



**Critical Evaluation of Leachate Clogging Potential in Gravity Collection Systems and  
Management Solutions  
Final Report**

**June 2020**

**Author  
Daniel E. Meeroff, Ph.D.**

Florida Atlantic University, Department of Civil, Environmental & Geomatics Engineering

**And  
Co-Authors  
Bishow Shaha, Ph.D., E.I.**

Florida Atlantic University, Department of Civil, Environmental & Geomatics Engineering

**Hinkley Center for Solid and Hazardous Waste Management**  
University of Florida  
P. O. Box 116016  
Gainesville, FL 32611  
[www.hinkleycenter.org](http://www.hinkleycenter.org)

Report # (leave blank)

**PROJECT TITLE: CRITICAL EVALUATION OF LEACHATE CLOGGING POTENTIAL  
IN GRAVITY COLLECTION SYSTEMS AND MANAGEMENT SOLUTIONS**

**PRINCIPAL INVESTIGATOR(S):**

Daniel E. Meeroff, Ph.D., Professor & Associate Chair, Dept. of Civil, Environmental & Geomatics Engineering, Florida Atlantic University,  
Phone: (561) 297-2658, E-Mail: dmeeroff@fau.edu

**PROJECT WEBSITE:** [labees.civil.fau.edu](http://labees.civil.fau.edu)

**PROJECT DURATION:** October 1, 2018 – June 1, 2020

**ABSTRACT:**

Leachate clogging in the Leachate Collection System (LCS) due to chemical precipitations and biofilms produced by microbial activities is a common phenomenon in any Municipal Solid Waste (MSW) landfill. This study focuses on quantifying the factors that impact the micro-environment of leachate; and microbial activities that help the precipitates to form and attach to the LCS. It also evaluates the performance of operational changes that have been implemented or the potential alternatives and recommends the possible measures to reduce the severity of clogging. A field scale side-by-side pipe network, and several laboratory setups were used in this study. Calcite is identified to be the predominant phase present in the precipitates using XRD/XRF analysis which, concur with the previous studies. Microbial growth and activities enhance the precipitation of  $\text{CaCO}_3$  in LCS. Clogging in LCS pipes can be controlled if not eliminated by continuous monitoring along with frequent cleaning with physiochemical processes.

**Key words:**

Landfills, leachate clogging, municipal solid waste (MSW), Precipitation, calcite

## METRICS REPORTING:

### Student Researchers:

Full Name: Bishow Shaha, Ph.D., E.I.

Email: bshaha2015@fau.edu

Anticipated Degree: Ph.D.

Department: CEGE

### Metrics:

1. List research publications resulting from **THIS** Hinkley Center project

Shaha, B. N. (2020). *Critical Evaluation of Leachate Clogging Potential in Gravity Collection Systems and Management Solutions* (Doctoral dissertation, Florida Atlantic University).

Meeroff, D. E., Shaha, B., Bloetscher, F., Esiobu, N., Mercer, B., McCorquordale, D., ... & Bennett, M. (2019). Characterization of biofilms and mineralogical scale in underground injection well disposal of landfill leachate and industrial wastewater streams. *Journal of Geoscience and Environment Protection*, 7(11), 69.

2. List research presentations resulting from **THIS** Hinkley Center project

Shaha, B.N. and Meeroff, D.E. (2019). *Impacts of pH on leachate chemistry, CaCO<sub>3</sub> precipitation, and scaling potential (Oral presentation)*. In World Environmental and Water Resources Congress, May 2019, Pittsburgh, PA.

3. List who has referenced or cited your publications from this project.

6 papers have cited this presentation publication:

- Ahmad, Z. U., Yao, L., Lian, Q., Islam, F., Zappi, M. E., & Gang, D. D. (2020). The use of artificial neural network (ANN) for modeling adsorption of sunset yellow onto neodymium modified ordered mesoporous carbon. *Chemosphere*, 127081.
- Zhao, R., Li, M., Ma, S., Yang, T., & Jing, L. (2020). Material selection for landfill leachate piping by using a grey target decision-making approach. *Environmental Science and Pollution Research*, 1-9.
- Li, M., Zhao, R., Ma, S., & Yang, T. (2020). Scale Deposition Inhibiting Composites by HDPE/Silicified Acrylate Polymer/Nano-Silica for Landfill Leachate Piping. *Materials*, 13(16), 3497.
- Shaha, B. N., & Meeroff, D. E. (2020). Prediction of H<sub>2</sub>S Concentration in Landfill Gas Resulting from Construction and Demolition Debris and the Selection of Treatment Method. *Journal of Environmental Engineering*, 146(6), 04020045.
- Lian, Q., Yao, L., Uddin Ahmad, Z., Gang, D. D., Konggidinata, M. I., Gallo, A. A., & Zappi, M. E. (2020). Enhanced Pb (II) adsorption onto functionalized ordered mesoporous carbon (OMC) from aqueous solutions: the important role of surface property and adsorption mechanism. *Environmental Science and Pollution Research*, 1-15.

- Meeroff, D. E., Shaha, B., Bloetscher, F., Esiobu, N., Mercer, B., McCorquordale, D., ... & Bennett, M. (2019). Characterization of biofilms and mineralogical scale in underground injection well disposal of landfill leachate and industrial wastewater streams. *Journal of Geoscience and Environment Protection*, 7(11), 69.

3 have cited the second peer-review paper

- Ahmad, Z. U., Yao, L., Lian, Q., Islam, F., Zappi, M. E., & Gang, D. D. (2020). The use of artificial neural network (ANN) for modeling adsorption of sunset yellow onto neodymium modified ordered mesoporous carbon. *Chemosphere*, 127081.
- Shaha, B. N., & Meeroff, D. E. (2020). Prediction of H<sub>2</sub>S Concentration in Landfill Gas Resulting from Construction and Demolition Debris and the Selection of Treatment Method. *Journal of Environmental Engineering*, 146(6), 04020045.
- Lian, Q., Yao, L., Uddin Ahmad, Z., Gang, D. D., Konggidinata, M. I., Gallo, A. A., & Zappi, M. E. (2020). Enhanced Pb (II) adsorption onto functionalized ordered mesoporous carbon (OMC) from aqueous solutions: the important role of surface property and adsorption mechanism. *Environmental Science and Pollution Research*, 1-15.

4. How have the research results from **THIS** Hinkley Center project been leveraged to secure additional research funding? What grant applications have you submitted or are planning on submitting?

“Investigation of Leachate Management Solutions at the Solid Waste Authority of Palm Beach County (Year III),” Solid Waste Authority of Palm Beach County, \$32,500, 10/1-2018 – 09/30/2019.

5. What new collaborations were initiated based on **THIS** Hinkley Center project?

Bud Goblisch, CES Consultants

6. How have the results from **THIS** Hinkley Center funded project been used (not will be used) by the FDEP or other stakeholders?

The operations personnel at SWA receive regular reports of our experimental results to inform their ongoing efforts to keep leachate collection system clogging under control. Other facility managers have contacted us regarding our expertise in leachate clogging including Lee County (Rebecca Rodriguez and Linda Monroy) as well as Tim Laube and David Schwabe from Kroff Chemical.

## ACKNOWLEDGEMENTS

The researchers would like to acknowledge the William W. “Bill Hinkley Center for Solid and Hazardous Waste Management for funding this project. The researchers would also like to thank the Technical Advisory Group members and all the stakeholders for their invaluable advice, feedback, and support of this work.

Full Name: Bishow Shaha, Ph.D., E.I.

Email: bshaha2015@fau.edu

Degree: Ph.D.

Department: FAU CEGE

Bio: Bishow Shaha is a solid waste researcher and has been working in this field since 2015. He completed his M.S. in Civil Engineering (environmental track) and a Ph.D. in Sustainable Infrastructure track from Florida Atlantic University. In the last five years, He worked on several solid waste management projects including Landfill gas (LFG) emission modeling, Leachate water quality analysis, Leachate clogging, Deep-well injection, and recycling alternatives. He competed three times in the solid waste student design competition organized by Solid Waste Association of North America (SWANA), finished second in 2015, and won the competition in 2017 and 2019. His Ph.D. dissertation titled “Critical evaluation of leachate clogging potential in gravity collection system” is focused on the understanding of the mechanism of calcium carbonate precipitation in gravity pipes that leads to the failure of a leachate collection system. He intends to be a solid waste professional and serve the industry. He lives in Boca Raton, Florida.

### **TAG members:**

Mark Eyeington, Mark Maclean, Mark Bruner, Owrang Kashef, D.V. Reddy, Craig Ash, Ravi Kadambala, Ron Schultz, Jeff Roccapriore, André McBarnette, Dan Schauer, Damaris Lugo, Amanda Krupa, Richard Meyers, Amede Dimonnay, Art Torvela, Ted Batkin.

# TABLE OF CONTENTS

LIST OF FIGURES .....	viii
LIST OF TABLES .....	xi
<b>1 INTRODUCTION .....</b>	<b>1</b>
<b>1.1 Background.....</b>	<b>1</b>
<b>1.2 Objectives.....</b>	<b>2</b>
<b>1.3 Literature Review.....</b>	<b>2</b>
<b>1.3.1 Leachate Clogging Mechanism .....</b>	<b>2</b>
<b>1.3.2 Factors Affecting Clogging .....</b>	<b>8</b>
<b>1.4 Historical Leachate Clogging and Management Strategies at the Study Site .....</b>	<b>11</b>
<b>1.4.1 Leachate Clogging at the Study Site.....</b>	<b>11</b>
<b>1.4.2 Management Strategies.....</b>	<b>12</b>
<b>2 METHODOLOGY .....</b>	<b>15</b>
<b>2.1 Site Description and LCS Clogging .....</b>	<b>15</b>
<b>2.2 Experimental Setup.....</b>	<b>20</b>
<b>2.2.1 Field Scale Experiment Model .....</b>	<b>20</b>
<b>2.2.2 Laboratory Setup.....</b>	<b>24</b>
<b>2.3 Leachate Collection .....</b>	<b>29</b>
<b>2.4 Analytical Methods for Parameters of Interests .....</b>	<b>31</b>
<b>2.4.1 pH .....</b>	<b>32</b>
<b>2.4.2 Temperature .....</b>	<b>33</b>
<b>2.4.3 Electrical Conductivity and Specific Conductance.....</b>	<b>34</b>
<b>2.4.4 Total Calcium .....</b>	<b>34</b>
<b>2.4.5 Alkalinity .....</b>	<b>35</b>
<b>2.5 Bacteriological Analysis.....</b>	<b>37</b>
<b>2.5.1 Petri Dish (Heterotrophic Plate Count) .....</b>	<b>37</b>
<b>2.5.2 Microscopic Analysis .....</b>	<b>39</b>
<b>2.5.3 Gravimetric Solids (TDS, TSS, and VSS) .....</b>	<b>41</b>
<b>2.5.4 Sulfides .....</b>	<b>43</b>
<b>2.5.5 Sulfates .....</b>	<b>44</b>
<b>2.6 Heat Sterilization and Precipitation .....</b>	<b>46</b>
<b>2.7 Test Method for Alternate and Submerge Dry Condition .....</b>	<b>47</b>

2.8	Saturation Indices .....	48
2.9	XRD Analysis with Rietveld Refinement .....	50
2.9.1	<i>Crystal Analysis Using PXRD/XRF</i> .....	50
2.9.2	<i>Post Processing Using Rietveld Refinement</i> .....	53
3	RESULTS.....	56
3.1	Leachate Characteristics and CaCO <sub>3</sub> Precipitation Potential .....	56
3.2	Types of CaCO <sub>3</sub> Scale Formation .....	56
3.3	Impacts of Flow Regime on CaCO <sub>3</sub> Scaling.....	59
3.4	Impacts of pH on CaCO <sub>3</sub> Scaling Potential .....	67
3.5	Impacts of Microbial Activities on CaCO <sub>3</sub> Scaling.....	81
3.5.1	<i>UV Disinfection</i> .....	82
3.5.2	<i>Heat Sterilization</i> .....	83
3.6	Impacts of Alternate Submerged and Dry Conditions on LCS Clogging.....	91
3.7	Impacts to the Deep Injection Well .....	93
4	CONCLUSIONS.....	100
4.1	Summary of Findings.....	100
4.2	Recommendations .....	103
	BIBLIOGRAPHY .....	106
	Appendix A: Water Quality Analyses .....	115
	Appendix B: PXRD/XRF Diffraction Pattern Analyses and Refinement.....	120
	Appendix C: Summary of Phase Identification and Rietveld Refinement .....	123

## LIST OF FIGURES

Figure 1. Various chemical processes that have shown the ability to generate supersaturated environments essential for calcite precipitation. Adapted from (Zhu and Dittrich, 2016).....	6
Figure 2. Simplified representation of the process that happens during ureolytic induced carbonate precipitation. Adapted from (Muynck et al., 2010a).....	10
Figure 3. High pressure water jetting results for the SWA Class I leachate collection system headers - 2012 and 2013 results (CDM Smith 2013) .....	12
Figure 4. Aerial photograph of the SWA site (adapted from Google Earth).....	15
Figure 5. A schematic of SWA Palm Beach County landfill cells and leachate collection system as of 2013.....	16
Figure 6. Landfill liner and leachate collection system design schematic (adapted from Shaha 2016).....	18
Figure 7. Schematic of gravity leachate collection line and pump station locations (yellow circles represent manholes, and the leachate flows in the direction of the arrows shown).....	19
Figure 8. Schematic layout of onsite side-by-side pipe network.....	20
Figure 9. Field scale side-by-side pipe network with UV unit.....	21
Figure 10. Satellite view of the pipe network and GPS location (26.764398, -80.139975) of pump station A.....	21
Figure 11. Reservoir (left), UV unit retrofitting (middle), and UV unit (right) .....	22
Figure 12. UV unit obtained for the field experiment ( <a href="https://www.pelicanwater.com/viqua-pro-uv.php">https://www.pelicanwater.com/viqua-pro-uv.php</a> ).....	23
Figure 13. 25 mm (1”) bypass line with 0.3 m (1 ft) long removable pieces retrofitted from the newly installed Y-strainers on both sides .....	24
Figure 14. Laboratory scale cyclone separator, front view (left), cross sectional view (right) ...	25
Figure 15. Photocatalytic Safety Cabinet used to disinfect leachate in the laboratory.....	26
Figure 16. Laboratory setup for pH adjustment with N <sub>2</sub> , CO <sub>2</sub> , and Air .....	27
Figure 17. Variable rate (0-3.5 lpm) gas regulator for 600 L gas cylinder.....	28
Figure 18. Addition of CO <sub>2</sub> and Air into the leachate .....	28
Figure 19. Selected sampling locations at SWA Class I landfill .....	30
Figure 20. Sampling procedure from the manholes.....	31
Figure 21. pH measuring meters (YSI 556 MPS, left; Model Hq40d meter, right) .....	33
Figure 22. Handheld thermal infrared thermometer (Ryobi IR001).....	34
Figure 23. Hach digital titrator setup for calcium measurement .....	35
Figure 24. Hach digital titrator kit for alkalinity measurement .....	36
Figure 25. Petri dish for use in HPC testing .....	37
Figure 26. Serial dilution preparation.....	38
Figure 27. L-spreading tool.....	38
Figure 28. Microscope with automatic camera (TCA-3.0) set up .....	40
Figure 29. Microscope slides .....	40
Figure 30. Microscope cover glass .....	41
Figure 31. “LissView” program icon on the desktop (a) and the program window, (b) .....	41
Figure 32. Suction filtration setup for TDS, TSS, and VSS .....	42
Figure 33. Sulfide test flow path.....	44

Figure 34. Sulfate test flow path.....	45
Figure 35. Leachate sterilization using boiling (left), Sterilized sample and the control kept at room temperature for the duration of the sterilization process (right).....	46
Figure 36. Test method to test alternate dry and submerge condition.....	47
Figure 37. Samples collected at three different depths (0-200 ft, 200-1500 ft, 1500-2900 ft) for mineralogical analysis.....	50
Figure 38. Sample preparation for XRD analysis in which solids were dried at 105°C overnight (left) and cooled in a desiccator and grinded to powder using a mortar and pestle (right) .....	50
Figure 39. XRD analysis flow path.....	51
Figure 40. XRD diffraction pattern of pure calcite purchased from Wards Scientific .....	52
Figure 41. XRF diffraction pattern of pure calcite purchased from Wards Scientific.....	52
Figure 42. Phase identification and Rietveld refinement using MATCH! 3.2.0, 3.9.0 and FullProf suite, respectively.....	54
Figure 43. Rietveld refinement of a pure calcite sample purchased from Wards Scientific .....	55
Figure 44. Historical clogging samples collected to analyze using XRD for phase identification .....	57
Figure 45. Comparison of historical LSI with that of current study.....	64
Figure 46. Observed changes in pH during the experiment with addition of nitrogen (N <sub>2</sub> ), carbon dioxide (CO <sub>2</sub> ), and air.....	68
Figure 47. Changes in pH due to addition of CO <sub>2</sub> at different rates.....	71
Figure 48. Changes in pH by exposing leachate to open air.....	71
Figure 49. Changes in pH by external turbulence (500 rpm) .....	71
Figure 50. pH adjustment and the impact on CaCO <sub>3</sub> precipitation rate: loose scale. A visible floating layer (left) and the layer attached to the beaker surface after pouring out leachate from the beaker (right) (7 days).....	72
Figure 51. pH adjustment and the impact on CaCO <sub>3</sub> precipitation rate: hard scale attached to the surface (7 days).....	72
Figure 52. pH changes during the incubation at 35°C for 7 days.....	73
Figure 53. Changes in alkalinity during the incubation at 35°C for 7 days.....	73
Figure 54. Changes in dissolved calcium during the incubation at 35°C for 7 days .....	74
Figure 55. Changes in dissolved sulfide during the incubation at 35°C for 7 days.....	74
Figure 56. Impact of initial pH of leachate on scale rate .....	75
Figure 57. Loose scale under microscope (x400) .....	75
Figure 58. Impact of increased pH using NaOH on dissolved calcium.....	76
Figure 59. Impact of increased pH using NaOH on alkalinity .....	77
Figure 60. Saturation index on Day 0 and Day 7.....	77
Figure 61. Saturation index (LSI) at Day 0 and Day 7 for the leachate sample from MH 13 .....	78
Figure 62. Saturation index (LSI) at Day 0 and Day 7 for leachate sample from MH 11 .....	79
Figure 63. Saturation index (LSI) at Day 0 and Day 7 for leachate sample from Deep well.....	79
Figure 64. Enhanced precipitation of calcium carbonate with pH adjustment with the addition of NaOH; 1mL (left), 3mL (middle), and 5 mL (right).....	80
Figure 65. Alkalinity and calcium concentration changes with pH.....	81

Figure 66. Boiling leachate (left), and visual comparison of sterilized and control leachate (right) ..... 84

Figure 67. Visible adherent scale formation in 250 mL beaker for control (1st and 2nd from left) and sterilized sample (3rd and 4th from left)..... 85

Figure 68. Changes in Langelier Saturation index (LSI) during different stages of experiment.. 85

Figure 69. Precipitation rate obtained from trial 1..... 86

Figure 70. HPC plates after incubation at 35°C for 48-72 hours (Autoclaved sample) ..... 87

Figure 71. HPC plates after incubation at 35°C for 48-72 hours (Oven sterilized sample) ..... 87

Figure 72. HPC plates and bacteria growth in 48 hours after with samples stored 10 days at 35°C (Autoclave: left; Oven sterilized: right)..... 88

Figure 73. Precipitate in the vessel surface and 4.5-micron glass microfiber filters for control, oven sterilized and autoclaved leachate sample from left to right, respectively ..... 88

Figure 74. Precipitation rate obtained from trial 2 with much stronger leachate compared to trial 1..... 89

Figure 75. Precipitation rate of sterilized sample with aerobic and anaerobic incubation ..... 90

Figure 76. Precipitation rate of raw and sterilized leachate with different incubation period at 35°C..... 90

Figure 77. Precipitation due to submerged and dry cycle in the laboratory ..... 92

Figure 78. IW-1 brushing and sample collection for mineralogical testing (a. brushing equipment setup (top left), b. a closer view of the setup and the sample port (green flexible hose) (top right), c. sample port assembly (bottom left), and d. 5-gallon sampling bucket filled with sample to collect settled particles..... 95

Figure 79. Stacked bar chart showing the composition of the samples at each depth compared to a pure calcite QA/QC standard ..... 98

## LIST OF TABLES

Table 1. List of urease producing bacteria that are capable of calcite precipitation.....	10
Table 2. Date of first waste disposal and status of each landfill cell .....	17
Table 3. Calibration gas concentration details.....	27
Table 4. Summary of sampling parameters .....	29
Table 5. Summary of water quality analysis method and calibration of instruments.....	31
Table 6. Sample volume and digit multipliers for alkalinity titrations (provided by Hach.com). 37	
Table 7. Sulfide analytical method (Hach Program 690) performance data (Hach DR 5000 methods: Method 8131) .....	44
Table 8. Sulfate analytical method (Hach Program 680) performance data (Hach DR 5000 methods: Method 8051) .....	45
Table 9. Estimated equilibrium constants and activity coefficients .....	48
Table 10. Precalculated value of pK and A .....	49
Table 11. Leachate characteristics and comparison with the literature review .....	56
Table 12. Summary of search match calculation and Rietveld refinement .....	58
Table 13. Field and laboratory water quality analysis of collected leachate sample between June and September, 2017.....	61
Table 14. Saturation indices (LSI and RI) calculation based on average water quality parameters for the samples collected between June and September 2017 .....	62
Table 15. Average water quality data based on 2018-2019 sampling .....	63
Table 16. Mass balance summary at NEFCO pH equal to 4.5 .....	65
Table 17. Mass balance summary at NEFCO pH equal to 5.0 .....	66
Table 18. Mass balance summary at NEFCO pH equal to 5.5 .....	66
Table 19. Turbidity and TSS reduction using a laboratory scale cyclone separator at 1.7 lpm flow rate.....	67
Table 20. Factors that impacts pH changes in leachate .....	68
Table 21. Summary of leachate water quality changes due to addition of N <sub>2</sub> , CO <sub>2</sub> , and Air .....	69
Table 22. Saturation indices calculation (LSI and RI).....	69
Table 23. Water quality of the three different leachates.....	78
Table 24. Summary of PXRD analysis and Rietveld refinement .....	80
Table 25. UV disinfection of leachate using the laboratory setup.....	82
Table 26. Average water quality parameters from the control and treated side during 120 min experiment.....	82
Table 27. HPC count for treated and untreated samples.....	83
Table 28. Pump station A leachate water quality parameters and precipitation potential .....	83
Table 29. Summary of leachate addition to adjust for the loss due to evapotranspiration .....	91
Table 30. Summary of groundwater addition to adjust for the loss due to evapotranspiration ....	92
Table 31. Summary of mass balance analysis based on the flow going to the deepwell in March 2017.....	93
Table 32. A summary of the mass balance based on individual waste streams going to the injection well.....	94

Table 33. Field data using YSI 556 multiparameter meter and turbidimeter on February 28, 2018. .....	96
Table 34. Summary of XRD pattern analysis and Rietveld refinement using MATCH! 3.9.....	97

# 1 INTRODUCTION

## 1.1 Background

Leachate is defined as the liquid that percolates through a landfill and carries contaminants dissolved from waste as it percolates through the cell to the leachate collection system (LCS). Rain falling on the landfill is the main contributor to leachate generation. In addition, existing moisture from wet waste and the metabolic water from waste decomposition also contribute to leachate formation. Release of leachate to the environment can be a threat to surface and groundwater (Raghab et al. 2013). Municipal solid waste (MSW) sanitary landfills in the United States are required by regulation (RCRA Subtitle D) to use double liners to protect the groundwater and soil from leachate exposure. LCS are required to remove the leachate above the liner. United States federal guidance on landfills (40 CFR Part 258) limits the hydraulic head of leachate above the bottom liner to be less than 30 centimeters (12 inches) (Koerner 2008). Therefore, it is critical that LCS components (sand, gravel, geotextiles, geonets, pipes etc.) perform as expected.

LCS clogging is a common phenomenon in MSW landfills throughout the United States (Rowe 2009; Cooke et al. 2005; Rowe et al. 2004; Bouchez et al. 2003; Maliva et al. 2000; Fleming et al. 1999; Rowe et al. 1998; Baveye 1998; Rittmann 1996; Koerner 1994; Brune 1991; Bass et al. 1985). There are several reasons for LCS failure including clogging due to deposits of silt or other fines (Fleming et al. 1999), chemical precipitation due to the presence of carbonates and sulfides in an anaerobic environment (Bass et al. 1983), biofilm buildup (Limoli et al. 2015; Vangulk & Rowe 2004; Rowe et al. 2002; Castanier et al. 2000; Flemming et al. 1999), pipe deterioration due to chemical attack or corrosion (Bass 1985), change of slope due to differential settling (Bass 1985), and others. Soil, silt or other fines can enter the LCS pipes and settle out or in the joints, turns, and intersections, particularly if the flow is insufficient. Clogging by chemical precipitation can occur as the result of simple chemical processes or more complex biogeochemical processes. These include the precipitation of calcium carbonate, magnesium carbonate (rhodochrosite) and other insoluble forms (such as sulfides and silicates). Excessive biological activity may also cause LCS clogging. Bacteria secrete extracellular polysaccharides to form a gelatinous matrix (biofilm), which traps particles that seed biogeochemical rocking (Limoli et al. 2015).

The Solid Waste Authority (SWA) of Palm Beach County landfill operators began documenting LCS clogging issues in 1999 (refer to Section 1.4). SWA implemented several management strategies including addition of groundwater for dilution and flow control in the gravity collection line and introduction of an electronic scale control system. In addition to that, they have also performed periodic cleaning of the leachate collection pipes using acid flushing and high-pressure water jetting to keep the pipes free of clogs. Even though literature review of LCS clogging suggested various mechanisms of clog formation within the pipe network, the exact trigger(s), as

well as the factors that worsen the condition are yet to be identified. In addition to that, visual inspection of historical leachate clogs that were collected from the study site are of different types and only suggest that there is more than one mechanism that causes these problematic clogs. Furthermore, the preventative measures that were implemented so far only helped to control the leachate clogging to a certain extent that did not hamper daily operation. However, the performance depends on various site-specific factors that need to be identified and evaluated. Therefore, this study will focus on the identification of mechanisms and factors that act as a trigger for the formation of biogeochemical rock in the LCS to suggest better preventative measures based on the findings.

## **1.2 Objectives**

To keep LCS clogging under control, it is necessary to understand the trigger mechanism, factors that impact the micro-environment of leachate, and microbial activities that aid precipitates to attach to the inner wall of the LCS pipes. In the literature, there is no consensus on the actual mechanism, and the critical factors of LCS clogging are yet to be fully understood. This study provides researchers with new data and knowledge regarding the mechanisms and the factors involved in LCS clogging, the probable mechanism of precipitates collected from the landfill based on laboratory replicates, impacts of LCS clogging on the leachate disposal system, and operational controls for preventing LCS clogging at landfills.

The main goal of this study is to: 1) better understand the mechanism of LCS clogging within the context of challenges in daily operation, 2) better understand the major factors that enhance clogging, and 3) review, evaluate, and suggest preventative measures based on the findings. To accomplish this goal, this study is organized in two main activities:

1. To simulate LCS clogging in the laboratory and field scale pipe network set up with different conditions (pH, temperature, UV treated leachate, heat sterilized) to replicate real LCS conditions and better explain the formation trigger mechanism of different types of clog samples collected from the site.
2. To review, evaluate and analyze the preventative measures to suggest the effective operational controls.

## **1.3 Literature Review**

### **1.3.1 *Leachate Clogging Mechanism***

#### **1.3.1.1 Chemical Precipitation**

Chemical precipitation of leachate clogs is mostly calcium carbonate ( $\text{CaCO}_3$ ) and is pH dependent (Meeroff et al. 2019; Shaha et al. 2019; Shaha 2016; Levine 2005; Mullah-Saleh 2007; Brune 1991; Bass 1985). Leachate is a complex liquid waste that tends to have elevated levels of calcium

ion in solution (Meeroff et al. 2019; Shaha et al. 2019; Shaha 2016). A small increase in pH due to chemical, biological, or temporal changes in the leachate can increase the formation of carbonate ( $\text{CO}_3^{2-}$ ) ion, which results in precipitation of calcium carbonate (calcite) as shown in equation 1.



This is the most commonly reported formation of calcium carbonate and also known as inorganic clogging in LCS. The most basic requirement for the precipitation of calcium carbonate ( $\text{CaCO}_3$ ) minerals such as calcite and aragonite, is that the product of the concentrations of calcium [ $\text{Ca}^{2+}$ ] and carbonate ions [ $\text{CO}_3^{2-}$ ] exceeds the solubility product of calcite (equation 2) and aragonite, respectively.

$$[\text{Ca}^{2+}][\text{CO}_3^{2-}] > 10^{-8.35} \quad (2)$$

One of the major changes that occurs during the transportation of leachate through the LCS is the degasification of carbon dioxide ( $\text{CO}_2$ ) (Shaha et al. 2019). Degasification is the removal of dissolved gases from liquids, especially water or aqueous solutions. Degasification of  $\text{CO}_2$  within the leachate affects the pH, the carbonate equilibrium, and thus the inorganic clogging. In addition, microbial growth and activity and removal of volatile fatty acids (VFAs) also impacts the pH and thus clogging (Rittmann et al. 2003). The solubility of  $\text{CO}_2$  is dependent on Henry's law, the partial pressure of gas in the atmosphere, temperature, leachate water quality (e.g. salinity, total solids, etc.) and turbulence intensity (Metcalf & Eddy 2003, Malusa et al. 2003).

### 1.3.1.2 Biochemical Precipitation/ Microbially Induced Precipitation

*Biofilm:* Based on the field and laboratory studies performed by Lozecznik (2010), clogging is a biologically-mediated process initiated by the formation of biofilm within the drainage material of LCS. The growth and activity of biofilms and suspended microorganisms induces the precipitation of carbonate minerals (e.g.  $\text{CaCO}_3$ ) and entrainment of suspended particles (Armstrong 1998, Fleming et al. 1999, Fleming and Rowe 2004, Rittman et al. 2003, Cooke et al. 1999, 2001, 2005, McIsaac et al. 2000, 2005, VanGulck et al. 2003, 2004a,b, Rowe et al. 2000a,b, 2004, 1998a,b, McIsaac and Rowe 2006). In general terms, a biofilm is a community of microorganisms and their extracellular polymers (EPS) attached to a solid surface. Different microorganisms produce different EPS (i.e proteins, lipopolysaccharides or capsular polysaccharides), which further affect the surface adhesion process and changes of the biofilm thickness and density (Vu et al. 2009). The compositions of biofilms vary widely for each case depending on growth conditions (Stoodley et al. 1999); these conditions include nutrient availability and hydrodynamic conditions (e.g. laminar or turbulent flow). Biofilms are mainly composed of water (> 90%), EPS (up to 90% of organic matter), cells, entrapped particles and precipitates, sorbed ions, and a mix of polar and nonpolar organic molecules (Flemming et al. 2000). Biofilms are porous; nutrients penetrate the pores and reach different layers of the biofilm and microbial colonies, thus affecting the growth of

the film via mass-transport mechanisms. Hydrodynamic conditions have a dual effect on mass transfer in biofilms with high turbulence facilitating substrate diffusion and shear stress increasing biofilm density. This reduces the diffusivity of substrates into the biofilm (Liu and Tay 2001). Biofilm density is a property that affects how the biofilm operates. This property is dependent on the bacterial species diversity, biofilm thickness, bulk composition, hydrodynamics of the environment and biofilm age (Vu et al. 2009). Because the adhesive properties of EPS help retain the suspended particles at the biofilm surface, these particles can contribute significantly to the overall mass of the biofilm (Flemming et al. 2000). They may also hinder the transport of nutrients inside of the biofilm that are required for the microorganism's survival.

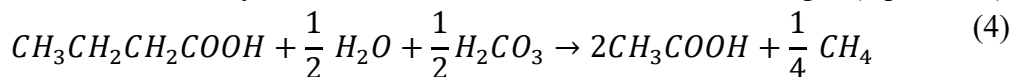
Bacterial cells are typically anionic due to the presence of carboxylate or phosphate moieties in the outer layer. The biofilm may then facilitate binding with metals cations ( $\text{Ca}^{2+}$ ,  $\text{Mg}^{2+}$  and  $\text{Fe}^{3+}$ ) that can precipitate on the surface (McClellan et al. 1999). Biofilm accumulation and growth also increases the frictional resistance in water distribution systems (Bryers and Characklis 1981), increasing the pressure drop and reducing the effective diameter of pipes. Given that the design and operation of current landfills and bioreactor landfills around the world have no control over leachate composition and biofilm formation in LCS, the expected conditions are ideal for uncontrolled biofilm growth to occur.

Rowe et al. (2004) reviewed past research of clogging in LCS and suggested that biofilm growth in LCS results largely from the growth of microorganisms conducting acetogenesis of propionate and butyrate, and by the methanogenesis of acetate. Microbial consumption of these VFAs (propionate, butyrate, acetate) generates carbonic acid ( $\text{H}_2\text{CO}_3$ ), as shown in the following equations.

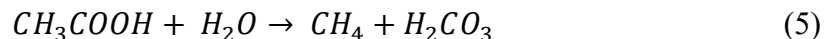
Fermentation of propionate to acetate, carbonic acid and methane gas (equation 3):



Fermentation of butyrate to acetate, carbonic acid and methane gas (equation 4):



Fermentation of acetate to methane and carbonic acid (equation 5):



The accumulation of  $\text{H}_2\text{CO}_3$  increases the total available carbonate species in solution; when combined with metals such as  $\text{Ca}^{2+}$ , which is abundant and likely supersaturated in leachate, readily precipitates as  $\text{CaCO}_3$  scale. The consumption of VFAs and the production of  $\text{CO}_2(\text{g})$ , a portion of which dissolves in water to form carbonic acid - a weaker acid, tends to increase pH,

potentially inducing the precipitation of carbonate-based minerals formed in the leachate. Particles such as sand grains, which are commonly used as daily cover, travel with the leachate. They are transported with the bulk liquid and can be deposited in the drainage layer or in slow-moving pipes, thus contributing to the inorganic layer of clogging. The porosity of the medium decreases as clogging occurs, increasing the leachate velocity through the drainage material. This may control the rate of VFA consumption and the attachment/detachment of suspended or attached microorganisms; net growth in this layer occurs as a result. As clogging occurs, the change in fluid flow through the porous media may affect the attachment/detachment of inorganic particles (Rittmann 1996; Rowe et al. 1998; Lozeczniak 2010).

Biologically-induced mineralization is usually carried out in open environments, and the process is often linked to microbial cell surface structures and metabolic activities. Microbial EPS can trap and bind remarkable amounts of calcium to facilitate calcium carbonate precipitation, and most likely also play an essential role in calcium carbonate precipitation morphology and mineralogy (Arp et al. 1999; Braissant et al. 2007; Dupraz et al. 2005). The mineralization process associated with microbial metabolic activities usually leads to an increase in alkalinity, thereby facilitating calcium carbonate precipitation (Douglas and Beveridge 1998; Castanier et al. 1999). Among these metabolic activities, the most common is urea hydrolysis catalyzed by urease enzymes, which commonly occurs in large varieties of microorganisms (Moblely and Hausinger 1989). The microbial urease enzyme hydrolyzes urea to produce carbonate and ammonia, increasing the pH and carbonate concentration, which then combines with free calcium to precipitate calcium carbonate, which is more insoluble at elevated temperatures (Hammes et al. 2003; Muynck et al. 2010).

Previously, the formation of calcium carbonate precipitation was proposed to occur via different mechanisms (**Figure 1**) such as photosynthesis (Thompson and Ferris 1990; McConnaughey and Whelan 1997), urea hydrolysis (Stocks-Fischer et al. 1999; De Muynck et al. 2010; Dhami et al. 2013a), sulfate reduction (Castanier et al. 1999; Warthmann et al. 2000; Hammes et al. 2003a), anaerobic sulfide oxidation (Warthmann et al. 2000), and biofilm EPS (Kawaguchi and Decho 2002; Arias and Fernandez 2008).

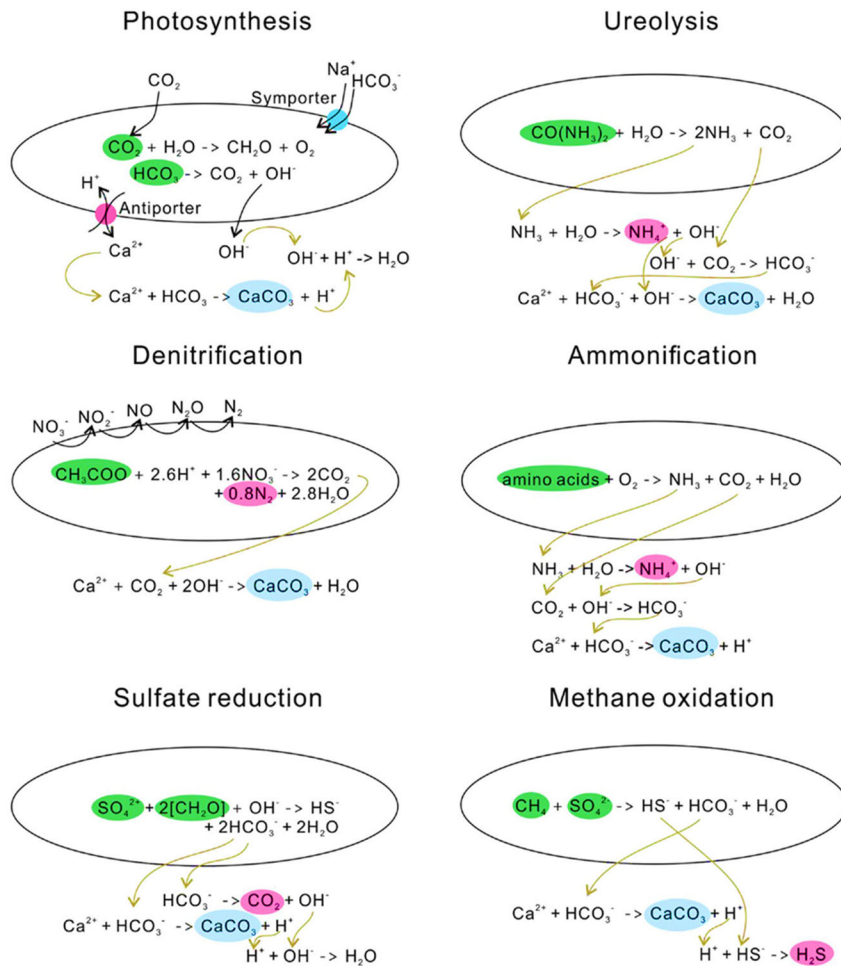
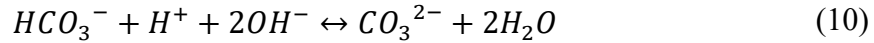
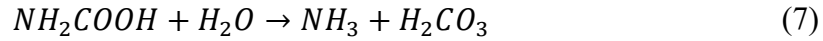
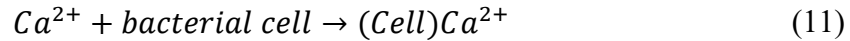


**Figure 1. Various chemical processes that have shown the ability to generate supersaturated environments essential for calcite precipitation. Adapted from (Zhu and Dittrich, 2016)**

However, the precipitation of calcium carbonate by bacteria via urea hydrolysis is one of the more widely accepted mechanisms (Hammes and Verstraete 2002; DeJong et al. 2010; De Muynck et al. 2010). The ability of urease (urea amidohydrolase; EC 3.5.1.5) to induce carbonate precipitation in microorganisms has already been discussed by several researchers (Hammes et al. 2003a; Burbank et al. 2012; Li et al. 2013; Stabnikov et al. 2013). Urease catalyzes the hydrolysis of urea into ammonia and carbamic acid (equation 6), which is spontaneously hydrolyzed to an additional mole of ammonia and carbonic acid (equation 7) (Stocks-Fischer et al. 1999; Burne and Chen 2000; Hammes et al. 2003a). These two products ( $\text{NH}_3$  and  $\text{H}_2\text{CO}_3$ ) are further equilibrated in water to form bicarbonate (equation 8) and two moles of ammonia and two moles of hydroxide ions (equation 9). The hydroxide ions result in an increase of pH, which can shift the bicarbonate equilibrium, resulting in the formation of carbonate ions (Fujita et al. 2008) (equation 10). This shift can then precipitate the metal ions in solution, and the reaction continues spontaneously to eventually form insoluble calcium carbonate (Ferris et al. 1996; Mitchell and Ferris 2005).



CaCO<sub>3</sub> precipitation occurs at the bacterial cell surface if there are sufficient concentrations of Ca<sup>2+</sup> and CO<sub>3</sub><sup>2-</sup> in solution (Qian et al. 2010) (equations 11 & 12)



Calcite (CaCO<sub>3</sub>) is the most common and stable bacterial carbonate polymorph among the three crystal polymorphs of calcium carbonate (calcite, aragonite and vaterite) (Rodriguez-Navarro et al. 2012). The production of the polymorphs depends both on their growing environments and bacterial strains. It was reported that different bacteria precipitated different types of calcium carbonate of either spherical or polyhedral crystalline forms (Cañaveras et al. 2001). Bacterial-induced carbonate minerals have often been reported in a large number of bacteria, such as cyanobacteria (Jansson and Northen 2010), sulphate-reducing bacteria (Warthmann et al. 2000), bacilli (Goddette et al. 1992; Betzel et al. 1998; Jørgensen et al. 2000), myxococci (Rodriguez-Navarro et al. 2003; Gonzalez-Muñoz et al., 2010), Halobacteria (Sánchez-Román et al., 2011) and *Pseudomonas* sp. (Jha et al. 2009). Groth et al. (2001) tested the crystal-producing ability among cave bacteria and found that all produced calcite except for *Bacillus* sp., which precipitated vaterites. Rodriguez-Navarro et al. (2003) reported that *Myxococcus xanthus* was able to induce precipitation of calcite and vaterite. Emerging evidence suggests that bacteria do not directly influence calcium carbonate morphology or polymorph selection (Chekroun et al. 2004; Bosak et al. 2005; Rodriguez-Navarro et al. 2012). The morphological features instead may be influenced by the composition of the culture medium, the specific bacterial outer structures and their chemical nature, which might be critical for the bacterial crystallization process (Gonzalez-Muñoz et al. 2010).

In summary, there are three different mechanisms involved in the biologically-mediated formation of carbonate minerals:

- 1) Biologically controlled mineralization, which consists of cellular activities that specifically direct the formation of minerals (Lowenstam and Weiner 1989; Benzerara et al. 2011; Phillips et al. 2013). In this process, microorganisms control nucleation and growth of minerals, which are directly synthesized at a specific location within or on the cell, but only under certain conditions.

- 2) Biologically influenced mineralization, in which passive mineral precipitation is caused by the presence of cell surface organic matter such as EPS associated with biofilms (Benzerara et al. 2011; Phillips et al. 2013)
- 3) Biologically induced mineralization in which the chemical modification of an environment by biological activity results in supersaturation and subsequent precipitation of minerals (Lowenstam and Weiner 1989; Stocks-Fischer et al. 1999; De Muynck et al. 2010; Phillips et al. 2013).

### 1.3.2 *Factors Affecting Clogging*

Calcium carbonate precipitation is a chemical process governed by several key factors: 1) pH, 2) temperature, 3) Chemical strength of leachate/saturated and unsaturated condition, 4) a catalyst (e.g. urease or carbonic anhydrase), and 5) the flow regime (Declat et al. 2016; Shaha 2016; Wei et al. 2015; Rowe & Yu 2010).

#### 1.3.2.1 pH

Studies (Helmi et al. 2016, Ferris et al. 2003) have been carried out to assess the relative impact of different environmental conditions on the biomineralization process. Investigations of mineral precipitation mediated by different groups of bacteria have identified that pH has an important influence on carbonate precipitation (Helmi et al. 2016, Ferris et al. 2003). The precipitation of calcite in a solution can be tracked by measuring the pH, as the urease enzyme will only be active at pH values that support urea hydrolysis ( $\text{pH} \leq 8.0$ ). The optimum pH for urease activity is 8.0, and if the pH is above 8.0, the enzyme activity decreases by half (Stocks-Fischer et al. 1999, Gorospe et al. 2013). Aerobic bacteria release  $\text{CO}_2$  via cell respiration, which is paralleled by an increase in pH due to ammonia production (Ivanov and Chu 2008). Upon the decrease of pH, carbonates will dissolve (Hammes and Verstraete 2002).

Most calcite precipitation occurs under alkaline conditions from pH 8.7 to 9.5 (Ferris et al. 2003, Stocks-Fischer et al. 1999, Sanchez-Roman et al. 2007). Stabnikov et al. (2013) investigated the activity of halophilic and alkaliphilic urease producing bacteria at high concentrations of inorganic salt and pH above 8.5. The results showed that halophilic and alkaliphilic bacteria are more tolerant to conditions in which other urease producing bacteria cannot survive. This demonstrates that certain groups of bacteria capable of precipitating calcium carbonate do exist and can survive the extreme conditions of high concentrations of inorganic salts and highly alkaline pH regimes that are characteristic of leachate.

#### 1.3.2.2 Temperature

Temperature dictates the growth of bacteria and the ability of urease enzyme to facilitate the precipitation of calcium carbonate. Experimental studies tested on carbonate precipitating isolates were able to grow and precipitate carbonate crystals at temperatures between 10 and 40°C (Zamarreño et al. 2009b). However, at 40°C, only certain bacteria were able to grow and

precipitate crystals. The optimum temperature for efficient carbonate precipitation is 35°C (Zamarreño et al. 2009b, Helmi et al. 2016). Temperatures in this range are common for leachate collection systems.

#### 1.3.2.3 Chemical Strength of Leachate/Saturated and Unsaturated Condition

Several researchers found that “lightly-loaded” permeating leachate with low concentrations of organic acids and cations (such as calcium) causes little if any clogging; whereas most clogging occurred with “highly-loaded” leachate with higher concentrations of organic acids and cations (Brune et al. 1991, Rowe et al. 2002, Armstrong 1998). In addition, Rowe et al. (2002) demonstrated that for similar chemical strength and flow rate, columns permeated with synthetic leachate with negligible suspended solids experienced less clogging than those permeated with real landfill leachate (Armstrong 1998) with much higher suspended solids. Thus, the composition of the leachate (e.g. organic acids, inorganic cations and suspended solids concentrations) entering the LCS has an important role to play with respect to the rate of clogging.

Saturation indices are indicators of chemical stability and take into consideration the pH, alkalinity, dissolved solids, calcium concentration, and temperature of leachate. The most common and widely used indices in predicting calcium carbonate precipitation potential are Langelier Saturation Index (LSI), Ryzner Index (RI), and calcium carbonate precipitation potential (CCPP). LSI and RI indicate the thermodynamic driving force, while CCPP is the total mass of  $\text{CaCO}_3$  reacted to obtain equilibrium (de Moel et. al. 2013). Although these indices provide qualitative information about the saturation condition of leachate, in predicting clogging they have some inherent limitations such as: 1) dealing with high levels of suspended solids, 2) microbial activity, and 3) accurate measurement of leachate alkalinity. Therefore, although these indicators provide qualitative information if the leachate is oversaturated, neutral, or undersaturated, they do not predict the magnitude or the severity of the clogging issue.

#### 1.3.2.4 Effect of Urease Towards Calcite Precipitation

The conversion of urea to ammonia is an important proposed mechanism for carbonate precipitation. Urease producing bacteria (UPB) are the most commonly used bacteria for precipitation studies (**Table 1**).

**Table 1. List of urease producing bacteria that are capable of calcite precipitation**

Bacteria	References
<i>Bacillus megaterium</i>	(Stocks-Fischer et al. 1999, Lian et al. 2006)
<i>Sporosarcina pasteurii</i>	(Okwadha and Li 2010, Tobler et al. 2011)
<i>Bacillus</i> sp. VS1	(Chu et al. 2012, Chu et al. 2013, Chu et al. 2014)
MCP-11 ( <i>Bacillus sphaericus</i> )	(Cheng and Cord-Ruwisch 2012 and 2013)
<i>Bacillus</i> sp. CR2	(Achal and Pan 2014)
<i>Sporosarcina pasteurii</i> WJ-2	(Kang et al. 2014b)
<i>Methylocystis parvum</i> OBBP	(Ganendra et al. 2014)
<i>Lysinibacillus sphaericus</i> CH5	(Kang et al. 2014a)
<i>Bacillus licheniformis</i>	(Helmi et al. 2016)

Upon addition of urea to these bacteria communities, dissolved inorganic carbon (DIC) and ammonium (AMM) are released in the microenvironment (**Figure 2A**).

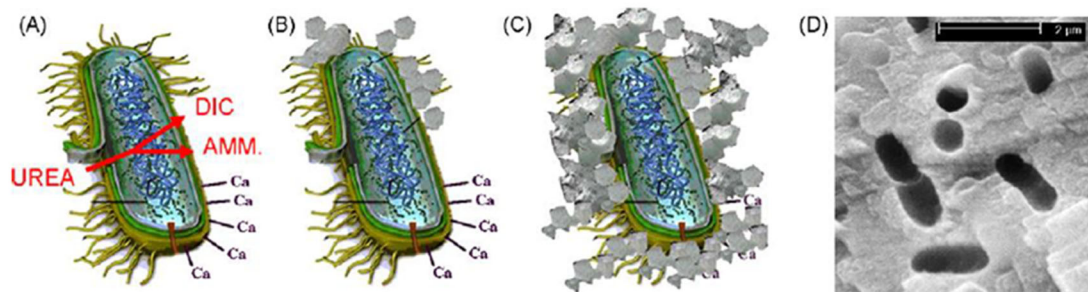


**Figure 2. Simplified representation of the process that happens during ureolytic induced carbonate precipitation. Adapted from (Muynck et al., 2010a)**

Calcium ions in solution are attracted to the bacterial cell wall due to the negative charge of the latter creating calcium supersaturation locations (**Figure 2B**). This causes bacterial encapsulation due to a limited amount of nutrient transfer, which results in cell death (**Figure 2C**). The imprints of bacterial cells involved in carbonate precipitation remain in the carbonate crystals (**Figure 2D**).

#### 1.3.2.5 Impact of Flow Regime in the Pipes

Flow regime includes quantity and quality of leachate, variation in leachate mix from different sources or cells (active or inactive), leachate flow through the gravity collection system, as well as addition of dilution water to increase the flow to avoid stagnation (Schert et al. 2015; Shaha 2016; Shaha et al. 2019). Quantity and quality of leachate vary with the waste composition landfilled and precipitation if all other parameters remain constant. Higher leachate strength with low volume during dry seasons has higher precipitation potential and enhances precipitation in the leachate collection system. It is also evident from the previous studies (Schert et al. 2015; Shaha 2016) that, the addition of dilution water into the gravity collection system increases the leachate flow and reduces precipitation of  $\text{CaCO}_3$ . However, there was no statistical evidence of changes in leachate

water quality or saturation indices due to the dilution activity (Shaha 2016). In addition, turbulence and disturbance in the leachate flow allow aeration of leachate in the gravity collection system. Aeration has been shown to increase the leachate pH (Schert et al. 2015; Shaha 2016; Shaha et al. 2019), which also leads to localized precipitation.

## **1.4 Historical Leachate Clogging and Management Strategies at the Study Site**

### **1.4.1 *Leachate Clogging at the Study Site***

In March 1999, SWA observed a loss of leachate flow from Cell 6 of the Class I landfill. Upon inspection, it was found that a hard-mineral substance filled portions of the leachate collection lines within Cell 6 (laterals and headers) and the leachate transmission lines outside the landfill (“stub” lines from cells to manholes, gravity lines between manholes, and leachate force main). Precipitates in these lines were found up to 120 feet into the cell and more than 300 feet outside the cell (Maliva 2000). Cell 6 was constructed in 1995, and waste was first deposited in the cell in September, 1996; so, it was concluded that the mineral deposit formed over a period of less than 2.5 years (Maliva, 2000). Due to heavy rainfall in 1999 and leachate disposal volume restrictions, leachate was held in Cell 6 for a period of three months; leachate laterals, headers, and drainage media (aggregate around pipes and sand drainage and protective layer) were, presumably, saturated with leachate for some or all of the three-month period.

Samples of precipitates from Cell 6 were analyzed by X-ray diffraction (XRD) and the only mineral detected was calcite ( $\text{CaCO}_3$ ), which was found in two main forms: bundles of radial fibrous crystals or microcrystalline formations. The researchers described the mineral deposition as a combination of pure abiotic precipitation and microbially-mediated precipitation (Maliva 2000).

Levine (2005) sampled and analyzed leachate from Cell 6 of the Class I landfill in March and November of 2004 and concluded that there was “significant evidence of microbial activity in the leachate.” In addition, the elemental composition of suspended particles was analyzed by scanning electron microscopy and energy dispersive spectroscopy (SEM/EDS) to determine that calcium was the predominant species (~90%) with some evidence of magnesium, phosphorous, and silica (Levine 2005), while the clog-forming precipitates themselves had a similar composition (90% calcium with traces of silica, chloride, potassium, and sulfur). Levine (2005) also studied the difference in clogging depending on the type of waste landfilled (MSW Monofill, Ash Monofill, or mixed waste) and concluded that lower levels of microbial activity in the “Ash Monofill” leachate results in lower levels of carbonate species resulting in less clogging. The dominant constituents in the clog material from the landfill LCS are calcium, carbonate, sulfur, phosphorous, iron, and silica.

Mullah-Saleh (2006), in an extension of Levine’s work, analyzed leachate data and also conducted geochemical modeling using “The Geochemist’s Workbench®, Release 6.0” (GWB) –

specifically, the Reaction Module (REACT) found within GWB. Model simulations with respect to the Cell 6 leachate sample indicated that  $\text{CaCO}_3$ ,  $\text{MgCa}(\text{CO}_3)_2$ ,  $\text{Ca}_{10}(\text{PO}_4)(\text{OH})_2$ ,  $\text{FeS}_2$ , and  $\text{FeCO}_3$  were all possible insoluble species that could be present in the leachate.

Shaha (2016) studied the leachate clogging issue at the SWA landfill, collected periodic leachate samples and clog materials previously formed in the leachate collection pipe, conducted XRD analysis and found out that the major component of the clog is calcium carbonate (calcite) and quartz (Shaha 2016; Shaha et al. 2019) along with some impurities including halite (salt) and microbiological residues.

### 1.4.2 Management Strategies

SWA uses high pressure water jetting periodically to manage the clogging issue in the leachate collection headers. **Figure 3** presents the results of high-pressure water jetting in 2012 and 2013 conducted by CDM Smith.

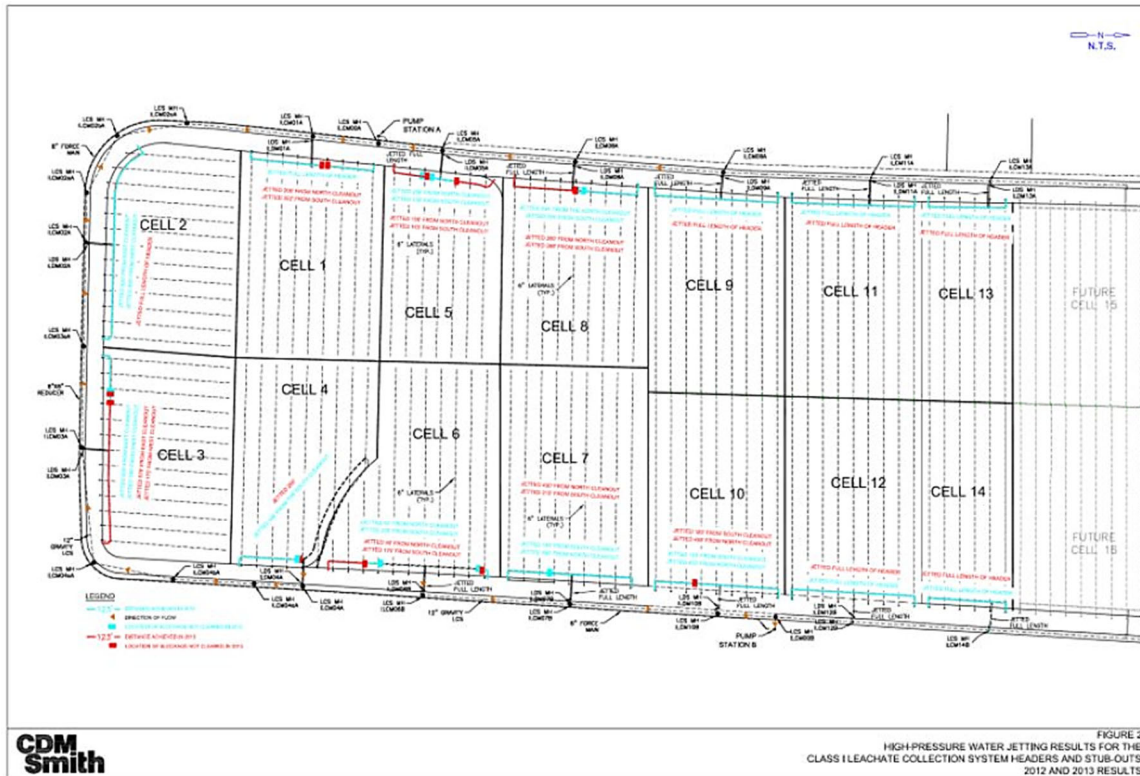


**Figure 3. High pressure water jetting results for the SWA Class I leachate collection system headers - 2012 and 2013 results (CDM Smith 2013)**

To keep LCS clogging under control, several methods were proposed. These included physically clearing the clogs or preventative measures to stop clogs from forming. Mayer (2014) discussed clogging at MSW landfills and reviewed clogging mechanisms suggested by other literature. In addition, Mayer (2014) discussed methods of cleaning the LCS pipe and surrounding gravel pack

in landfills in general and specifically discussed results from LCS pipe cleaning at the landfill. Methods discussed included: 1) high pressure water jetting; 2) cutters and milling machines; and 3) chemical treatment. To compare the effectiveness and cost of the cleaning technologies, high pressure water jetting and chemical cleaning were used at the landfill, and the results of the two cleaning methods were compared. Mayer (2014) found that both high pressure water jetting and chemical cleaning removed clog material from the LCS pipes. One difficulty encountered with high pressure water jetting was that large pieces of clog material dislodged during the cleaning would build up at points where sharp turns in the LCS pipe were encountered (e.g., where lateral pipes intersect with header pipes); so, labor-intensive, continuous dislodging and removal of large pieces of clog material at these points was necessary. This resulted in a slow, staged cleaning approach that increased the time and cost. This method also required access points for removal of larger dislodged clog material. Mayer (2014) concluded that high pressure water jetting was best suited for routine annual maintenance of long segments of perforated pipe. Chemical cleaning was also found to be successful in removing most of the clog material in the LCS pipes including the solid walled pipes (headers and pipes from internal sumps to external manholes) without some of the difficulties associated with dislodging of large pieces of clog material as experienced with high pressure jetting. It was determined that 1,500 linear feet per week of pipe could be cleaned with high pressure water jetting at a cost of \$10 to \$60 per foot of pipe (Mayer 2014). Mayer (2014) also found that 2,000 feet per week of pipe could be cleaned with chemicals at a cost of \$20 to \$40 per foot of pipe (Mayer, 2014). Following this demonstration work, a broader scope cleaning project was implemented at the landfill using the chemical cleaning technology that resulted in the removal of clog material from more than 10,000 feet of perforated laterals, 4,000 feet of perforated headers, and 4,000 feet of gravity mains.

The chemical cleaning technology consisted of a combination of surging, recirculation, and foaming of a proprietary acid solution consisting of hydrochloric acid, carboxylic acid, alkanolamine, and sodium alkyl sulfonate that also contained proprietary catalysts, dispersants, and inhibitors to protect the components of the LCS susceptible to acid attack. In single access LCS piping with perforations, the surging method employed was shown to be effective from 100 to 150 feet. In these instances, a high-pressure water jet was used to carry an acid delivery hose to the end of the lateral. Gravity carried the acid back to the internal landfill sump and then to the manhole outside the cell. The acid was collected at the manhole and recirculated using a pump. Finally, Mayer (2014) suggested that stagnant leachate and minimal leachate flows are correlated to clog formation, empirically.

The facility also implemented two preventative measures in 2014: 1) addition of groundwater directly into the gravity collection line to dilute the leachate and to facilitate higher active flow rates in the LCS, and 2) an electronic scale control (ESC) unit was installed upstream at manhole 11 on the west side of the LCS. The combined effect of these two measures seemed to effectively reduce downstream clogging impacts.

The ESC unit produces a pulsing current to create time-varying magnetic fields inside the pipe, which induces an electric field described by Faraday's law (equation 13)

$$\int E ds = - \frac{d}{dt} \int B dA \quad (13)$$

where E = induced electric field vector; s = line vector along the circumferential direction; B = magnetic field strength vector; and A = cross-sectional area of pipe. The induced electric field oscillates with time and provides the necessary molecular agitation such that calcium and bicarbonate ions collide and precipitate but get flushed downstream. Once dissolved ions are converted to insoluble mineral crystals, the level of supersaturation of the water decreases; thus, new scale deposits on the pipe surface are reduced or prevented (Cho et al. 1997; Fan 1997; Cho and Choi 1999; Kim 2001; Cho et al. 2005; Xiaokai 2008; Tijing 2011). Shaha et al. (2019) studied the measurable effect of ESC on the leachate water quality or the composition of the solid scale generated in the pipes. There were no observable differences in water quality parameters as well as in the precipitate composition between electronically treated and untreated leachate at this urban landfill site.

## 2 METHODOLOGY

### 2.1 Site Description and LCS Clogging

The Solid Waste Authority of Palm Beach County (SWA) manages a variety of solid waste disposal units including two Waste-to-Energy Plants (WTE-1 and WTE-2), a Class III (construction and demolition waste) landfill, a partially closed landfill facility (Dyer Park), and a Class I landfill on property it owns in Palm Beach County, Florida. The waste disposed of to the landfill includes municipal solid waste (MSW), a mixture of bottom ash and fly ash from the two waste-to-energy plants on the property adjacent to the Class 1 landfill, and inert waste and reject waste from processing of the refuse derived fuel from WTE-1. **Figure 4** provides an aerial view of the locations of the major SWA facilities considered and discussed in this study. The Class I landfill was permitted in 1989 and began accepting waste in December of that year. More than 13,500,000 tons of waste have been disposed in the subsequent 26 years.



**Figure 4. Aerial photograph of the SWA site (adapted from Google Earth)**

From 1989 to 1996, only MSW was disposed at the landfill. In 1997, SWA began operating a refuse-derived fuel (RDF) waste-to-energy plant (WTE-1) on property they own adjacent to the landfill. Waste disposed at the landfill after the WTE-1 plant came on-line (1989) was a mixture of: 1) MSW that by-passed the WTE-1 plant; 2) unprocessable waste (items removed from the WTE tipping floor); 3) process residue (“unders” removed from the RDF processing stream; and 4) mixed bottom and fly ash from the combustion of the MSW delivered to the plant. Except for a period of refurbishment, the WTE-1 plant has typically received more than 800,000 tons of MSW each year since 1997 (SWA, 2012). It currently processes in excess of 850,000 tons of MSW per year (tpy) (Palm Beach Renewable Energy Facility-1 2016). SWA began operating a new 1,000,000 tpy mass burn MSW incinerator (WTE-2) on property adjacent to the landfill in mid-

2015. MSW presently being delivered directly to the landfill for disposal is now incinerated at WTE-2, and the resultant ash is delivered to the landfill for disposal.

The Class I landfill (**Figure 5**) in 2019 was roughly rectangular in shape (4,475 ft in length and 1,550 ft in width) and included 16 cells each approximately 10 acres in area.

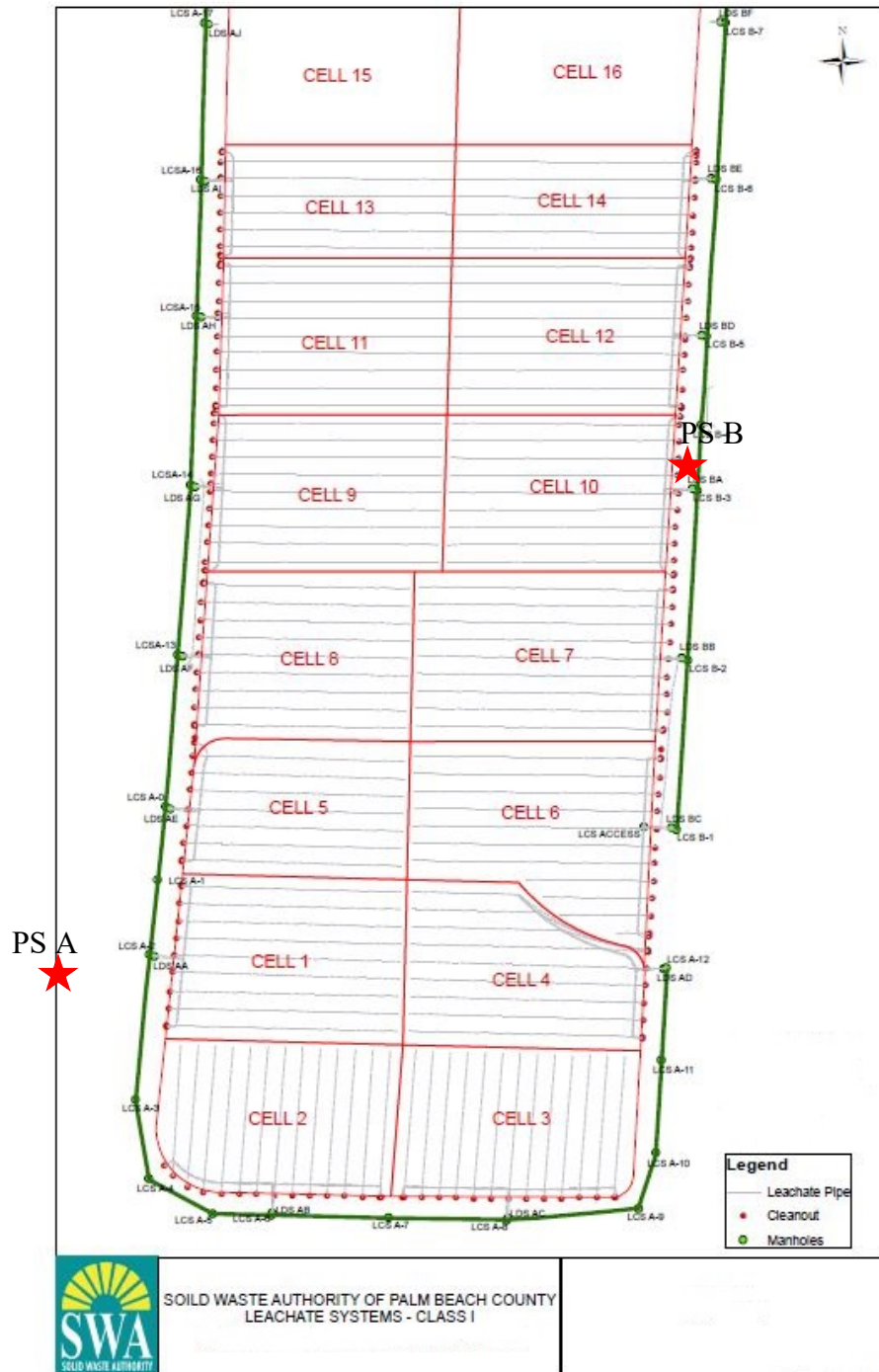


**Figure 5. A schematic of SWA Palm Beach County landfill cells and leachate collection system as of 2013**

**Table 2** presents the age of each cell and the current status of waste acceptance. Based on CDM Smith (2015), the first 10 cells (Cell 1-10) were filled to the permitted limit and were capped and closed. The SWA took initiative to estimate the airspace remaining based on a 3:1 build-out side slope in 2017 and reopened cell 5 and cell 6 in January 2017. They continued to open and fill the remaining airspace for Cells 7 to 10 that were filled and capped previously. The four active cells (Cell 11-14) are receiving waste on a day-to-day basis and have either a 6-inch daily cover or a 12-inch interim soil cover. Cells 15 and 16 are newly constructed, Cell 15 began receiving waste in September, 2018 and Cell 16 is yet to receive any waste as of the date of this report.

**Table 2. Date of first waste disposal and status of each landfill cell**

Cell No.	First Waste Disposal	Years to Date (2020)	Status
1	07/1989	30.6	Closed
2	12/1989	30.2	Closed
3	01/1991	29.1	Closed
4	02/1992	28.0	Closed
5	10/1993	26.3	Reopened in January, 2017
6	09/1996	23.4	Reopened in January, 2017
7	08/1998	21.5	Reopened between January, 2017 and December 2019
8	04/1998	21.8	Reopened between January, 2017 and December 2019
9	01/2006	14.1	Reopened between January, 2017 and December 2019
10	01/2006	14.1	Reopened between January, 2017 and December 2019
11	04/2010	13.8	Active
12	12/2008	11.2	Active
13	11/2009	10.3	Active
14	02/2013	7.0	Active
15	09/2018	1.4	Active

A perimeter berm surrounds the constructed landfill cells and forms the outer edge of the class I landfill. Small isolation berms separate each cell; however, liner systems in adjacent cells are connected. While the liner between cells is continuous, the leachate collection system (LCS) in each cell is independent and separated by the isolation berm as well as by the landfill bottom grades, which isolate leachate within each cell by elevation and gravity. The cells are constructed in a sawtooth design with a high point that runs along a center ridge running north-south along the length of the landfill. This ridge divides the width of the landfill in two, with respect to the long axis. Leachate flows from this high middle ridge to either the east or west side collection sumps located at the foot of the perimeter berm. The landfill liner slopes from the center ridge to the perimeter sumps at a minimum of 0.5%. A cross-section of the liner is shown in **Figure 6**.

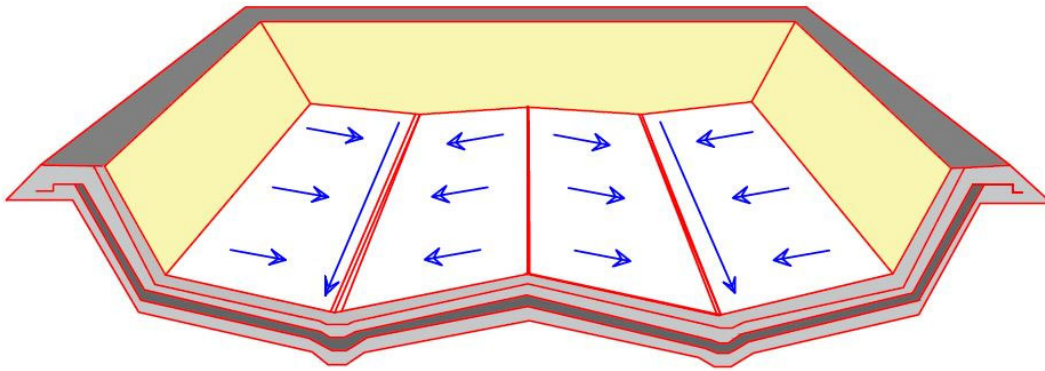


**Figure 6. Landfill liner and leachate collection system design schematic (adapted from Shaha 2016)**

Leachate collected in the sump flows by gravity through a “stub line” and discharges in a manhole located in the perimeter road. Each landfill cell has its own manhole. The manholes for the cells on the east side of the landfill are connected, and leachate flows by gravity from one manhole to the next until it reaches the nearest pump station (Pump Station B). The manholes for the cells along the south and west sides of the landfill are also connected and flow to a separate pump station (Pump Station A). From the two pump stations, the collected leachate is pumped into a force main around the landfill perimeter to a deep injection well (Deep Well), where the combined leachate is disposed approximately 3,000 feet beneath ground surface. Liquid from the secondary collection system (leak detection system) is captured in separate sumps within the cells and pumped through a flow meter to the manholes, where it mixes with the collected primary leachate. **Figure 7** shows the general location of gravity leachate lines and leachate pump stations.

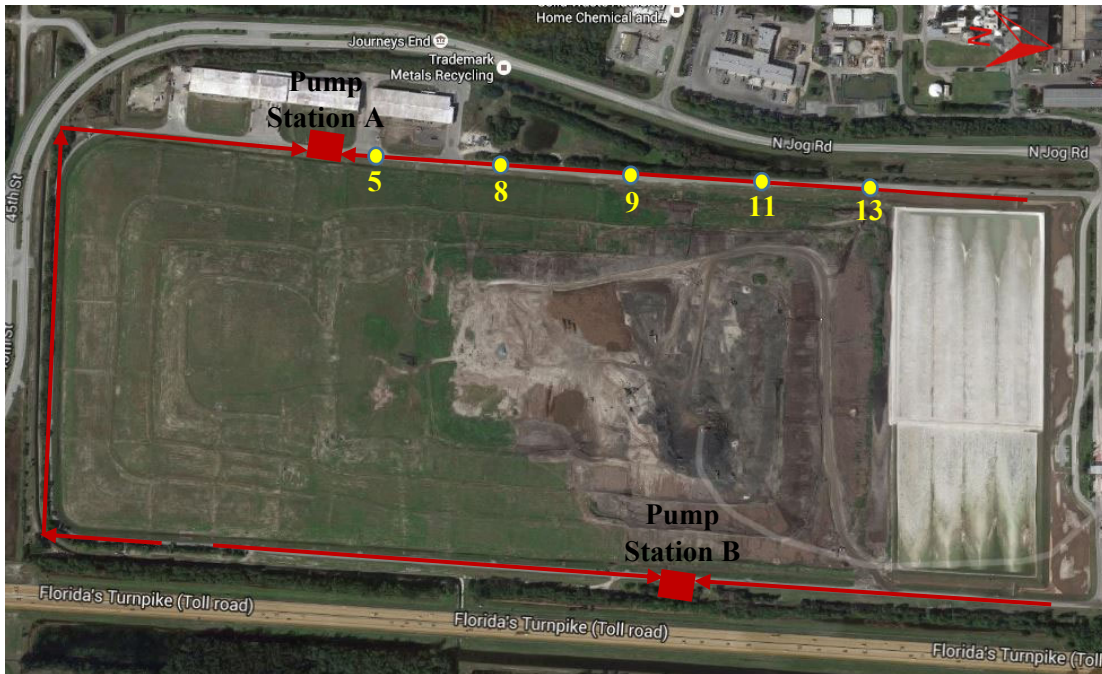


**Figure 7. Schematic of gravity leachate collection line and pump station locations (yellow circles represent manholes, and the leachate flows in the direction of the arrows shown)**

In 1999, the Solid Waste Authority (SWA) of Palm Beach County, Florida became aware of clogging of some of the LCS pipes in disposal cells within the landfill and in a leachate forcemain that conveys collected leachate to disposal in an on-site deep well. Clean-out lines associated with the LCS pipes are designed to allow access to the pipes. SWA has periodically inspected and cleaned these pipes since discovering the clogging issue. In addition, redundant LCS components (drainage layer sand, liner slopes, and rock drainage media around leachate pipes) have allowed SWA to continually remove collected leachate from the landfill. The clogged portion of the landfill perimeter forcemain was removed in 1999.

In 2000, SWA embarked on a study (Maliva 2000) to better understand the cause of the clogging and to identify suggested treatment methods, operational changes, or design modifications that would mitigate the impact of the clogging. This work provided some insight into the clogging mechanism and treatment, design, and maintenance approaches. Between 2000 and 2012 there were several studies (Maliva 2000; Levine 2005; Mullah-Saleh 2006; Mullah-Saleh 2007) conducted to understand the LCS clogging mechanism. They found that calcite is the predominant species and results from either chemical, biological, or the combination of both processes.

In 2012, SWA entered into a contract with the Hinkley Center for Solid Waste Management to conduct critical examinations of LCS clogging at SWA disposal facilities. Researchers from University of Florida (UF) and Florida Atlantic University (FAU) were actively involved in this project. In 2013, a major clogging issue was discovered in the gravity line between manholes (MH)

8 and 9. In 2014, SWA implemented the addition of groundwater dilution in the gravity lines (at MH 11) to reduce the clogging effect based upon the recommendation from the FAU researchers. In addition to that, SWA also introduced an electronic scale control device (FlowMark) in MH 11. These measures provided SWA with positive results but did not completely solve the issue of LCS clogging.

## 2.2 Experimental Setup

### 2.2.1 Field Scale Experiment Model

**Figure 8** provides a schematic of the closed loop leachate pipe network that was used for this study.

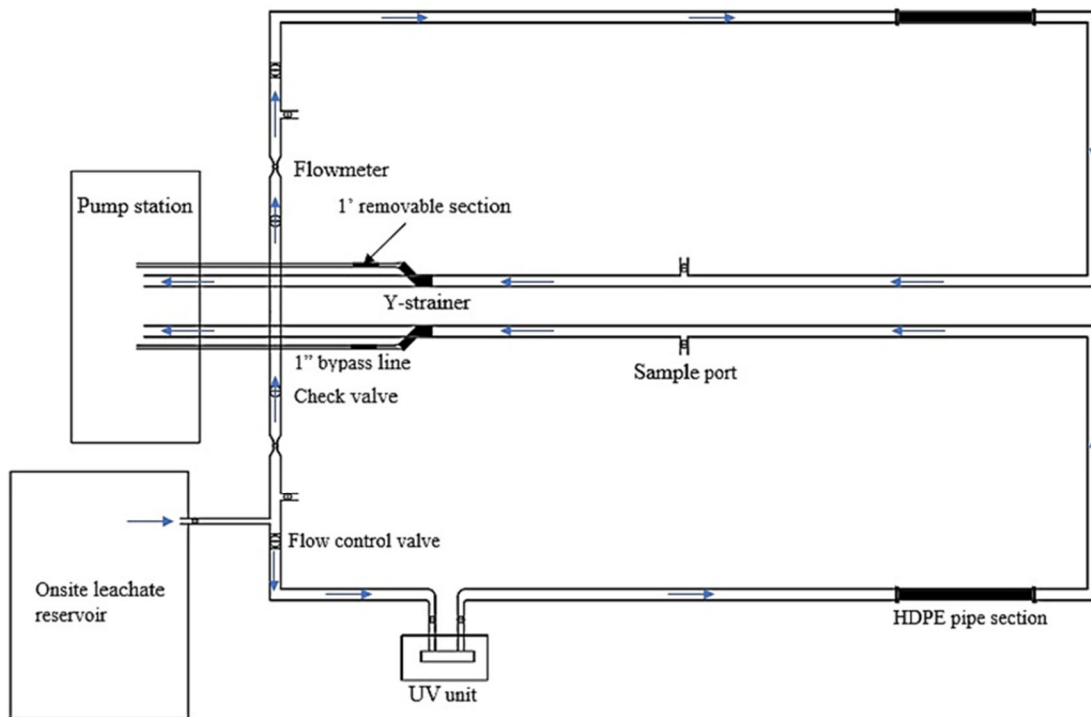


**Figure 8. Schematic layout of onsite side-by-side pipe network**

This pipe network photographed in **Figure 9** was initially developed between 2015 and 2016 to validate the effectiveness of an electronic scale control system (ESC) (Shaha et al. 2019, Shaha 2016) and utilized in this study with necessary modification. This 12.2 m × 6.1 m network was built with 150 mm PVC pipe and included two 1.8-meter long, 150 mm removable HDPE pipe sections introduced to replicate actual LCS pipe material and collect any solid precipitates. The network was divided into one ultraviolet (UV) treated or disinfected loop and another identical untreated control loop. Each loop has a 150 mm check valve to prevent backflow, a 25 mm flowmeter, two 50 mm sample ports, a 150 mm flow control valve to balance the flows, and a 150 mm Y-strainer (mesh size: 0.8 mm) to capture precipitates.



**Figure 9. Field scale side-by-side pipe network with UV unit**

**Figure 10** shows the satellite view of the study location, pipe network, and the global positioning system (GPS) location of pump station A.



**Figure 10. Satellite view of the pipe network and GPS location (26.764398, -80.139975) of pump station A**

The influent was supplied in the pipe network (gravity flow) using a 50 mm pipe from an onsite 900-gallon leachate reservoir (**Figure 11: left**). A submerged pump filled the reservoir prior to beginning the test from pump station A. The ultraviolet (UV) light disinfection unit to quantify the impacts of microbial activity on clogging was retrofitted to the existing pipe network (**Figure 11: middle**). Based on literature review (Chevrefils et al 2006, Malayeri 2016) and the average flow rate through the pipe network, Viqua Model PRO 10 Ultraviolet System (**Figure 12**) with UV intensity monitor (**Figure 11: right**) was installed in the pipe network to disinfect leachate in one loop; whereas the other loop remained untreated (control). This unit is capable of transmitting 40 mJ/cm<sup>2</sup> fluence at 10 gallons per minute (gpm) flow with a chamber size of 22" x 4". This unit complies with NSF/ANSI/CAN 60: *Drinking Water Treatment Chemicals – Health Effects*. The pipe network flow measured during previous experiments was on the order of 10 gpm for each side (Schert et al. 2015).



**Figure 11. Reservoir (left), UV unit retrofitting (middle), and UV unit (right)**



## PRO 10

**Figure 12.** UV unit obtained for the field experiment (<https://www.pelicanwater.com/viqua-pro-uv.php>)

In addition to the previously described modifications, one 25 mm (1 inch) bypass line with 0.3 m (1 ft) long removal section was retrofitted at the y-strainer from each side of the network (**Figure 13**). One 25 mm (1-inch) PVC inline true union ball valve was installed on each side before the removable section to control the flow rate through the section. These sections were installed to periodically investigate the precipitation in them and to quantify the physical and chemical differences.



**Figure 13. 25 mm (1") bypass line with 0.3 m (1 ft) long removable pieces retrofitted from the newly installed Y-strainers on both sides**

Prior to each experiment, 1) all upstream prevention measures (e.g. dilution with ground water and any chemical addition activities) were suspended for at least 3 days prior to the experiment date, 2) the onsite reservoir was filled with 700-800 gallons of leachate on the experiment date, 3) all field equipment including YSI 556 MPS were calibrated per manufacturer's specifications, and 4) the initial weight of each 25 mm dia 1-ft long pipe sections from both sides were measured.

After these checks were performed, leachate influent was allowed to flow through the loop system. Volumetric flow measurements showed that about 430 - 470 cm<sup>3</sup>/s (6.9-7.4 gpm) of leachate flows through each side and about 100 cm<sup>3</sup>/s (1.6 gpm) flows through the 25 mm (1-inch) bypass line. At least 10 minutes was allowed to prime the network and to wash away any remaining liquid and settled solids from any previous test. The duration of each test varied between 90 minutes and 150 minutes and a subsequent stagnation period, in which the pipe network was kept full with leachate, was maintained for up to two weeks to inspect scale formation periodically.

Samples were collected at 0, 15, 30, 90, and 120 minutes from both the UV treated side and control side. An YSI 556 MPS was used for field data collection, and samples were stored in at 4°C and transferred to the Lab.EES facilities in Boca Raton, FL for heterotrophic plate count (HPC) testing.

## 2.2.2 *Laboratory Setup*

### 2.2.2.1 Cyclone Separator

A laboratory scale cyclone separator was built (**Figure 14**) with 100 mm (4-inch) PVC pipe and reduced to a 12.5 mm (½-inch) outlet in three steps: 100 mm to 50 mm, 50 mm to 37.5 mm, 37.5 mm to 6.3 mm (4-inch to 2-inch, 2-inch to 1 ½-inch, and 1 ½-inch to ½ inch) to form the cone section for solid accumulation, thickening and subsequent removal.

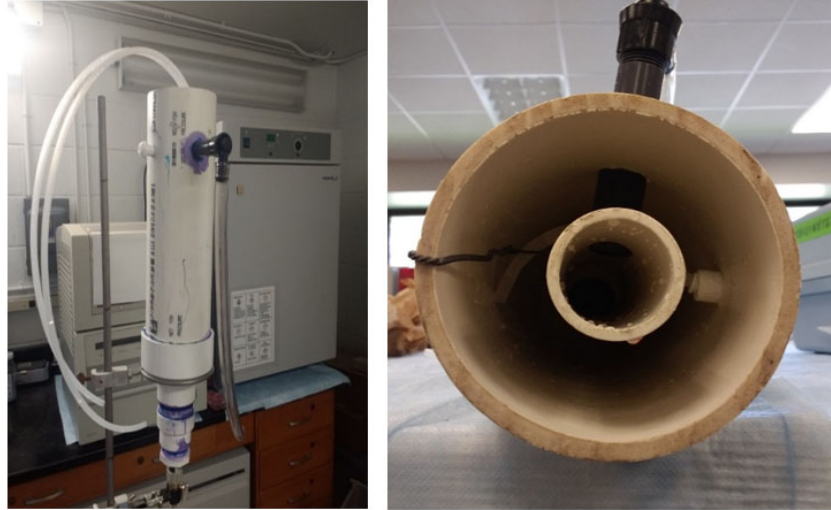


**Figure 14. Laboratory scale cyclone separator, front view (left), cross sectional view (right)**

The measured capacity of the unit was 2.8 liters (0.74 gallons). The inlet is 6.3 mm ( $\frac{1}{4}$  inch) dia and the outlet is 12.5 mm ( $\frac{1}{2}$  inch) dia. Pump flow rate was determined using volumetric flow measurements with a graduated cylinder and stopwatch and found to be 1.7 liters per minute (lpm) (0.45 gpm). The first test was conducted on April 24, 2018 with 4 liters (1.1 gallons) of NEFCO biosolids processing wastewater. The objective was to determine the performance of the unit in reducing turbidity as well as TSS. Samples were collected at 5 min intervals for 15 minutes. Turbidity was measured using a calibrated HACH turbidimeter, and TSS was measured using the standard gravimetric solid analysis method.

#### 2.2.2.2 Leachate Disinfection

UV disinfection: A laboratory scale UV source with  $2.1 \text{ mJ/cm}^2\cdot\text{s}$  fluence (**Figure 15**) was used to conduct preliminary disinfection experiments of leachate. A volume of 100 mL leachate sample in transparent quartz test tubes were exposed to UV radiation at three different distances (3.55 cm, 7.65 cm, and 12.5 cm) from the source in a closed photochemical safety cabinet for 30 minutes. Immediately upon conclusion of ultraviolet exposure, a heterotrophic plate count (HPC) test was conducted to quantify the log reduction of microbes. An untreated leachate sample was used as control and 3 samples were irradiated at each distance to replicate the outcome.



**Figure 15. Photocatalytic Safety Cabinet used to disinfect leachate in the laboratory**

Heat Sterilization: The following steps were followed during the experiment to accomplish heat sterilization of leachate:

- Two 800 mL samples were prepared in 1L glass beakers
- Hardness, alkalinity, COD, TDS, and TSS were measured initially
- One beaker was heat sterilized for 15 min at 100°C (boiling point), while the other sample was kept as the control
- The sterilized sample was cooled to room temperature, and then analyzed for the water quality constituents previously measured
- Three 200 mL samples from each 1L sample were taken and kept in an incubator for 7 days at 35°C to accelerate precipitation
- Measured final water quality parameters, precipitate weight (floating, attached to the surface), and sample volume were measured at the end of the time period

#### 2.2.2.3 pH Adjustment Setup

A laboratory experimental setup (**Figure 16**) was designed based on preliminary studies (Shaha 2016), in which it was observed that the pH increases by almost 1 unit within one hour with simple exposure to atmosphere.



**Figure 16. Laboratory setup for pH adjustment with N<sub>2</sub>, CO<sub>2</sub>, and Air**

Three different mixtures of gas cylinders (CO<sub>2</sub>, N<sub>2</sub>, and synthetic LFG) were obtained from Geotech Environmental Equipment, Inc., Denver, CO. Calibration gas concentrations are summarized in **Table 3**.

**Table 3. Calibration gas concentration details**

<b>Gas Cylinder</b>	<b>Components, % by volume</b>	<b>Cylinder volume</b>	<b>Regulator</b>
<b>Carbon dioxide, CO<sub>2</sub></b>	CO <sub>2</sub> : 0.01-49.99%	103L	2 lpm
<b>Synthetic LFG</b>	CO <sub>2</sub> : 15.0% CH <sub>4</sub> : 15.0% N <sub>2</sub> : Balance	600L	0-3.5 lpm
<b>Nitrogen, N<sub>2</sub></b>	N <sub>2</sub> : 99.99%	103L, 600L	2 lpm, 0-3.5 lpm

For each gas, an appropriate gas regulator was connected to the cylinder, and the other end was connected with laboratory tubing to facilitate the gas flow into the leachate stored in a transparent plastic two-liter bottle reaction chamber. At the end of the tubing, a bubbling stone was attached using silicone gel to achieve uniform distribution of gas bubbles. A gas release valve attached with tubing was mounted in the bottle cap to remove the excess gas from the mixture. A sampling port with stop valve was connected to the plastic bottle to collect samples during the experiments. A leachate sample volume between 500 mL and 1000 mL was used. In the initial experiments with the fixed regulator, the gas flow rates were constant at 2 lpm. However, after obtaining a variable

rate regulator (0-3.5 lpm) (**Figure 17**) along with 600 L gas cylinder, the gas flow rates varied within the range. The duration of each exposure test varied between 30 minutes and 180 minutes. Leachate water quality parameters (pH, temperature, conductivity, specific conductance, and TDS) were recorded using an YSI 556 MPS. Samples were collected and analyzed for alkalinity and calcium with 5-10 minutes interval following standard methods.



**Figure 17. Variable rate (0-3.5 lpm) gas regulator for 600 L gas cylinder**

In case of air, an aquarium air pump (120 volts AC, 60Hz, 1.5 Volts, 1.0 psi) was used to supply the gas into the 500 mL leachate in an 1L glass beaker, and the water quality parameters were continuously monitored using YSI MPS 556. In some instances, a 1-L beaker was also used for all other gases (**Figure 18**) so that the YSI meter can record continuous data with 1-minute interval during the test period.

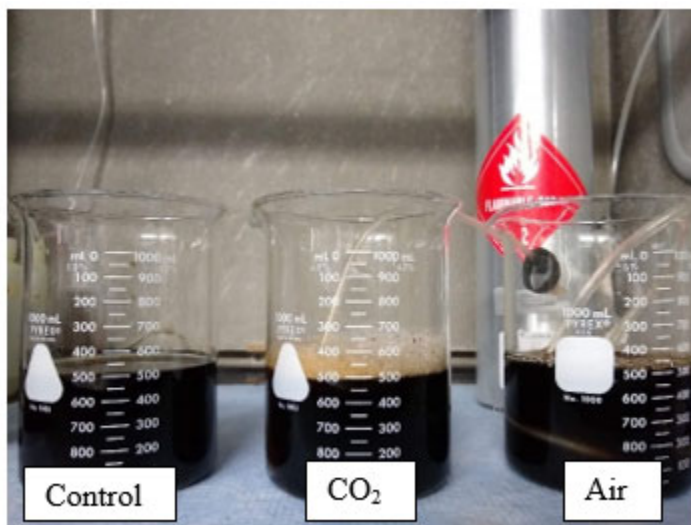


**Figure 18. Addition of CO<sub>2</sub> and Air into the leachate**

### 2.3 Leachate Collection

Guidance regarding sample collection was obtained from:

- Standard Methods 1060 Collection and Preservation of Samples;
- Surface Water Sampling Operating Procedures, USEPA, Region 4, Science and Ecosystem Support Division, Athens, Georgia; and,
- Groundwater Sampling Operating Procedures, USEPA, Region 4, Science and Ecosystem Support Division, Athens, Georgia.

Unless otherwise noted, grab samples were taken from the various sample points in clean, labeled polyethylene (or equivalent) containers. Temperature, specific conductance, pH, and dissolved oxygen (DO) were determined in the field typically within minutes of sample collection using a YSI 550MPS. Analyses not performed in the field were preserved as indicated in **Table 4**.

**Table 4. Summary of sampling parameters**

<b>Parameter</b>	<b>Preservation</b>	<b>Storage</b>	<b>Sample Type</b>
<b>pH</b>	Analyze immediately	Two hours	Grab
<b>Alkalinity</b>	Refrigerate/Analyze immediately	24 hours	Grab
<b>Total Solids</b>	Refrigerate	7 days	Grab
<b>Total Dissolved Solids</b>	Refrigerate	7 days	Grab
<b>Calcium</b>	Refrigerate/Analyze immediately	6 months	Grab
<b>Electrical Conductivity</b>	Refrigerate/Analyze immediately	28 days	Grab

The different types of grab sampling utilized at the landfill were collected at the locations shown in **Figure 19**.



**Figure 19. Selected sampling locations at SWA Class I landfill**

- Samples of composite leachates from Pump Station A were taken from the sampling ports of the pipe network developed for previous experiments (Shaha 2016). Leachate was collected in a 2-gallon bucket and was transferred to clean, labeled polyethylene sample bottles and securely capped and placed in coolers at 4°C if not analyzed immediately in the field.
- Samples from leachate pumped into manholes were collected with clean plastic buckets (2-gallon) attached to lines lowered to a point beneath the discharge pipe in the manhole

(Figure 20). Collected leachate was then poured into clean, labeled polyethylene sample bottles, stored in ice at 4°C and transported to the FAU laboratory for analysis.



Figure 20. Sampling procedure from the manholes

#### 2.4 Analytical Methods for Parameters of Interests

Alkalinity, dissolved calcium, and total calcium were tested immediately after collecting samples in the field using standard titration methods (Water Environment Federation & American Public Health Association 2017). Gravimetric solids tests were completed within a week in the lab at FAU (Table 5) shows the water quality test method and calibration procedure used in the study.

Table 5. Summary of water quality analysis method and calibration of instruments

Parameters	Method	Device	Calibration	Detection limit	Dilution ranges
<b>pH</b>	SM4500-H <sup>+</sup> B, Electrometric Method	YSI556 Multi-parameter System (MPS)	Calibrated with standard pH buffers of 4, 7, and 10	0-14 (0.001pH)	N/A
<b>Temperature</b>	SM2550B and field sampling procedures outlined in DEP-SOP-001/01 FT 1400	YSI556 MPS or HACH Hq40d. handheld thermal infrared thermometer (Ryobi IR001)	Manufacturer's calibration	Nearest 0.1 or 1°C	N/A
<b>Conductivity</b>	SM2510B	YSI 556 Multi-parameter System (MPS)	Calibrated using 100 mS/cm standard solution	0.1 and 1%	N/A
<b>Calcium hardness</b>	Hach Method 8204 (EPA approved, equivalent of SM3500-Ca B or D)	Hach digital titrator (EDTA titration method)	Manufacturer's calibration	10-4,000 mg/L as CaCO <sub>3</sub>	1:100

Parameters	Method	Device	Calibration	Detection limit	Dilution ranges
<b>Alkalinity</b>	Hach Method 8203 (EPA approved, equivalent of SM2320 B)	Hach digital titrator (H <sub>2</sub> SO <sub>4</sub> titration method)	Manufacturer's calibration	10-4,000 mg/L as CaCO <sub>3</sub>	1:100
<b>Solids</b>	TDS: SM2540C/EPA Method 160.2; TSS: SM2540D/EPA Method 106.4; VSS: SM2540E/EPA Method 106.4	Glass-microfiber filter disk (934-AHTM, 47 mm diameter);	N/A	N/A	Volume: 60 to 100 mL sample
<b>Sulfide</b>	USEPA methylene blue method (method 8131) equivalent to SM4500-S2-D	Hach DR5000 UV/V spectrophotometer	Manufacturer's calibration	5 to 800 µg/L S <sup>2-</sup>	1:1 to 1:100
<b>Sulfate</b>	SulfaVer 4 method equivalent to SM10248	Hach DR5000 UV/V spectrophotometer	Manufacturer's calibration	2 to 70, 20 to 700, 200 to 7,000 mg/L SO <sub>4</sub> <sup>2-</sup>	1:1 to 1:100

\*N/A- not applicable

#### 2.4.1 *pH*

The pH of leachate samples was measured using SM4500-H<sup>+</sup> B. Electrometric Method using a YSI556 Multi-Parameter System (MPS) or a Hach (Model Hq40d portable meter) (**Figure 21**). Field sampling procedures followed DEP-SOP-001/01 FT 1100 Field Measurement of Hydrogen Ion Activity (pH). Probes were calibrated periodically with standard pH buffers (4, 7, and 10). Sensors were rinsed with deionized water and dried with kim wipes in between sample readings.



**Figure 21. pH measuring meters (YSI 556 MPS, left; Model Hq40d meter, right)**

#### **2.4.2 *Temperature***

Water temperature was measured following SM2550B and field sampling procedures outlined in DEP-SOP-001/01 FT 1400 Field Measurement of Temperature. Readings were collected with either the onboard temperature probe of the YSI556 MPS or HACH Hq40d (**Figure 21**). Water surface temperatures were recorded using a handheld thermal infrared thermometer (Ryobi IR001) (**Figure 22**).



**Figure 22. Handheld thermal infrared thermometer (Ryobi IR001)**

### 2.4.3 *Electrical Conductivity and Specific Conductance*

The electrical conductivity (mS/cm) was measured following SM2510B and was recorded during the sample collection using either an YSI 556 MPS or a Hach Hq40d portable meter with conductivity probe or in the field (**Figure 21**). A calibration standard of 100 mS/cm was used to calibrate the probe due to the high amount of TDS expected in leachate samples. YSI 556 displays TDS in g/L as a function of specific conductance. Based on the past 2 year's data this ratio between specific conductance and TDS is found to be 1.54. Thus, the field TDS is obtained by equation 14, as follows:

$$TDS \left( \frac{g}{L} \right) = \frac{\text{Specific conductance} \left( \frac{mS}{cm} \right)}{1.54} \quad (14)$$

### 2.4.4 *Total Calcium*

For the total calcium hardness, Hach Method 8204 (EPA approved, equivalent of SM 3500-Ca B or D) was used. For this analysis, a Hach digital titrator was used (**Figure 23**).



**Figure 23. Hach digital titrator setup for calcium measurement**

A sample volume of 100 mL was selected with a dilution ratio of 100, such that 1 mL of raw sample and 99 mL of deionized water were combined to make a total volume of 100 mL. A Hach digital titrator was loaded with a 0.800 M EDTA titration cartridge for all analyses.

After pouring the sample into a clean 250 mL Erlenmeyer flask, 2 mL of 8 N Potassium Hydroxide Standard Solution was added and swirled to mix. After that, one CalVer® 2 Calcium Indicator Powder Pillow was added, and the flask was swirled to mix with a resulting pink color. The number of digits of EDTA solution required to titrate the sample from pink to blue multiplied by the dilution factor (100) and the digit multiplier (1) from is the Calcium hardness (mg/L as CaCO<sub>3</sub>).

#### 2.4.5 Alkalinity

For the total alkalinity measurements, SM 2320 B titration method (Hach Method 8203, EPA approved, equivalent of SM 2320 B) was used. For this analysis, a Hach digital titrator was used (**Figure 24**).



**Figure 24. Hach digital titrator kit for alkalinity measurement**

A sample volume of 100 mL was selected with a dilution ratio of 100, such that 1 mL of raw sample and 99 mL of deionized water were combined to make a total volume of 100 mL. A Hach digital titrator was loaded with a 1.600 N H<sub>2</sub>SO<sub>4</sub> titrant cartridge for all analyses. After pouring the sample into a clean 250 mL Erlenmeyer flask, one phenolphthalein indicator powder pillow was added to the sample. If the sample turned pink, titrant was added until the phenolphthalein endpoint was reached (pink to clear), if necessary. The reading on the digital titrator was recorded as corresponding to the phenolphthalein alkalinity in mg/L as CaCO<sub>3</sub> by multiplying the dilution factor by the number of digits. No phenolphthalein alkalinity was measured during any of the experiments, meaning that all alkalinity was in the form of bicarbonate ion. Then the Bromcresol Green-Methyl Red indicator was added to the sample, and again titrant was added until the second endpoint was reached (blue-green to light pink). This is the Bromcresol Green Methyl-Red alkalinity. The total digits required to reach the final end point were multiplied by the dilution factor (100) and the digit multiplier of 1 (**Table 6**). This value corresponded to the total alkalinity (phenolphthalein alkalinity plus Bromcresol Green Methyl-Red alkalinity).

**Table 6. Sample volume and digit multipliers for alkalinity titrations (provided by Hach.com)**

Range (mg/L as CaCO <sub>3</sub> )	Sample Volume (mL)	Titration cartridge	Digit multiplier
10-40	100	0.1600 N H <sub>2</sub> SO <sub>4</sub>	0.1
40-160	25	0.1600 N H <sub>2</sub> SO <sub>4</sub>	0.4
100-400	100	1.600 N H <sub>2</sub> SO <sub>4</sub>	1
200-800	50	1.600 N H <sub>2</sub> SO <sub>4</sub>	2
500-2000	20	1.600 N H <sub>2</sub> SO <sub>4</sub>	5
1000-4000	10	1.600 N H <sub>2</sub> SO <sub>4</sub>	10

## 2.5 Bacteriological Analysis

### 2.5.1 Petri Dish (*Heterotrophic Plate Count*)

The heterotrophic plate count (HPC) is a procedure for estimating the number of viable aerobic or facultatively anaerobic bacteria in an environmental sample. There are three different methods for performing HPC test: 1) spread plate, 2) pour plate, and 3) membrane filtration. Spread plate method was used in this study.

The first step is to prepare the R2A media plates. Using a balance, 18.1 gram of agar media was measured onto weigh paper, then transferred to a 1000 mL volumetric flask and dissolved in 1000 mL deionized water. The flask was agitated/shaken until the media was completely dissolved. The solution was then poured into 250 mL autoclavable bottles and sterilized in an autoclave at 121°C for 15 minutes. It is important to note that the bottle caps were kept loose to facilitate pressure release during the sterilization process. After the sterilization was completed, the bottles containing the agar media were taken out, and an appropriate amount of the media was poured into each pre-sterilized petri dish to form a uniform layer. This process was completed in a biosafety cabinet to avoid any contamination. The petri dishes (**Figure 25**) with the media were kept in the biosafety cabinet until they solidified. Next, the petri dishes were capped and stored in the refrigerator for up to several weeks before inoculation.



**Figure 25. Petri dish for use in HPC testing**

The second step of the process was to prepare the appropriate dilution of the sample. HPC values are reported in the term “colony forming units” (CFU) per mL, and plates with counts between 20-300 CFU/mL are the most accurate. Plates with counts more than 300 CFU/mL should be labeled as “TNTC”, which stands for “too numerous to count”. Therefore, a serial dilution (**Figure 26**) was prepared for the leachate samples and only the plates with counts within the allowable range were used.

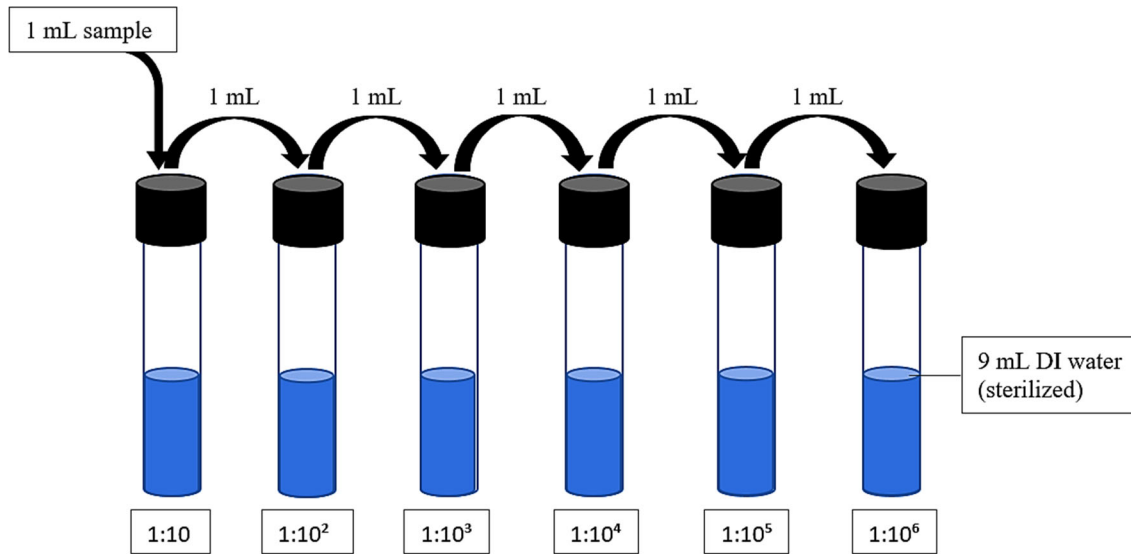


**Figure 26. Serial dilution preparation**

Once the serial dilution was prepared, 0.1 mL of diluted sample from each dilution was transferred to the appropriately labelled petri dish using a P200 pipet. Then, using a tilting motion, the 0.1 mL sample was spread uniformly across the agar surface. Then using a sterile L-spreading tool (**Figure 27**) the liquid was distributed uniformly on the plate.



**Figure 27. L-spreading tool**

Once the plates were inoculated, each plate was labelled and incubated inverted at 35°C for 48 hours in an incubator. After 48 hours of incubation, the plates were taken out, and the colony numbers were counted manually. Plates that counted between 20-300 CFU were used for this study and multiplied by the dilution ratio and reported as CFU/mL of sample.

### 2.5.2 *Microscopic Analysis*

A laboratory microscope (**Figure 28**) with digital camera was used to take zoomed (up to 400x) photographs of microbial colonies as well as the chemical precipitates. These photographs helped to understand the typical microbial colonies found in leachate as well chemical components of the precipitates. The following steps were followed to take microscopic photographs:

- Step 1: Prepare the instruments
  - Switch on the computer with the preinstalled microscopic digital camera program (“LissView”).
  - Connect the microscope power, and connect the USB cable to the computer.
  - Turn on the microscope
  - Double click on the “LissView” program to start the program.
  - Once the program window opens, click on the “Detect camera” button to automatically detect the camera on the microscope (TCA-3.0).
  - At this stage, the microscope, the camera, and the program are ready to take the digital photographs of the sample and store them in the selected drive.
- Step 2: Prepare the microscopic slides to view under microscope
  - Take a very small drop/amount of sample (microbial colony, precipitate, or leachate) using sterile swab or pipette.
  - Smear it for 2 to 3 seconds on the microscopic slide (**Figure 29**).
  - Place a small drop of sterilized deionized water or a drop of oil on the slide.
  - Place a coverslip (**Figure 30**) on top. Remove excess solution around the coverslip with a paper towel or tissue.
- Step 3: View under microscope and take photographs
  - View in the compound microscope at 4× or 10× initially, before moving to higher magnification. Bacteria appear small even at the highest magnification.
  - Once the sample was focused under the microscope and the “LissView” program is running, click on the “start preview” button on the program window (**Figure 31**). This should allow the camera to preview the real-time view of the microscopic view in the computer. Then click on the “take picture” button on the program window and save it to the desired location of the computer.
- Step 4: Postprocessing photographs
  - Compare the photographs with the available known database and identify the components of precipitates / microbial colony.



**Figure 28. Microscope with automatic camera (TCA-3.0) set up**

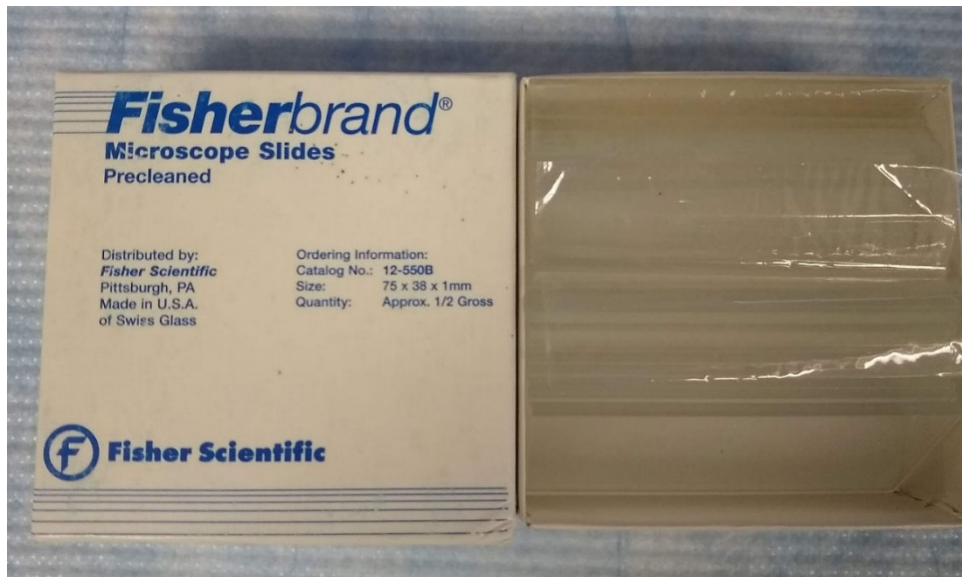


**Figure 29. Microscope slides**



Figure 30. Microscope cover glass

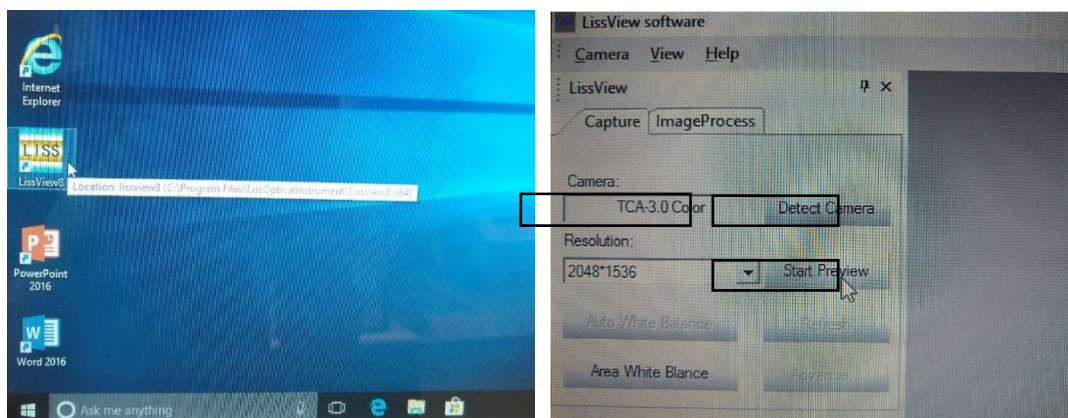
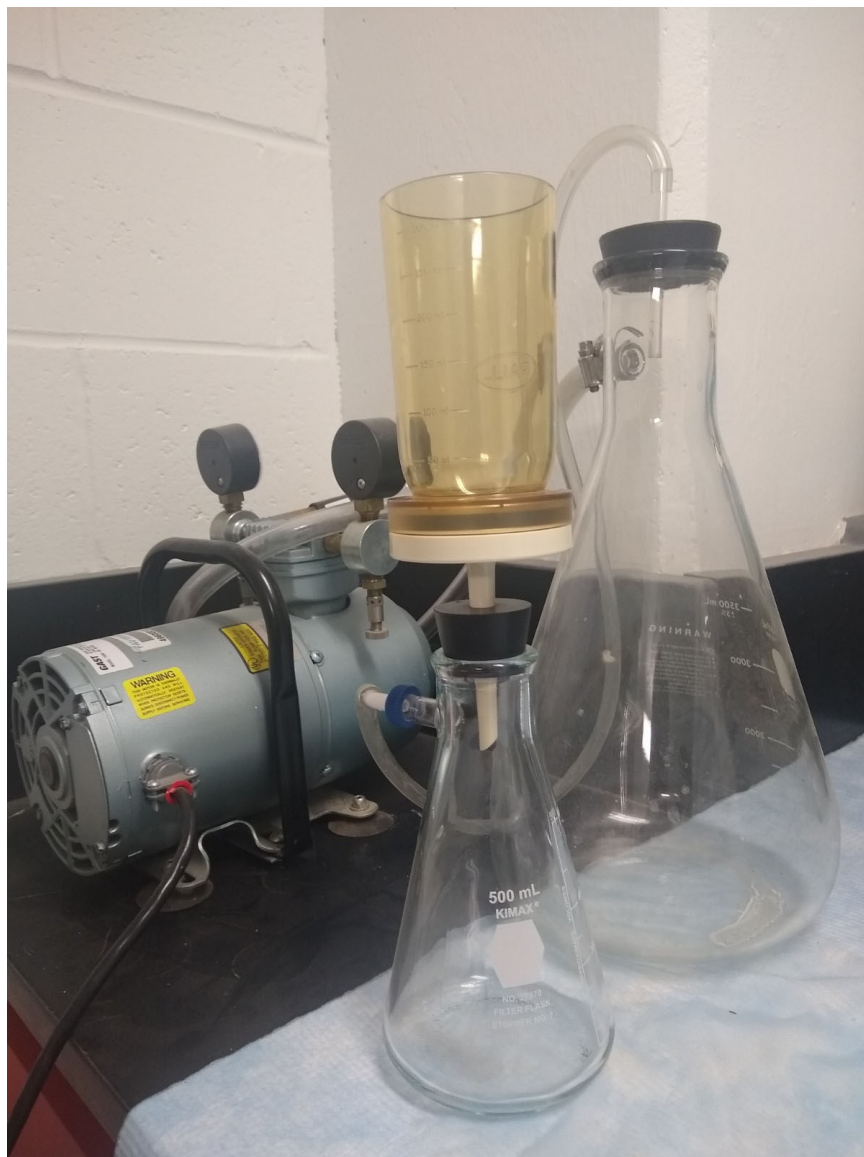


Figure 31. “LissView” program icon on the desktop (a) and the program window, (b)

### 2.5.3 Gravimetric Solids (TDS, TSS, and VSS)

Solid analyses were done using the gravimetric technique using a vacuum filter apparatus (Figure 32). For total dissolved solids (TDS), SM2540C/EPA Method 160.2 was used. For total suspended solids (TSS), SM2540D/EPA Method #106.4 was used, and for volatile suspended solids (VSS),

SM2540E/EPA Method #106.4 was used. Briefly, glass-microfiber filter disk (934-AHTM, 47 mm diameter), aluminum weighing dishes and porcelain evaporating dishes were prepared as described in SM 2540. Glass-microfiber filter disks and aluminum and porcelain dishes were ignited at 550°C for 15 minutes in a muffle furnace prior to use and then stored in a desiccator at room temperature until needed.



**Figure 32. Suction filtration setup for TDS, TSS, and VSS**

For each sample, one aluminum dish, one glass-microfiber filter disk and a porcelain evaporating dish was used to analyze for TDS, TSS and VSS. A sample volume of 60-100 mL was selected for analysis. The first step of the analysis was to pre-weigh the aluminum dishes along with the glass-microfiber filter disk (A1) and the evaporating dish (B1). After that, a well-mixed sample of known volume was filtered using a vacuum filter apparatus and 0.45-micron glass-microfiber filter

disk. After filtration, the filter disk was removed from the magnetic filtration apparatus and transferred to the aluminum dish using metal forceps and placed in a drying oven at 104°C for at least 1 hour, cooled in a desiccator for at least 1 hour, and weighed (A2). To measure the volatile suspended solids, the weighed aluminum dish along with the filter (A2) was further ignited in a muffle furnace for 20 minutes at a temperature of 550°C, cooled in a desiccator for 1 hour and weighed again (A3). Total filtrate with washings was then transferred from the filter flask to a pre-weighed evaporating dish and evaporated to dryness in a drying oven (at 103°C - 105°C for 24 hours) and cooled in a desiccator for at least 1 hour before weighing (B2).

For TDS, the weight difference of evaporating dish B1 and B2 divided by the sample volume and multiplied by 10<sup>6</sup> is the TDS of the sample in mg/L (equation 15).

$$TDS (mg/L) = \frac{(B1 - B2)}{V} \times 10^6 \quad (15)$$

For, TSS, the weight difference of aluminum dish and filter A1 and A2 divided by the sample volume and multiplied by 10<sup>6</sup> is the TSS of the sample in mg/L (equation 16).

$$TSS (mg/L) = \frac{(A1 - A2)}{V} \times 10^6 \quad (16)$$

For, VSS, the weight difference of aluminum dish and filter A2 and A3 divided by the sample volume and multiplied by 10<sup>6</sup> is the VSS of the sample in mg/L (equation 17).

$$VSS (mg/L) = \frac{(A2 - A3)}{V} \times 10^6 \quad (17)$$

Reported single-laboratory analyses of 77 samples of a known TDS of 293 mg/L were made with a standard deviation of differences of 21.20 mg/L. For TSS, the standard deviation was 5.2 mg/L (coefficient of variation 33%) at 15 mg/L, 24 mg/L (10%) at 242 mg/L, and 13 mg/L (0.76%) at 1707 mg/L in studies by two analysts of four sets of 10 determinations each. For VSS, the standard deviation was 11 mg/L at 170 mg/L volatile total solids in studies by three laboratories on four samples and 10 replicates. Bias data on actual samples cannot be obtained.

#### 2.5.4 *Sulfides*

Sulfides were measured using the USEPA methylene blue method (method 8131), which is equivalent to SM4500-S2-D. This is a spectrophotometric method which can measure sulfide concentration ranges between 5 to 800 µg/L S<sup>2-</sup>. A Hach DR5000 UV/Vis spectrophotometer and the recommended 10 mL sample cell (2495402) were used. After starting the spectrophotometer, program 690 Sulfide was selected. A sample cell (**Figure 33-1**) was filled with 10 mL of deionized water and a second cell was filled with 10 mL leachate or a volume of 10 mL diluted leachate

sample. Using a dropper, 0.5 mL of sulfide 1 reagent was added to each cell and swirled to mix (**Figure 33-2**). A second dropper was used to add 0.5 mL sulfide 2 reagent to each cell and swirled to mix again (**Figure 33-3**). A pink color developed initially, and the blue color of the solution indicates the presence of sulfides. After the five minutes of reaction time (**Figure 33-4**) expired, the blank was cleaned and inserted into the cell holder to zero the instrument. Next, the sample cell was cleaned and inserted into the cell holder. After pushing the read function, the results were displayed as  $\mu\text{g/L}$  (**Figure 33-5**). **Figure 33-6** shows the color of the sample before and after the test. Because of the high turbidity and solids of leachate, a dilution ratio of 1, 10, or 100 were used. In case of the diluted samples, the reading displayed in the spectrophotometer was multiplied by the dilution ratio to obtain the actual sulfide concentrations in  $\mu\text{g/L}$ .

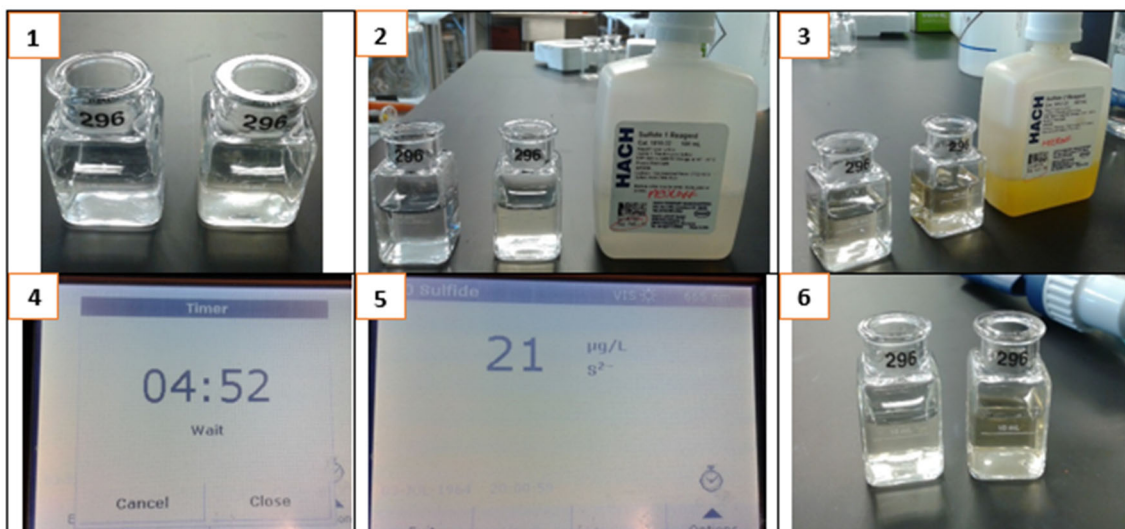


**Figure 33. Sulfide test flow path**

The method performance data (**Table 7**) was derived from laboratory tests that were measured on a spectrophotometer during ideal test conditions.

**Table 7. Sulfide analytical method (Hach Program 690) performance data (Hach DR 5000 methods: Method 8131)**

Standard	Precision (95% confidence interval)	Sensitivity Concentration change per 0.010 Abs change
520 $\mu\text{g/L S}^{2-}$	504 – 536 $\mu\text{g/L S}^{2-}$	5 $\mu\text{g/L S}^{2-}$

### 2.5.5 Sulfates

Sulfate was measured using the Hach SulfaVer 4 method (SM10248), which is a spectrophotometric method that measures sulfate concentration ranges between 2 to 70, 20 to 700, 200 to 7000  $\text{mg/L SO}_4^{2-}$ . A DR5000 UV/Vis spectrophotometer and the recommended 10 mL

sample cell (2495402) were used. After starting the spectrophotometer, program 680 Sulfate was selected. A sample cell was filled with 10 mL leachate or a volume of 10 mL diluted leachate sample (**Figure 34-1**). The blank was inserted in to the cell holder to zero the instrument (**Figure 34-2**). After that, one Sulfaver 4 reagent powder pillow was added and swirled to mix (**Figure 34-3**). The sample cloudiness indicates the presence of sulfate. A reaction time of 5 minutes was selected in the spectrophotometer (**Figure 34-4**). After pushing the read function, the results were displayed as mg/L (**Figure 34-5**). **Figure 34-6** shows the color of the sample after test. Because of the high turbidity and solids of leachate, a dilution ratio of 1, 10, 20, 50, or 100 was used. In case of the diluted samples, the reading displayed in the spectrophotometer were multiplied by the dilution ratio to get the actual sulfate concentrations in mg/L.



**Figure 34. Sulfate test flow path**

Barium interferes at all concentration levels. Calcium only interferes at a concentration more than 20,000 mg/L as CaCO<sub>3</sub>. Chlorides concentration more than 40,000 mg/L as Cl<sup>-</sup> interferes with the results. Also, magnesium more than 10,000 mg/L as CaCO<sub>3</sub>, and more than 500 mg/L of SiO<sub>2</sub> may interfere with the sulfate concentration. The dilution (1:10 to 1:100) made sure that there is no interference from the above contaminants. The method performance data (**Table 8**) was derived from laboratory tests that were measured on a spectrophotometer during ideal test conditions (Hach Method 8051).

**Table 8. Sulfate analytical method (Hach Program 680) performance data (Hach DR 5000 methods: Method 8051)**

Standard	Precision (95% confidence interval)	Sensitivity Concentration change per 0.010 Abs change
40 mg/L SO <sub>4</sub> <sup>2-</sup>	30 – 50 mg/L SO <sub>4</sub> <sup>2-</sup>	0.4 mg/L SO <sub>4</sub> <sup>2-</sup>

## 2.6 Heat Sterilization and Precipitation

Heat sterilization of leachate was achieved using three different methods: 1) boiling at 100°C for 15 minutes under a laboratory hood, 2) boiling in an oven at 150°C for 30 minutes, and 3) autoclaved at 121°C for 30 minutes at 15 lb/in<sup>2</sup> pressure. In case of method 1, a sample volume between 500-800 mL was taken in a 1000 mL glass beaker. A duplicate sample was also prepared with equal sample volume and kept at room temperature as a control. Water quality parameters were measured using a YSI 556 MPS and a small sub-sample of 10 mL was collected for calcium and alkalinity measurement. The sample was then heated using a laboratory heater and magnetic stirrer, and the temperature was monitored continuously until it reached to 100°C. Once, the sample temperature reached to 100°C, a 15-minute timer was started, and the sample was boiled for 15 minutes (**Figure 35**). The sample was then kept at room temperature, and the temperature was monitored periodically until it reached room temperature between 20-25°C. Then a second set of water quality measurements was taken to quantify the difference between control and sterilized sample.



**Figure 35. Leachate sterilization using boiling (left), Sterilized sample and the control kept at room temperature for the duration of the sterilization process (right)**

For sterilization using a laboratory oven, all the steps mentioned above were followed except the sample was put into a laboratory oven (preheated to 150°C) instead of heating using a magnetic stirrer and heater. For the method 3 (autoclave) procedure, 1000 mL sample was poured into an autoclavable bottled with loosely tightened cap. Initial water quality was measured using YSI MPS 556 and standard methods. The sample was then placed into the autoclave, and the preset liquid sterilization function (121°C for 30 minutes) was started. The sample was taken out after 3-4 hours from the autoclave and cooled to ambient temperature. A second set of water quality measurements was performed at ambient temperature.

Once the sterilization process and the sterilized water quality analyses were completed, a set of 100 mL sterilized samples was poured into 250 mL glass beakers. The glass beakers used for this experiment were acid washed to remove any precipitate attached to the surface, rinsed with deionized water, dried in a laboratory oven at 105°C for an hour, and finally cooled in a desiccator. The beakers were numbered and weighed with a laboratory scale and recorded to the nearest 0.001 gram. The beakers with 100 mL samples were then kept in an incubator at 35°C for 7 days to facilitate precipitation. The samples were then taken out from the incubator on day 7, and the leachate was decanted and discarded. Each beaker was dried at 105°C for at least one hour, cooled to room temperature in the desiccator and weighed again to determine the amount of precipitate, by mass.

A similar set of experiments were conducted by comparing the precipitation amount between the samples incubated aerobically and anaerobically. The beakers were closed with aluminum foil to prevent contact with air for anaerobic condition, whereas other beakers were kept open for replicating aerobic conditions.

## 2.7 Test Method for Alternate and Submerge Dry Condition

Based on the field observations, it was hypothesized that the alternating dry and submerged conditions in the leachate collection system enhances the clog formation and by accelerating attachment to the pipe surface. To test this supposition, the following procedure was conducted, as depicted in **Figure 36**:

- Five (5) 100-mL samples were poured into glass beakers and the mass was recorded
- Beakers were placed in incubation at 35°C for 21 days
- Sample mass was measured on days 1, 3, 5, 7, 12, 19, and 21
- Samples were refilled with room temperature leachate to match initial sample weight after each measurement
- Final precipitate mass was measured after decanting any remaining leachate and then drying the beaker and contents at 105°C for one hour

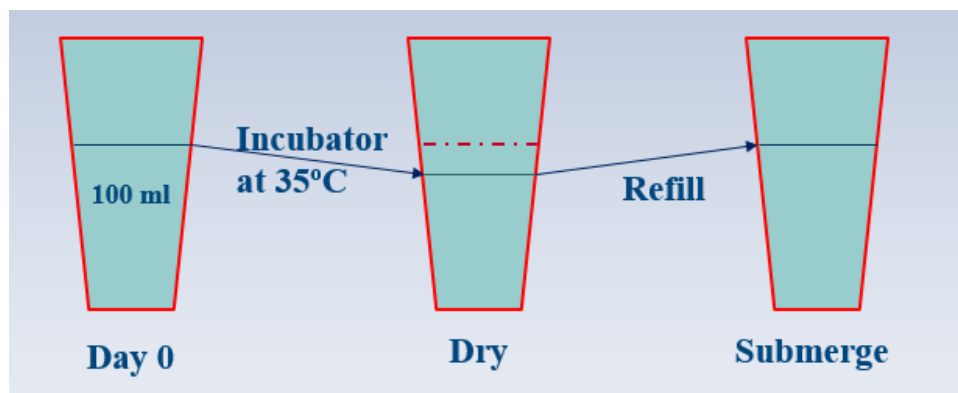


**Figure 36. Test method to test alternate dry and submerge condition**

## 2.8 Saturation Indices

The saturation indices used were Langelier Saturation Index (LSI) and Ryznar Stability Index (RI). LSI is based on the effect of pH on the equilibrium solubility of CaCO<sub>3</sub>. The pH at which water is saturated with CaCO<sub>3</sub> is known as the pH of saturation (pH<sub>s</sub>). The LSI can be defined mathematically by the following equations (Equations 18 & 19):

$$LSI = pH - pH_s \quad (18)$$

$$pH_s = pK_2 - pK_s + p[Ca^{2+}] + p[HCO_3^-] + 5pf_m \quad (19)$$

Where, pK<sub>2</sub> is second dissociation constant for carbonic acid, pK<sub>s</sub> is the solubility product of CaCO<sub>3</sub>, [Ca<sup>2+</sup>] is the calcium ion concentration in g-moles/L, [HCO<sub>3</sub><sup>-</sup>] is the bicarbonate ion concentration in g-moles/L, f<sub>m</sub> is the activity coefficient for monovalent species at the specified temperature, and ‘p’ preceding a variable designates the negative log base 10 (-log<sub>10</sub>) of that variable.

**Table 9** shows the estimated equilibrium constants and activity coefficients required to calculate pH of saturation, and **Table 10** displays the pre-calculated values for pK and A at selected temperatures.

**Table 9. Estimated equilibrium constants and activity coefficients**

Equation	Temperature Range
When complete mineral analysis is available: $I = \frac{1}{2} \sum_{i=1}^i [X_i] Z_i^2$	-
When only conductivity is available: $I = 1.6 \times 10^{-5} C$	-
When only TDS is available: $I = TDS/40,000$	-
$pf_m = A \left[ \frac{\sqrt{I}}{1+\sqrt{I}} - 0.3I \right]$ (valid to I < 0.5)	-
$A = 1.82 \times 10^6 (ET)^{-1.5}$	-
$E = 60,954/(T + 116) - 68.937$	-
$pK_2 = 170.8871 + 0.03252849T - 5151.79/T - 38.92561 \log_{10} T + 563713.9/T^2$	273-373
$pK_w = 4471/T + 0.01706T - 6.0875$	280-338
$pK_{sc} = 171.9065 + 0.077993T - 2839.319/T - 71.595 \log_{10} T$	273-363
$pK_{sa} = 171.9773 + 0.077993T - 2903.293/T - 71.595 \log_{10} T$	273-363
$pK_{sv} = 172.1295 + 0.077993T - 3074.688/T - 71.595 \log_{10} T$	273-363
*I = ionic strength	E = dielectric constant
[X <sub>i</sub> ] = concentration of compound I, g-moles/L	T = temperature, °K (°C+273.2)
Z <sub>i</sub> = charge of species i	K <sub>2</sub> = second dissociation constant for carbonic acid
C = conductivity, μmhos/cm	K <sub>w</sub> = dissociation constant for water
TDS = total dissolved solids, mg/L	K <sub>sc</sub> = solubility product constant for calcite
pY = -log <sub>10</sub> of the value of any factor Y	K <sub>sa</sub> = solubility product constant for aragonite
f <sub>m</sub> = activity coefficient for monovalent species	K <sub>sv</sub> = solubility product constant for vaterite

**Table 10. Precalculated value of pK and A**

Temperature °C	pK <sub>2</sub>	pK <sub>s</sub>			pK <sub>w</sub>	A
		Calcite	Aragonite	Vaterite		
5	10.55	8.39	8.24	7.77	14.73	0.494
10	10.49	8.41	8.26	7.80	14.53	0.498
15	10.43	8.43	8.28	7.84	14.34	0.502
20	10.38	8.45	8.31	7.87	14.16	0.506
25*	10.33	8.48	8.34	7.91	13.99	0.511
30	10.29	8.51	8.37	7.96	13.83	0.515
35	10.25	8.54	8.41	8.00	13.68	0.520
40	10.22	8.58	8.45	8.05	13.53	0.526
45	10.20	8.62	8.49	8.10	13.39	0.531
50	10.17	8.66	8.54	8.16	13.26	0.537
60	10.14	8.76	8.64	8.28	13.02	0.549
70	10.13	8.87	8.75	8.40	-	0.562
80	10.13	8.99	8.88	8.55	-	0.576
90	10.14	9.12	9.02	8.70	-	0.591

Source: Data from [APhA \(1998\)](#).

Note: All values determined from the equations of Table 1, *A* is also used to calculate *pf<sub>m</sub>* (see Table 1).

The water stability characteristics are interpreted as follows:

- If LSI > 0, water is supersaturated and tends to precipitate scale.
- If LSI = 0, water is neutral and is saturated (in equilibrium) with CaCO<sub>3</sub>. In other words, a scale layer of CaCO<sub>3</sub> is neither precipitated nor dissolved. LSI values between -0.4 and +0.4 are considered to be neutral (Prisyazhniuk 2007).
- If LSI < 0, water is undersaturated and tends to dissolve solid CaCO<sub>3</sub> as it is aggressive or corrosive in nature (Ozair 2012).

Ryzner defined a “Stability Index” in 1944 (Ryzner 1944, Montgomery 1985) as follows (Equation 20):

$$RI = 2pH_s - pH \quad (20)$$

Where, pH<sub>s</sub> is Langelier’s saturation pH. RI values between 6.5 and 7.0 are considered to be approximately at saturation equilibrium with CaCO<sub>3</sub>. RI values > 7.0 are interpreted as undersaturated and, therefore, would tend to dissolve any existing solid CaCO<sub>3</sub>. Waters with RI values < 6.5 are saturated and, hence, would tend to be scale-forming (Frederick 1990). However, Muller-Steinhagen and Branch (1988) observed that for higher concentrations of calcium and higher surface temperatures, RI predicts scaling for CaCO<sub>3</sub> concentration well below the saturation concentration and thus should always be checked against LSI.

## 2.9 XRD Analysis with Rietveld Refinement

### 2.9.1 Crystal Analysis Using PXRD/XRF

Precipitate samples collected from the field were prepared for XRD analysis by being dried (Figure 37) under a laboratory hood (24 hours approximately) and powdered using a mortar and pestle (Figure 38) to pulverize the crystals into a fine powder prior to analysis by powder X-ray diffraction/X-ray fluorescence (BTX II Benchtop XRD).

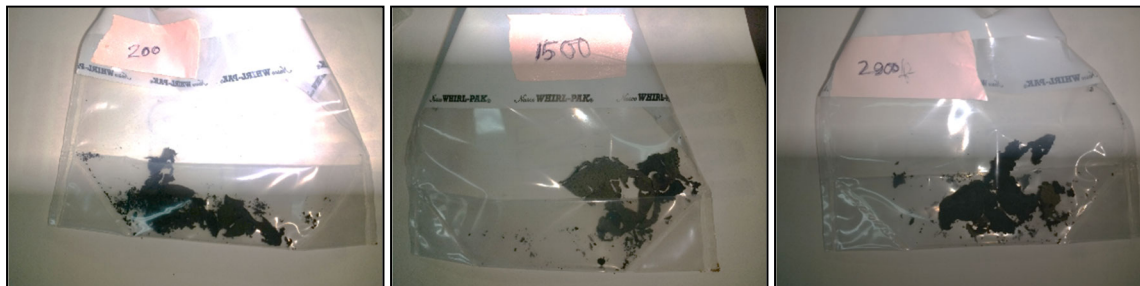


**Figure 37. Samples collected at three different depths (0-200 ft, 200-1500 ft, 1500-2900 ft) for mineralogical analysis**

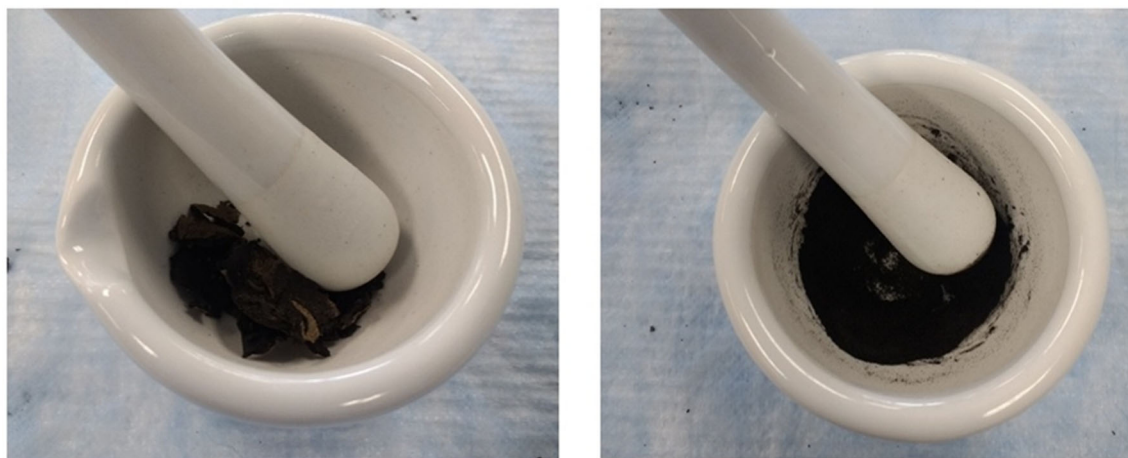


**Figure 38. Sample preparation for XRD analysis in which solids were dried at 105°C overnight (left) and cooled in a desiccator and grinded to powder using a mortar and pestle (right)**

The powder was loaded into a sample holder and analyzed using a BTX 425 Benchtop XRD system located in the organic chemistry lab (Physical science building, room-240). Diffractogram patterns obtained from each sample were then analyzed using a search match program (MATCH! 3.9.0) to identify the composition and quantity of each compound if possible, using FullProf Suite.

Powder X-ray diffraction/X-ray fluorescence requires fine powder of crystal to be analyzed. Samples were prepared using a mortar and pestle to pulverize the crystals into a powder form

(**Figure 39-1**). Powder was inserted into the sample holder through a very small window using auto vibration (**Figure 39-2**). After the sample holder was filled approximately three quarter's full, the vibration was stopped, and the sample holder was placed into the PXRD with proper orientation (**Figure 39-3**). The default target metal to emit x-rays was cobalt (Co), and the default wavelength was 1.79 Å (K $\alpha$ ). **Figure 39-4** displays the number of iteration setup and the progress of the data acquisition process.

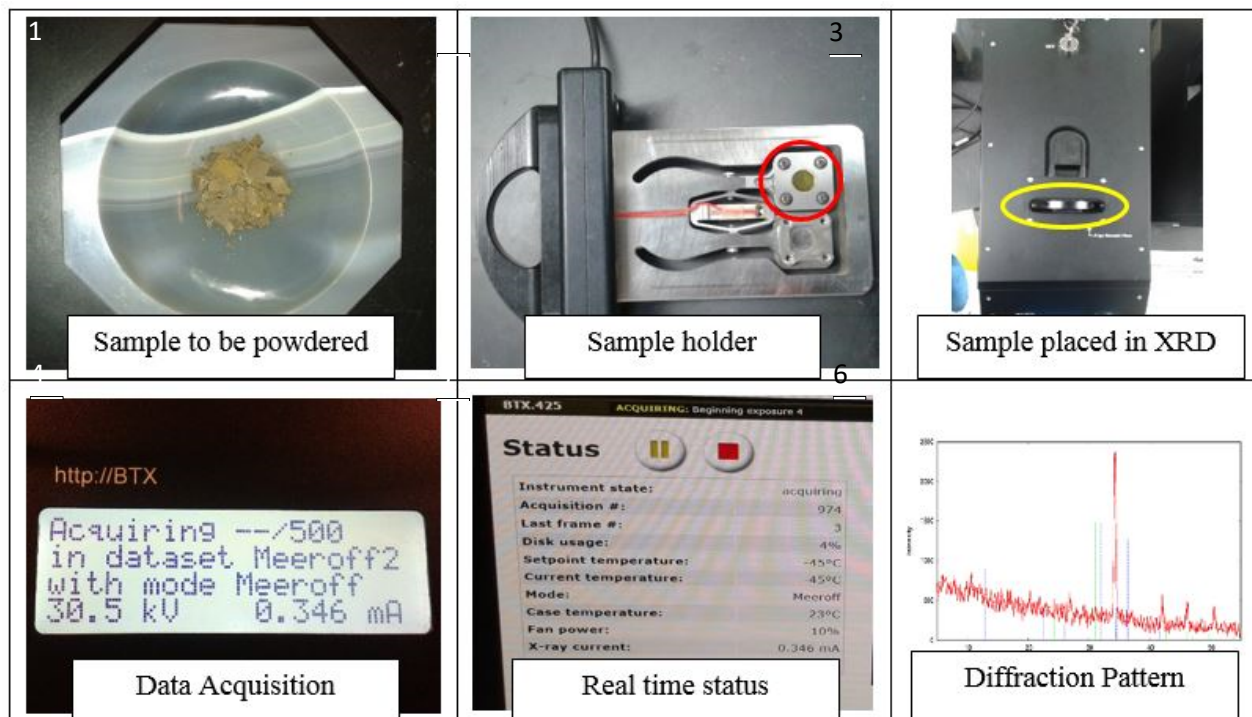


**Figure 39. XRD analysis flow path**

The range of  $2\theta$  was selected between 5-55 degrees, and number of grains varied between 50 and 200 (**Figure 39-5**). A typical diffraction pattern of pure calcite from the PXRD is shown in **Figure 39-6** and **Figure 40**. As different samples have varying intensity, the intensity axis (y-axis) has been converted to relative intensity as discussed earlier to make it easier to visualize the differences when comparing diffractograms.

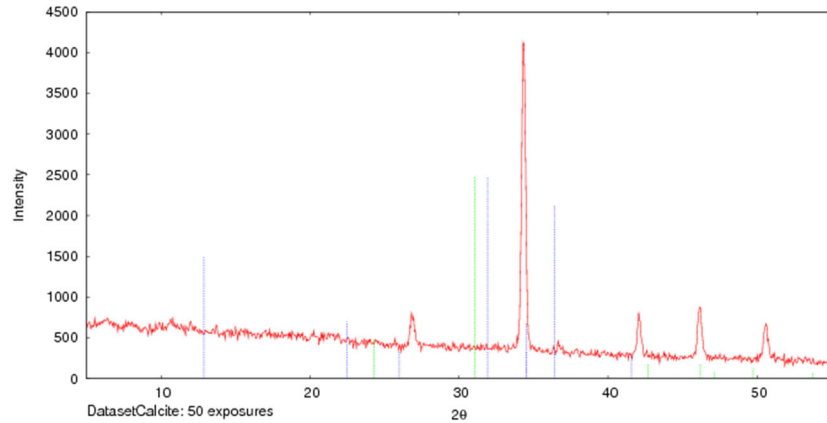


**Figure 40. XRD diffraction pattern of pure calcite purchased from Wards Scientific**

An x-ray fluorescence (XRF) spectrum (**Figure 41**) is the graphical representation of x-ray intensity peaks as a function of energy peaks. The peak energy identifies the element, and the intensity is generally an indication of the concentration. An XRF spectrum is generally formed simultaneously during the PXRD diffraction analysis.

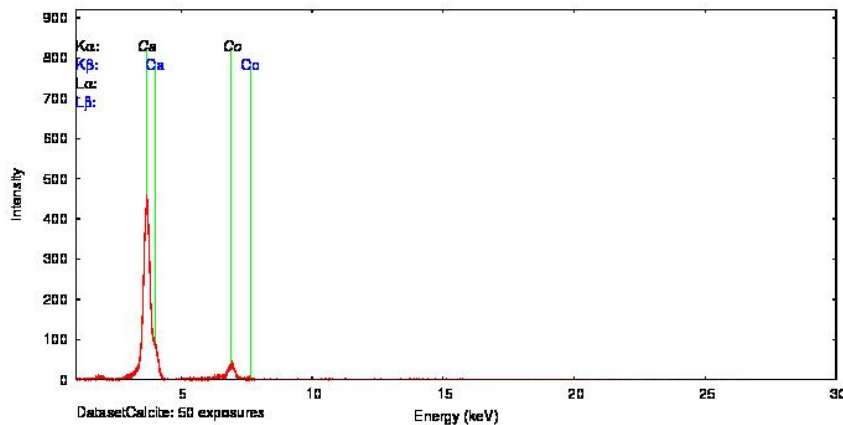


**Figure 41. XRF diffraction pattern of pure calcite purchased from Wards Scientific**

The intensity of the diffracted x-ray pattern is continuously recorded as the sample and detector rotate through their respective angles. A peak in intensity occurs when the mineral contains lattice planes with d-spacings appropriate to diffract x-rays at that value of  $\theta$ . Although each peak consists of two separate reflections ( $K\alpha_1$  &  $K\alpha_2$ ), at small values of  $2\theta$ , the peak locations overlap with  $K\alpha_2$  as a hump on the side of  $K\alpha_1$ . Greater separation occurs at higher values of  $\theta$ . Typically, these combined peaks are treated as one. The  $2\lambda$  position of the diffraction peak is typically measured as the center of the peak at 80% peak height.

Results are commonly presented as peak positions at  $2\theta$  degree and x-ray counts (intensity) in the form of a table or an x-y plot (**Figure 40**). The relative intensity is the ratio of the peak intensity at any  $2\theta$  to the most intense peak. Mathematically, this is represented as follows (Equation 21):

$$\text{Relative intensity} = \frac{I}{I_0} \times 1000 \quad (21)$$

To determine an unknown crystal, the d-spacing of each peak is then obtained by solution of the Bragg's equation for the appropriate value of  $\lambda$  and diffraction, which only occurs when Bragg's law is satisfied. Mathematical representation of Bragg's law is as follows (Equation 22):

$$n\lambda = 2d\sin\theta \quad (22)$$

Once all d-spacings have been determined, automated search/match programs compare the d values of the unknown crystal to those of known crystals from a crystal database. MATCH! Version 3.9.0 phase identification from powder diffraction software (crystalimpact.com) and crystallography open database (COD) available from crystallography.net were used for matching diffraction patterns of known materials (inorganic and organic compounds).

### 2.9.2 *Post Processing Using Rietveld Refinement*

For the quantitative analysis, Rietveld refinement was used. To run Rietveld refinement, FullProf suite was used, which works in the background during the qualitative analysis of diffraction pattern and can be controlled from the MATCH! program, when needed. **Figure 42** shows the step-by-step process for Rietveld refinement using FullProf suite. The default wavelength and the type of radiation was selected as 1.7903000Å (Co-K $\alpha$ ) and x-ray respectively. Next, the default background calculated by the program was selected and modified as needed.

This program can automatically select the peaks, but were selected manually so that there is no unnecessary peak selection by the program due to background noise. After selecting the peaks, the search match calculation was run, and after calculation, the program suggested possible matches starting with the most probable match. Then the best matched crystals were selected by making sure that there were no residual peaks. During this selection process, the program also shows an estimation of relative quantity of each crystal in the unknown sample.

The final step is to run Rietveld refinement for quantitative analysis. Only if the prediction of possible crystals present in the sample is correct, Rietveld refinement converges. Even after the refinement converges, the final weighted average Bragg R-factor and final reduced  $\chi^2$  indicates the quality of the refinement. The lower the value of these two factors, the better the refinement. If both of these values are low enough, the program displays the following message: "*Your refinement seems to be very good.*" Although sometimes it is challenging to achieve such low values of these two parameters, the refinement is still accurate within a certain percentage even if some peaks remain unknown. There are several reasons for this phenomenon such as the fineness of the powder, quality of the XRD pattern, excessive background noises, etc. But, as the refinement converges, that confirms the composition of the unknown sample selected is appropriate.

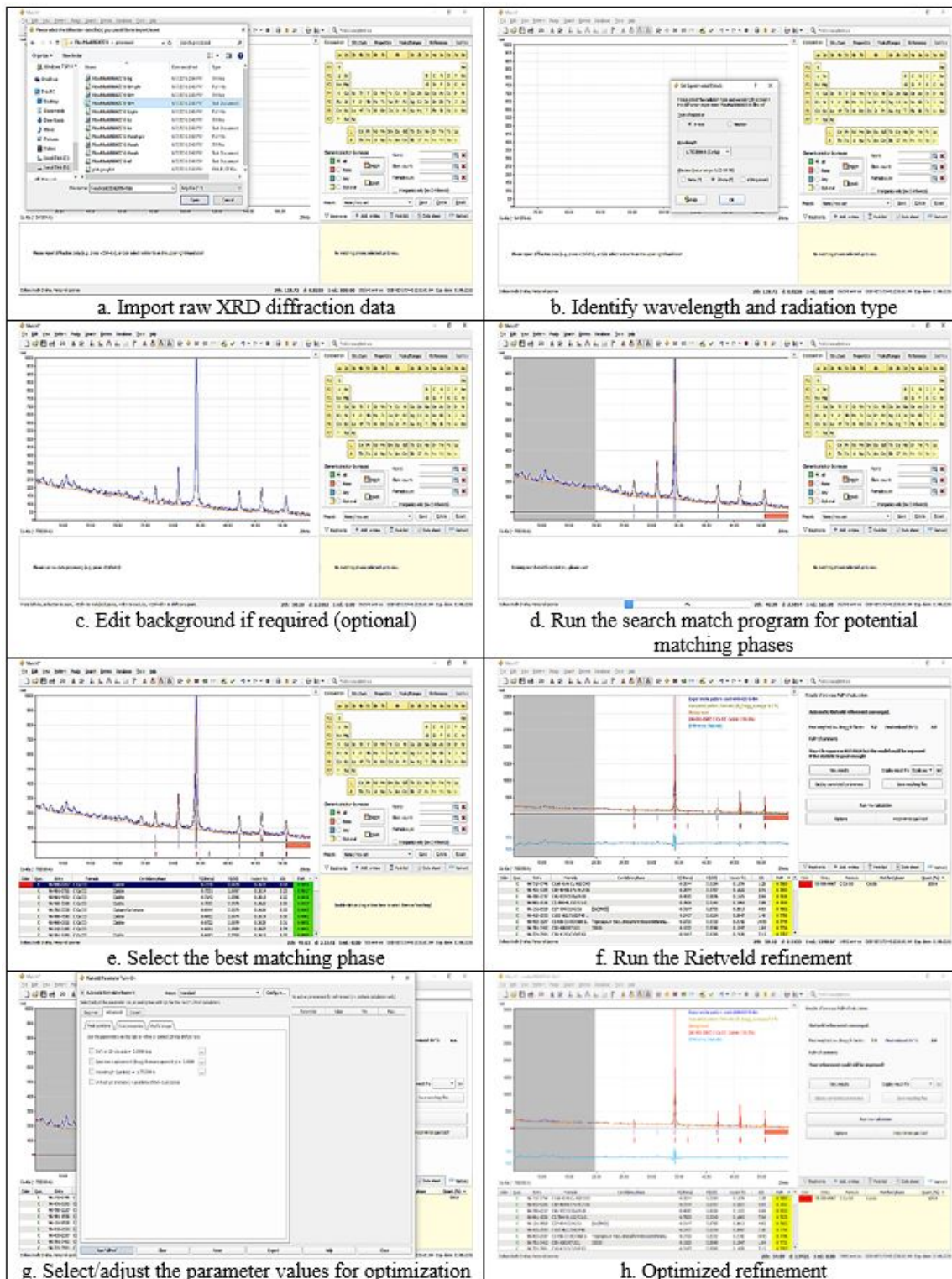
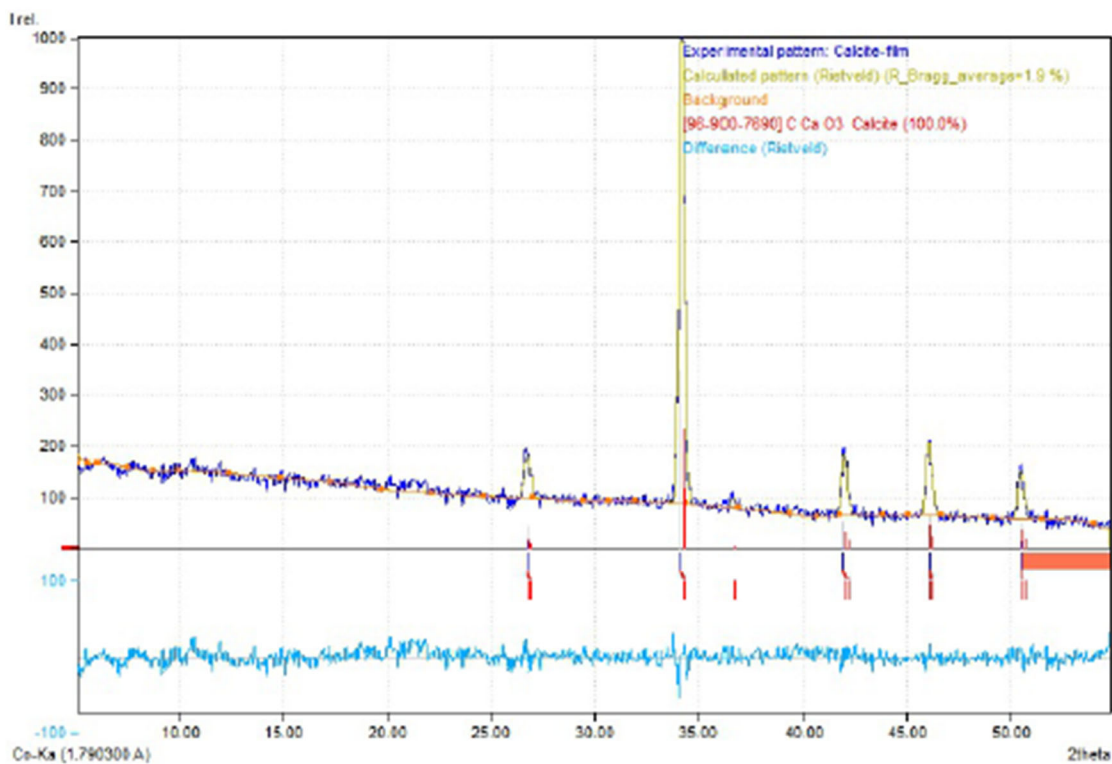


**Figure 42. Phase identification and Rietveld refinement using MATCH! 3.2.0, 3.9.0 and FullProf suite, respectively**

After refinement processing, an automated report can be downloaded from the program for printing or saving. The report generated by MATCH! Version 3.2.0 for the pure calcite sample is shown in **Appendix C**, and the graphical results are shown in **Figure 43**.



Match! Copyright © 2003-2015 CRYSTAL IMPACT, Bonn, Germany

**Figure 43.** Rietveld refinement of a pure calcite sample purchased from Wards Scientific

### 3 RESULTS

#### 3.1 Leachate Characteristics and CaCO<sub>3</sub> Precipitation Potential

Leachate water quality data from the present study was obtained from the 4 composite samples collected during the study period from Pump Station A (PS-A). Leachate from Cells 13, 11, 9, 8, and 5 passes through headers to the west side gravity collection system, which transports the mixed leachate along with gas condensate, leak detection leachate, and groundwater used for dilution (to reduce scaling) to PS-A. There are two gas condensate lines present at Manhole 8 and Manhole 9, which add very high concentrations of sulfide (32,400-54,100 µg/L S<sup>2-</sup>) as well as oil and grease to the composite leachate.

**Table 11** summarizes the leachate quality data from the present study and compares literature values from Meeroff and Youngman (2012) and Kjeldsen et al. (2002) compiled from Andreottola and Cannas 1992, Chu et al. 1994, Robinson 1995, Ehrig 1980, Ehrig 1983, Ehrig 1988, Garland and Mosher 1975, for context. Most of the water quality parameters monitored in this study are consistent with the literature values.

**Table 11. Leachate characteristics and comparison with the literature review**

Parameters	Kjeldsen et al. 2002*	Meeroff and Youngman 2012**	This study (2017-2019)
pH (standard units)	4.8-9.0	2.0-11.3	6.3-7.3
Conductivity (µS/cm)	2,500-35,000	5.2-95,000	3,600-58,300
Total Solids (mg/L)	2,000-60,000	10.1-133,000	3,100-34,800
Ca <sup>2+</sup> (mg/L as CaCO <sub>3</sub> )	10-7,200	Not recorded	800-4,100
Mg <sup>2+</sup> (mg/L as CaCO <sub>3</sub> )	30-15,000	14-140	100-1,000
Alkalinity (mg/L as CaCO <sub>3</sub> )	610-7,320	3,300-11,000	900-4,400

\*Compiled from Andreottola and Cannas (1992), Chu et al. (1994), Robinson (1995), Ehrig (1980), Ehrig (1983), Ehrig (1988), Garland and Mosher (1975).

\*\*Compiled from Abu Amr and Aziz (2012), Adlan et al. (2011), Anglada et al. (2011), Aziz et al. (2011), Bashir et al. (2010), Bekbölet et al. (1996), Bouhezila et al. (2011), Deng and Ezyske (2011), Iaconi et al. (2010), Jia et al. (2011), Kurniawan and Lo (2009), Li et al. (2009), Mahmud et al. (2011), Mohajeri et al. (2010), Poblete et al. (2012), Renou et al. (2008), Salem et al. (2008), Zhao et al. (2010).

#### 3.2 Types of CaCO<sub>3</sub> Scale Formation

Six scale samples (**Figure 44**) were collected from the landfill from the time period before the implementation of electronic water treatment as well as dilution water at MH 11. The first three samples were collected during June to November, 2013; whereas the later three were grabbed from the landfill in October 2015 by SWA staff, although the exact date of collection was not recorded. The samples are presented in **Figure 44**. Visual inspection of the samples indicate that they are of different colors, textures, and of different morphological structures. These six samples were prepared for XRD analysis, and diffraction patterns were obtained from the PXRD unit. These XRD patterns were then imported to the search match program MATCH! Version 3.2.0 and analyzed for phase identification (qualitative analysis) and Rietveld refinement for quantitative

analysis. The qualitative analysis of the sample collected in June 2013 from MH 5 shows that the two major components are quartz ( $\text{SiO}_2$ ) and calcite ( $\text{CaCO}_3$ ). The Rietveld refinement for quantitative analysis further identified the relative percentages (quartz-82.5%, calcite-17.5%) of the components. Also, there are many small peaks identified by the program that are not considered during the Rietveld refinement as no matching phases were identified. This results in a higher error percentage, but as the refinement converged, it can be concluded that quartz and calcite are the major components of the clog with some other minor impurities.

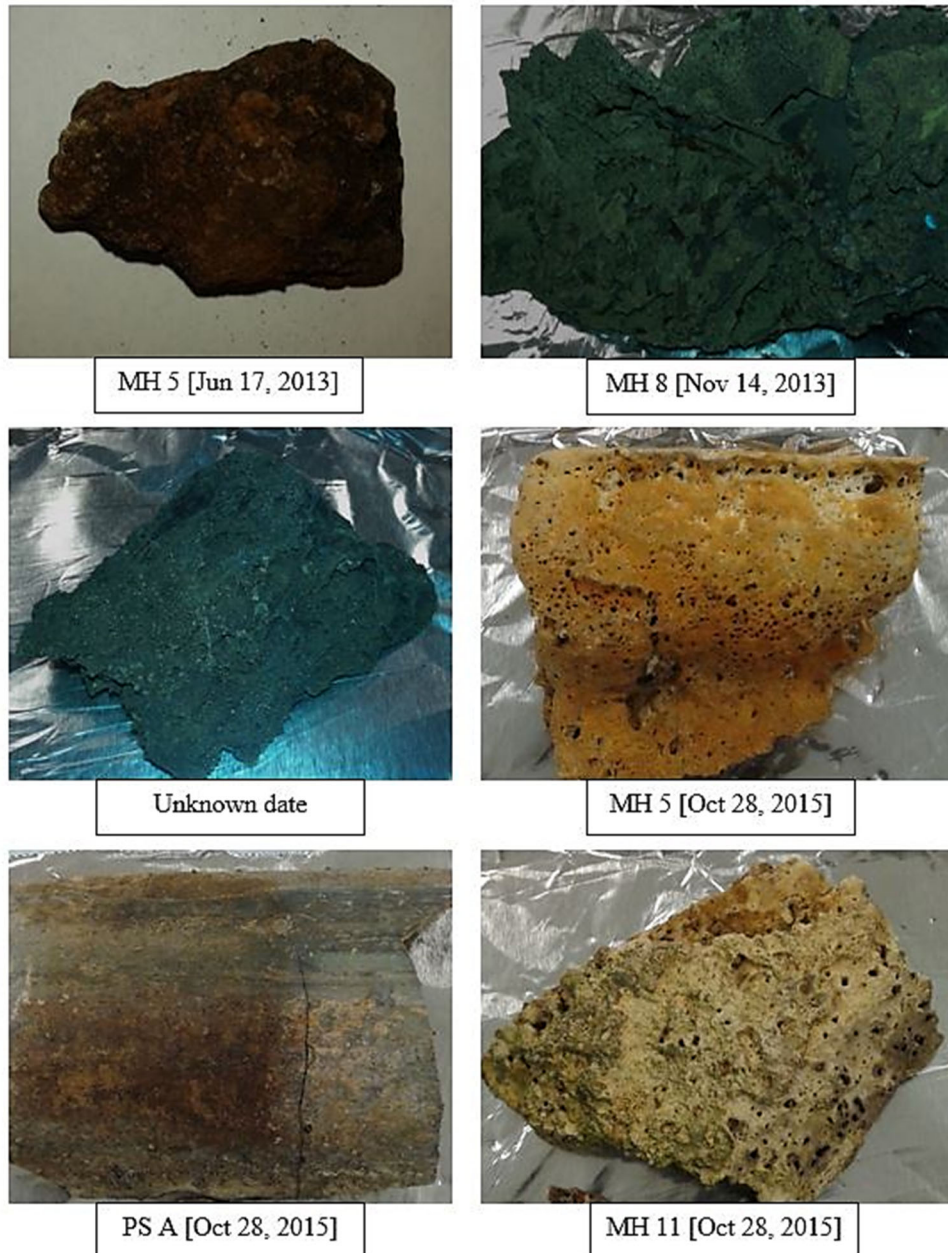


**Figure 44. Historical clogging samples collected to analyze using XRD for phase identification**

Similarly, for all other samples both qualitative and quantitative analysis were performed, and the results are summarized in **Table 12**.

**Table 12. Summary of search match calculation and Rietveld refinement**

Solids	Compounds	Coefficients	Comments
	Quartz - 82.5% Calcite - 17.5%	Bragg's R - 11.5 Final $\chi^2$ - 5.0	$\chi^2$ is not very high but model could still be improved if the statistics is good enough.
MH 5 [Jun 17, 2013]			
	Calcite - 100%	Bragg's R - 8.0 Final $\chi^2$ - 1.8	$\chi^2$ is low but high R-Bragg factor can be due to a bad structural model and/or rather poor statistics.
MH 8 [Nov 14, 2013]			
	Calcite - 100%	Bragg's R - 8.8 Final $\chi^2$ - 2.5	$\chi^2$ is low but high R-Bragg factor can be due to a bad structural model and/or rather poor statistics.
Unknown date			
	Calcite - 100%	Bragg's R - 34.9 Final $\chi^2$ - 7.0	$\chi^2$ is not very high but model could be improved if the statistics is good enough.
MH 5 [Oct 28, 2015]			
	Calcite - 100%	Bragg's R - 5.3 Final $\chi^2$ - 1.5	Refinement could still be improved.
PS A [Oct 28, 2015]			
	Calcite - 100%	Bragg's R - 7.3 Final $\chi^2$ - 1.9	Refinement could still be improved.
MH 11 [Oct 28, 2015]			

The analyses suggest that the major component of the precipitate is calcite ( $\text{CaCO}_3$ ) in most of the cases, with some other unidentified impurities. This finding agrees with the previous literature reviewed (Shaha 2016; Maliva 2000; Levine 2005; Mullah-Saleh 2006; Mullah-Saleh 2007,

Fleming et al. 1999, Fleming and Rowe 2004, Rittman et al. 2003, Cooke et al. 1999, 2001, 2005). Minor impurities and less important phases with very low concentrations were ignored for this analysis.

It is interesting to find out that although the samples were so different in visual inspection, the compositions are more or less similar based on the XRD analysis. This finding suggests that these precipitates are triggered by different factors and formed in a different chemical environment, giving them different appearances even though the mineral composition remains the same. One of the objectives of this research is to explain the formation and trigger mechanism of these precipitates, which are discussed with experimental findings in the following sections.

### **3.3 Impacts of Flow Regime on CaCO<sub>3</sub> Scaling**

To investigate the role of flushing, SWA personnel started dilution activities on the east side gravity system on March 20, 2017. A sampling plan was prepared to measure water quality impacts for pH, alkalinity, calcium, total dissolved solids, temperature, sulfides and sulfates to determine LSI/RI and solids characteristics at the following locations: MH6, MH10, P/S B, MH12, MH14, deep injection well composite, groundwater dilution water, and NEFCO wastewater. Biweekly sampling was conducted to observe the effects of operational changes in water quality parameters, if any, from June 1, 2017 to September 7, 2017. The initial field visit occurred on April 13, 2017 in which samples were collected from MH6, MH10, P/S B, injection well, groundwater dilution water, and NEFCO wastewater.

Field data (pH, conductivity, TDS, DO, and temperature) was obtained with a YSI 556 multiparameter meter, and surface temperature was recorded using an infrared thermometer. After collection and transport to FAU, laboratory measurements for TDS, COD, alkalinity, and calcium were conducted on the collected samples. The summary of field and laboratory analysis is presented in

**Table 13.**

**Table 13. Field and laboratory water quality analysis of collected leachate sample between June and September, 2017**

Sample ID	Date	pH (field)	Field Conductivity (mS/cm)	TDS (mg/L)	TDS (g/L)	COD (mg/L as O <sub>2</sub> )	Alkalinity (mg/L CaCO <sub>3</sub> )	Calcium (mg/L CaCO <sub>3</sub> )	Field TDS (g/L)	Temp. (°C)
MH 6	04/13/17	6.09*	50.74	20,370	20.37	8,000	6,950	350	28.91	32.36
MH 10	04/13/17	5.40*	29.92	18,950	18.95	4,280	3,800	1,800	17.75	29.95
P/S B	04/13/17	5.37*	19.85	13,850	13.85	5,570	4,700	700	19.85	29.92
DIW	04/13/17	4.99*	0.86	570	0.57	30	205	380	0.55	26.42
Deep well	04/13/17	5.35*	17.85	6,670	6.67	6,420	1,500	450	10.10	32.75
NEFCO	04/13/17	3.82*	6.14	1,900	1.90	4,810	190	250	3.48	32.64
MH 6	06/01/17	7.22	35.28	18,340	18.34	9,340	3,800	2,200	19.66	33.73
MH 10	06/01/17	7.37	41.64	18,500	18.50	16,340	7,200	1,800	22.38	35.93
PS/B	06/01/17	7.20	44.98	26,800	26.80	20,640	7,800	5,500	23.67	37.41
MH 12	06/01/17	7.35	41.76	18,400	18.40	8,560	6,400	1,100	22.65	35.34
MH 14	06/01/17	7.39	39.20	16,840	16.84	4,860	5,500	1,300	21.32	35.17
DIW	06/01/17	7.41	1.13	740	0.74	50	3,500	540	0.68	29.36
Deep well	06/01/17	6.86	10.75	5,040	5.04	2,300	950	1,400	5.67	37.22
NEFCO	06/01/17	5.74	8.76	2,300	2.30	6,330	750	410	4.46	39.56
MH 6	06/15/17	6.95	31.54	18,260	18.26	5,670	3,150	2,600	17.64	33.65
MH 10	06/15/17	6.85	28.40	17,450	17.45	13,600	3,600	3,200	15.97	33.20
PS/B	06/15/17	7.20	12.52	8,220	8.22	2,560	1,650	1,900	7.46	29.88
MH 12	06/15/17	7.13	8.70	5,950	5.95	1,470	1,350	1,350	5.17	30.01
MH 14	06/15/17	7.16	5.96	4,610	4.61	640	650	1,300	3.58	29.27
DIW	06/15/17	7.35	1.15	530	0.53	50	380	470	0.70	28.37
Deep well	06/15/17	6.79	11.88	6,860	6.86	2,290	1,700	1,600	6.83	31.92
NEFCO	06/15/17	5.95	6.28	1,640	1.64	4,110	500	800	3.43	35.04
MH 6	06/29/17	7.37	33.92	18,660	18.66	4,240	4,200	1,600	19.16	33.34
MH 10	06/29/17	7.36	33.64	18,200	18.20	5,355	5,000	1,600	18.94	33.13
PS/B	06/29/17	7.33	32.32	12,280	12.28	4,580	5,200	5,000	18.35	32.64
MH 12	06/29/17	7.33	5.74	4,220	4.22	190	900	730	3.39	30.34
MH 14	06/29/17	7.13	1.58	7,680	7.68	nr	300	500	0.95	29.42
DIW	06/29/17	7.38	1.24	620	0.62	60	360	500	0.74	29.99
Deep well	06/29/17	7.30	6.23	6,050	6.05	520	600	1,000	3.51	33.08
NEFCO	06/29/17	5.82	6.00	2,020	2.02	4,220	750	400	3.29	34.74
MH 6	07/27/17	7.51	44.96	22,300	22.30	5,660	6,000	1,000	25.60	32.45
MH 10	07/27/17	7.02	46.88	18,800	18.80	15,420	6,400	4,600	25.59	35.06
PS/B	07/27/17	7.18	44.34	25,400	25.40	10,660	4,700	3,300	24.93	33.24
MH 12	07/27/17	7.24	51.73	27,800	27.80	18,100	6,300	2,500	27.85	35.91
MH 14	07/27/17	7.34	40.91	20,180	20.18	6,140	4,900	1,900	22.55	34.38
DIW	07/27/17	7.44	1.24	790	0.79	70	390	460	0.74	29.36
NEFCO	07/27/17	5.64	9.94	4,700	4.70	6,800	300	800	5.55	33.55

\*pH probe was replaced. Standard pH 4, 7, and 10 were checked to be 1.99, 5.16, and 7.90. Average difference is 1.98. Data not used for analysis purposes.

nr = not reported.

The average pH of the samples collected was 7.04 (neutral) with a pH range of 5.64 to 7.51, and a standard deviation of 0.52. The lowest pH observed was in the NEFCO wastewater, in the range of 5.64 to 5.95. The average pH of leachate flowing through the gravity line and in the deep injection well increases to 7.22 with a standard deviation of 0.20 unit without considering NEFCO wastewater.

Field conductivity measurements were between 1.58 and 51.73 mS/cm. The conductivity of 1.58 mS/cm is very low. This reading was observed in the leachate collected from MH 14 on June 29, 2017, when it was submerged with groundwater during sample collection. The average

conductivity of the samples collected from the east side (MH 6, MH 10, PS/B, MH 12, and MH 14) was 32.95 mS/cm with a standard deviation of 14.18 mS/cm.

TDS measurement were between 4,220 and 27,800 mg/L. The addition of groundwater changes the concentration by a substantial amount. Alkalinity ranges between 300 and 7,800 mg/L as CaCO<sub>3</sub>; whereas calcium ranges between 350 and 5,500 mg/L as CaCO<sub>3</sub>. The average temperature was 32.6°C with a range of 26.4 to 39.6 and a standard deviation of 2.9. The average temperature of the samples was more than 0.5°C higher than the previous study (Schert et al. 2015) conducted in this landfill.

To determine if submerging the manholes has potential impacts on saturation indices, Langelier's saturation index (LSI) and Ryzner Index (RI) were calculated (**Table 14**). The NEFCO wastewater has the lowest LSI value of -0.6 with a RI value of 7.0, which indicates a neutral or slightly corrosive nature. However, leachates collected from the east side of the landfill have LSI values between +1.7 and +2.3, which indicates scale forming potential even after the submerged condition (dilution with groundwater between 20 to 100 gpm). In the previous study, the LSI of the leachate from the west side (MH 5, MH 8, MH 9, MH 11, and MH 13) ranged between +0.4 and +3.3 for the period between 2013 and 2015.

The average pH of the groundwater was found to be 7.40, which is about 0.5 units higher than it was in the previous study, and this results in higher LSI values (+1.3). In contrast, the injection well has an LSI of +1.1, which is lower than the east side leachates. This suggests that the addition of low pH NEFCO wastewater is helping to reduce the scaling potential of the mixed leachate for disposal.

**Table 14. Saturation indices (LSI and RI) calculation based on average water quality parameters for the samples collected between June and September 2017**

Sample ID	pH (field)	Field Conductivity (mS/cm)	TDS (g/L)	Alkalinity (mg/L CaCO <sub>3</sub> )	Ca Hardness (mg/L CaCO <sub>3</sub> )	Field TDS (g/L)	Temp. (°C)	LSI	RI
MH 6	7.26	39.29	18.90	4,820	1,550	22.19	33.11	2.0	3.2
MH 10	7.15	36.10	18.30	5,200	2,600	20.13	33.45	2.2	2.8
PS/B	7.23	30.80	15.30	4,810	3,280	18.85	32.62	2.3	2.6
MH 12	7.26	26.98	9.50	3,740	1,420	14.76	32.90	1.9	3.5
MH 14	7.26	21.91	9.70	2,840	1,250	12.10	32.06	1.7	3.9
DIW	7.40	1.12	0.60	970	470	0.68	28.70	1.3	4.8
Deep well	6.98	11.68	6.20	1,190	1,110	6.53	33.74	1.1	4.8
NEFCO	5.79	7.42	1.97	500	530	4.04	35.11	-0.6	7.0

In summary, based on saturation indices, the water quality did not change enough to neutralize the leachate. However, the addition of groundwater reduces the precipitation potential as the leachate flows downstream, which reduces further in the deep well by the addition of NEFCO wastewater. Furthermore, having more flow helps to reduce stagnant conditions in the gravity line and thus

reduces crystal formation. The critical question to answer is how much dilution flow provides adequate flushing that slows crystal formation in the gravity network.

In 2018, samples were collected from critical locations along the west side of the landfill including manholes (MH), pump stations (PS), composite leachate before deep injection at the wet well (wetwell), groundwater used for dilution purposes (DIW), and pelletizer wastewater (NEFCO). **Table 15** summarizes the average water quality data.

**Table 15. Average water quality data based on 2018-2019 sampling**

Sample Location	pH	Field Cond. (mS/cm)	TDS (mg/L)	Alkalinity (mg/L as CaCO <sub>3</sub> )	Ca Hardness (mg/L as CaCO <sub>3</sub> )	Field TDS (mg/L)	Temp. (°C)	pHs	LSI	RI
MH 5	6.97	53.56	28,220	3,800	3,500	31,700	30.34	4.88	2.09	2.79
MH 6	6.96	45.86	27,200	7,400	900	26,450	32.30	5.13	1.83	3.30
MH 8	6.87	39.46	20,670	2,300	1,875	23,080	30.39	5.22	1.65	3.58
MH 9	6.94	37.87	20,150	3,100	2,675	22,400	29.00	4.95	1.99	2.96
MH 11	7.03	58.17	34,900	4,400	4,075	34,280	30.37	4.87	2.16	2.72
MH 13	6.32	31.88	18,000	880	3,760	17,800	29.77	5.65	0.67	4.97
PS/A	6.89	6.60	4,770	500	1,260	4,220	25.40	6.31	0.58	5.73
PS/B	6.75	6.87	3,860	900	900	4,160	28.90	6.12	0.63	5.49
DIW	7.15	1.17	670	284	404	720	27.44	6.73	0.42	6.32
NEFCO	5.28	7.52	2,445	238	1,500	4,070	35.54	6.32	-1.04	7.35
Wetwell	7.47	9.74	6,360	1,425	1,075	6,240	25.82	5.96	1.51	4.45

Note: LSI>0.4: Supersaturated; LSI<0.0: undersaturated, and 0<LSI<0.4: Neutral

Most of the samples showed similar water quality results compared to the historical trends found in earlier studies conducted by FAU and UF since 2012 (Townsend et al. 2016; Shaha 2016). However, the wetwell sample had a pH of 7.47, which is almost 0.5 units higher than historical data, due to the operational changes (aeration during bypassing the leachate to the new wet well) in the landfill and/or leachate collection system that facilitated aeration or stagnation of leachate longer than usual.

LSI and RI saturation indices indicate supersaturation with respect to calcium carbonate precipitation for all of the leachate samples. The NEFCO pelletizer wastewater is undersaturated and corrosive. Groundwater (DIW) used for dilution purposes is neutral and helps to reduce the precipitation potential by facilitating higher flow in the gravity collection system as well as diluting the key constituents of calcium and alkalinity in the leachate. **Figure 45** shows the comparison of the historical saturation index (LSI) to that of the current study. The trend remains more or less similar except the lower LSI value observed at PS/A and PS/B because of the addition of groundwater to dilute the leachate, whereas MH 9 showed higher LSI value in this study. The higher LSI at MH 9 is likely related to the presence of a gas condensate line that directly discharges into MH 9.

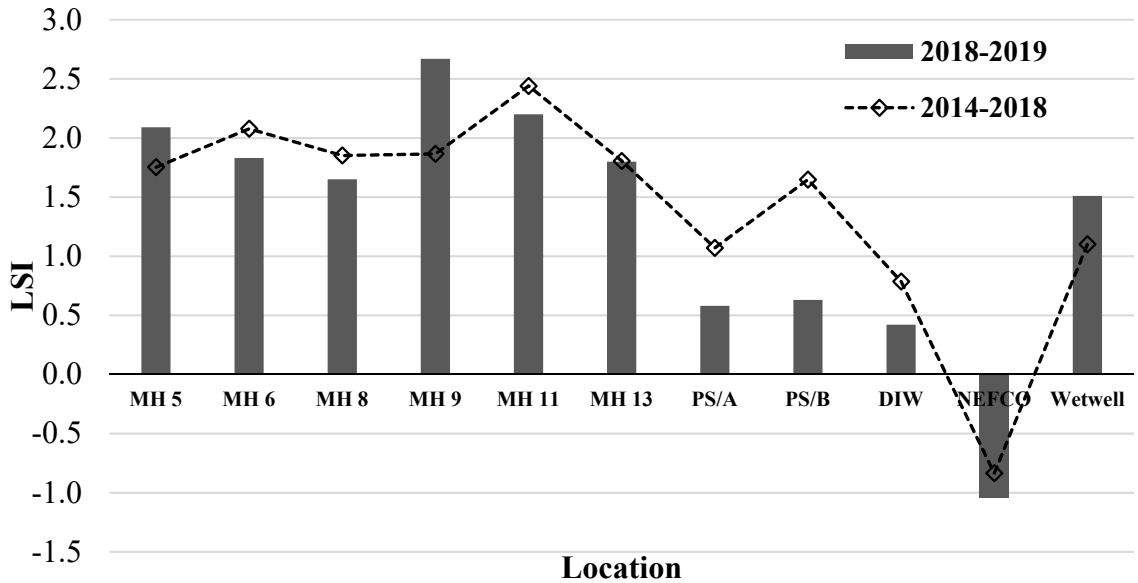


**Figure 45. Comparison of historical LSI with that of current study**

The NEFCO wastewater has an LSI value of  $-1.04 \pm 0.40$  (corrosive) and has the potential to be an alternate source of dilution water that may reduce dependency on the DIW groundwater that has a permitted limit of 100 gpm. FAU conducted several mass balance analyses with different volumetric ratios of leachate and NEFCO wastewater to estimate the optimum mixing ratio that provides neutral saturation indices. A 1:1 volumetric ratio of leachate to NEFCO wastewater results in an LSI of +0.5, which indicates the neutral nature of the mixture. However, NEFCO wastewater having total suspended (TSS) solids in the range of 400 to 600 mg/L (more than double or even triple in some instances compared to leachate) and the adhesive nature of those solids is a concern.

A theoretical mass balance was performed to identify the optimum ratio of leachate and NEFCO water that reduces precipitation potential. Leachate flowrate was varied between 20 and 90 gpm in 10 gpm increments; whereas, NEFCO flowrate was varied between 50 to 125 gpm in 25 gpm increments. In addition, mass balance calculations were performed at three different pH values (4.5, 5.0, 5.5) of NEFCO water. **Table 16,**

**Table 17**, and **Table 18** summarize these mass balance calculations. Based on theoretical mass balance, 1 gallon of NEFCO water can neutralize 1.2 gallons of leachate at initial NEFCO water pH of 4.5 ( $\frac{NEFCO}{leachate} = 0.8$ ), resulting in an LSI of +0.4 (which is considered neutral). The neutralizing capacity (volume of leachate neutralized per gallon of NEFCO water) decreases as the NEFCO water pH increases. For example, at pH 5.5, 60 gpm of leachate flow would require 100 gpm of NEFCO water to neutralize the precipitation potential ( $\frac{NEFCO}{leachate} = 1.7$ ).

**Table 16. Mass balance summary at NEFCO pH equal to 4.5**

NEFCO (gpm)	Leachate (gpm)	pH	TDS mg/L	Alk mg/L as CaCO <sub>3</sub>	Ca mg/L as CaCO <sub>3</sub>	Temp °C	Conductivity mS/cm	LSI	RI
50	20	5.28	5504	1581	956	34.46	14.16	-0.6	6.4
	30	5.52	6609	1918	1089	34.26	16.27	-0.2	5.9
	40	5.71	7468	2181	1192	34.10	17.91	0.1	5.6
	50	5.87	8155	2391	1275	33.97	19.22	0.3	5.3
	60	5.99	8717	2563	1343	33.87	20.29	0.4	5.1
75	20	5.07	4574	1296	844	34.63	12.39	-0.9	6.8
	30	5.28	5504	1581	956	34.46	14.16	-0.6	6.4
	40	5.45	6273	1815	1048	34.32	15.63	-0.3	6.1
	50	5.59	6918	2013	1126	34.20	16.86	-0.1	5.8
	60	5.71	7468	2181	1192	34.10	17.91	0.1	5.6
	70	5.82	7942	2326	1249	34.01	18.81	0.2	5.4
	80	5.91	8355	2452	1299	33.93	19.60	0.3	5.2
	90	5.99	8717	2563	1343	33.87	20.29	0.4	5.1
100	20	4.96	4032	1130	778	34.73	11.35	-1.1	7.1
	30	5.13	4825	1373	874	34.58	12.87	-0.8	6.7
	40	5.28	5504	1581	956	34.46	14.16	-0.6	6.4
	50	5.41	6093	1761	1027	34.35	15.29	-0.4	6.1
	60	5.52	6609	1918	1089	34.26	16.27	-0.2	5.9
	70	5.62	7064	2057	1144	34.17	17.14	-0.1	5.7
	80	5.71	7468	2181	1192	34.10	17.91	0.1	5.6
	90	5.79	7829	2291	1236	34.03	18.60	0.2	5.4
125	20	4.88	3676	1022	736	34.80	10.68	-1.2	7.3
	30	5.03	4364	1232	818	34.67	11.99	-0.9	6.9
	40	5.16	4969	1417	891	34.56	13.14	-0.7	6.6
	50	5.28	5504	1581	956	34.46	14.16	-0.6	6.4
	60	5.39	5982	1727	1013	34.37	15.07	-0.4	6.2
	70	5.48	6411	1858	1065	34.29	15.89	-0.3	6.0
	80	5.57	6797	1976	1111	34.22	16.63	-0.1	5.8
	90	5.64	7148	2083	1154	34.16	17.30	0.0	5.7

\*Values highlighted in green indicate the lowest dilution to meet the neutrality criterion of LSI≤+0.4

**Table 17. Mass balance summary at NEFCO pH equal to 5.0**

NEFCO (gpm)	Leachate (gpm)	pH	TDS mg/L	Alk mg/L as CaCO <sub>3</sub>	Ca mg/L as CaCO <sub>3</sub>	Temp °C	Conductivity mS/cm	LSI	RI
50	20	5.64	5504	1581	956	34.46	14.16	-0.2	6.0
	30	5.84	6609	1918	1089	34.26	16.27	0.1	5.6
	40	5.99	7468	2181	1192	34.10	17.91	0.3	5.3
	50	6.12	8155	2391	1275	33.97	19.22	0.5	5.1
75	20	5.47	4574	1296	844	34.63	12.39	-0.5	6.4
	30	5.64	5504	1581	956	34.46	14.16	-0.2	6.0
	40	5.78	6273	1815	1048	34.32	15.63	0.0	5.7
	50	5.89	6918	2013	1126	34.20	16.86	0.2	5.5
	60	5.99	7468	2181	1192	34.10	17.91	0.3	5.3
	70	6.08	7942	2326	1249	34.01	18.81	0.5	5.1
100	20	5.37	4032	1130	778	34.73	11.35	-0.6	6.7
	30	5.51	4825	1373	874	34.58	12.87	-0.4	6.3
	40	5.64	5504	1581	956	34.46	14.16	-0.2	6.0
	50	5.74	6093	1761	1027	34.35	15.29	0.0	5.8
	60	5.84	6609	1918	1089	34.26	16.27	0.1	5.6
	70	5.92	7064	2057	1144	34.17	17.14	0.2	5.4
	80	5.99	7468	2181	1192	34.10	17.91	0.3	5.3
	90	6.06	7829	2291	1236	34.03	18.60	0.4	5.2
125	20	5.31	3676	1022	736	34.80	10.68	-0.8	6.8
	30	5.43	4364	1232	818	34.67	11.99	-0.5	6.5
	40	5.54	4969	1417	891	34.56	13.14	-0.4	6.2
	50	5.64	5504	1581	956	34.46	14.16	-0.2	6.0
	60	5.72	5982	1727	1013	34.37	15.07	-0.1	5.8
	70	5.80	6411	1858	1065	34.29	15.89	0.1	5.7
	80	5.87	6797	1976	1111	34.22	16.63	0.2	5.5
	90	5.93	7148	2083	1154	34.16	17.30	0.3	5.4

**Table 18. Mass balance summary at NEFCO pH equal to 5.5**

NEFCO (gpm)	Leachate (gpm)	pH	TDS mg/L	Alk mg/L as CaCO <sub>3</sub>	Ca mg/L as CaCO <sub>3</sub>	Temp °C	Conductivity mS/cm	LSI	RI
50	20	5.99	5504	1581	956	34.46	14.16	0.2	5.7
	30	6.15	6609	1918	1089	34.26	16.27	0.4	5.3
75	20	5.86	4574	1296	844	34.63	12.39	-0.1	6.0
	30	5.99	5504	1581	956	34.46	14.16	0.2	5.7
	40	6.10	6273	1815	1048	34.32	15.63	0.3	5.4
	50	6.19	6918	2013	1126	34.20	16.86	0.5	5.2
100	20	5.79	4032	1130	778	34.73	11.35	-0.2	6.2
	30	5.90	4825	1373	874	34.58	12.87	0.0	5.9
	40	5.99	5504	1581	956	34.46	14.16	0.2	5.7
	50	6.08	6093	1761	1027	34.35	15.29	0.3	5.5
	60	6.15	6609	1918	1089	34.26	16.27	0.4	5.3
125	20	5.74	3676	1022	736	34.80	10.68	-0.3	6.4
	30	5.83	4364	1232	818	34.67	11.99	-0.1	6.1
	40	5.92	4969	1417	891	34.56	13.14	0.0	5.9
	50	5.99	5504	1581	956	34.46	14.16	0.2	5.7
	60	6.06	5982	1727	1013	34.37	15.07	0.3	5.5
	70	6.12	6411	1858	1065	34.29	15.89	0.4	5.4

However, the average TSS of NEFCO water was found to be 500 mg/L based on samples collected between 2015-2018. This is relatively high compared to 34 mg/L TSS of groundwater and about 250 mg/L for undiluted leachate. The addition of this large volume of solids to the gravity collection system is a concern, and a proper solid separation method needs to be identified before considering the use of NEFCO water for dilution of leachate in the LCS. Cyclone separation is a common physical method for solid-liquid separation that does not use any moving parts. A laboratory-scale cyclone separator was built and tested to determine the removal efficiency of NEFCO solids. Influent turbidity and TSS of the NEFCO water samples were 18.1 NTU and 80 mg/L, respectively. The accumulated solids resembled biological sludge and were highly adhesive to surfaces. In both test modes (single pass and batch mode), turbidity and TSS decreases were observed (turbidity reduction  $\geq 32\%$ , TSS reduction  $\geq 69\%$ ) in 10 minutes (**Table 19**). The average NEFCO wastewater flow at SWA is approximately six million gallons/month. A theoretical calculation was also performed to estimate the amount of solids that will need to be handled if the cyclone separator is to be implemented. Based on the six million gallons/month NEFCO wastewater flow with 500 mg/L of TSS and 70% TSS removal, approximately 580 lb/day of solids would need to be handled if cyclone pretreatment were instituted.

However, the sample collected at 15 minutes showed an increase in turbidity as well as TSS resulting from the accumulation of solids beyond the designed storage capacity of the unit. In other words, separated solids were resuspended in the solution again. This can be easily addressed in the field by periodic solids removal from the bottom of the solid accumulation zone.

**Table 19. Turbidity and TSS reduction using a laboratory scale cyclone separator at 1.7 lpm flow rate**

ID/time	Turbidity		TSS	
	NTU		mg/L	
	Single pass	Batch	Single pass	Batch
0	18.1	18.1	80	80
5	13.9	nr	80	80
10	12.1	12.3	20	25
15	12.2	16.2	40	75
% Removal @ 10 min	33%	32%	75%	69%
% Removal @ 15 min	33%	10%	50%	6%

*\*nr = not recorded*

### 3.4 Impacts of pH on CaCO<sub>3</sub> Scaling Potential

The different factors (**Table 20**) that influence changes in pH of leachate, which impact the precipitation/scale formation, include addition of CO<sub>2</sub>, exposing to air, mechanical turbulence (500 rpm), as well as aeration with air. All of these factors were investigated in this study.

**Table 20. Factors that impacts pH changes in leachate**

Factors	Change in pH
Open to atmosphere	+
Turbulence (500 rpm)	+
Aeration	+
Addition of base (NaOH)	+
Addition of CO <sub>2</sub>	-
Addition of acid (HCl)	-

The first experiment was conducted on July 23, 2017, with 103-L gas cylinders. The gas exposure duration was about 30 minutes, with initial adjustments. Samples were collected for 90 minutes from the beginning of the experiment. A third beaker (2L) half-filled with leachate was also aerated to replicate a previous experiment (Schert et al. 2015). As shown in **Figure 46**, aeration with ambient air degasified the CO<sub>2</sub> from the leachate and increased the pH from 7.5 to 8.4 in 1-1.5 hours, which confirms the previous results (Schert et al. 2015). The nitrogen control also increased the pH by approximately 0.5 units, presumably from the same degasification mechanism. However, the addition of carbon dioxide (2 lpm or 5.2 kg/day at standard temperature and pressure) decreased the pH by 0.5 units (7.4 to 6.9) by reacting with leachate and forming carbonic acid. At these conditions, the reaction achieved a steady state after only 20-30 minutes.

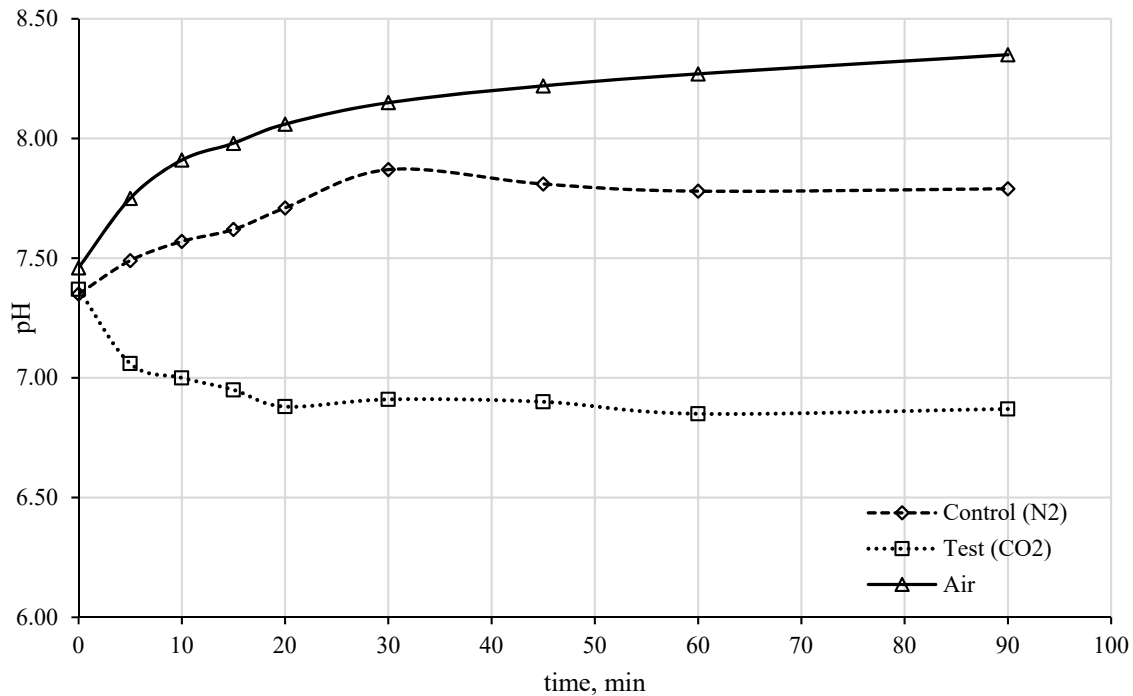


**Figure 46. Observed changes in pH during the experiment with addition of nitrogen (N<sub>2</sub>), carbon dioxide (CO<sub>2</sub>), and air**

There were no changes observed in any other water quality parameters (conductivity, TDS, alkalinity, Ca, sulfate, sulfides), as summarized in **Table 21**. Some oxidation of sulfides to sulfates, and perhaps some stripping of hydrogen sulfide gas, in the first 30 minutes was observed but was expected. The gas cylinders were empty after 30 minutes of exposure; therefore, it was planned to repeat these experiments with larger gas cylinders (600-L) to extend the exposure times to three to six hours.

**Table 21. Summary of leachate water quality changes due to addition of N<sub>2</sub>, CO<sub>2</sub>, and Air**

Time, min	Sulfide, µg/L S <sup>2-</sup>			Sulfate, mg/L SO <sub>4</sub> <sup>2-</sup>			Ca, mg/L as CaCO <sub>3</sub>			Alkalinity, mg/L as CaCO <sub>3</sub>		
	Control (N <sub>2</sub> )	Test (CO <sub>2</sub> )	Air	Control (N <sub>2</sub> )	Test (CO <sub>2</sub> )	Air	Control (N <sub>2</sub> )	Test (CO <sub>2</sub> )	Air	Control (N <sub>2</sub> )	Test (CO <sub>2</sub> )	Air
0	778	740	613	490	480	500	1900	1750	1350	1230	1270	1600
30	588	423	549	480	550	580	1700	1900	1650	1300	1330	1400
60	747	621	510	470	490	550	1750	1800	1600	1270	1280	1150
90	710	550	608	470	510	540	1750	1800	1600	nr	nr	nr

\*nr-not recorded

The Langelier saturation index (LSI) and Ryzner index (RI) were calculated and summarized in **Table 22**. Positive LSI indicates scale forming potential; whereas negative LSI implies the corrosive nature of leachate. However, a range of LSI between -0.4 and +0.4 is considered neutral in most cases (Prisyazhniuk 2007). In addition, the RI value of 6.0 is considered neutral. A RI value of less than 6.0 represents the scale forming nature and higher than 6.0 represents corrosive nature of leachate.

**Table 22. Saturation indices calculation (LSI and RI)**

Time, min	pH	TDS field, g/L	Alk, mg/L as CaCO <sub>3</sub>	Ca, mg/L as CaCO <sub>3</sub>	Temp., °C	pH <sub>s</sub>	LSI	RI
<b>Control (N<sub>2</sub>)</b>								
0	7.35	6.86	1,230	1,900	18.37	5.9	1.5	4.4
30	7.87	6.81	1,300	1,700	21.27	5.9	2.0	3.9
60	7.78	6.76	1,270	1,750	21.76	5.9	1.9	3.9
90	7.79	6.66	1,280	1,750	22.36	5.8	1.9	3.9
<b>Test (CO<sub>2</sub>)</b>								
0	7.37	6.85	1,270	1,750	18.5	5.9	1.5	4.4
30	6.91	6.81	1,330	1,900	21.24	5.8	1.1	4.7
60	6.85	6.87	1,280	1,800	21.58	5.8	1.0	4.8
90	6.87	6.9	1,280	1,800	22.2	5.8	1.0	4.8
<b>Air</b>								
0	7.46	6.94	1,600	1,350	15.82	6.0	1.5	4.5
30	8.15	6.77	1,400	1,650	19.43	5.9	2.3	3.6
60	8.27	6.71	1,150	1,600	20.61	6.0	2.3	3.6
90	8.35	6.67	1,150	1,600	21.41	5.9	2.4	3.5

The addition of N<sub>2</sub> and air increases the pH, which directly results in higher LSI and increases scale forming potential. For instance, the addition of air increases the pH by 0.9 units (7.5 to 8.4) in 90 minutes and results in a near-equal increase in LSI (+1.5 to +2.4). In contrast, the addition

of carbon dioxide decreases the pH by almost 0.5 units and thus LSI also decreases by nearly the same amount, resulting in less scale forming potential.

To replicate LFG, a cylinder with a composition of 50% CH<sub>4</sub>, 15% CO<sub>2</sub> was purchased instead of only pure CO<sub>2</sub> to investigate the possibility of using LFG instead of pure carbon dioxide for pH adjustment. **Figure 47** shows the experimental results of carbon dioxide addition to leachate for a longer period. **Figure 48**, and **Figure 49** present the effect of leachate exposure to the atmosphere, and the effect of external turbulence, respectively. The addition of carbon dioxide reduces the pH by almost 0.5 standard units regardless of the rate of addition, whereas keeping the leachate in contact with air and external turbulences increases the pH. Based on the experimental condition, with 1 L of leachate and CO<sub>2</sub> flow rate of 0.1 lpm, it requires 3L of CO<sub>2</sub> to achieve the pH reduction of approximately 0.5 units. In the case of exposing leachate to air; pH increases and stabilizes within 30 minutes. However, external turbulences increased the pH almost linearly until 50 minutes in this study. Aeration increases the pH of leachate by almost 1.0 standard units found in previous studies conducted by FAU and UF (Townsend et al. 2016; Shaha 2016).

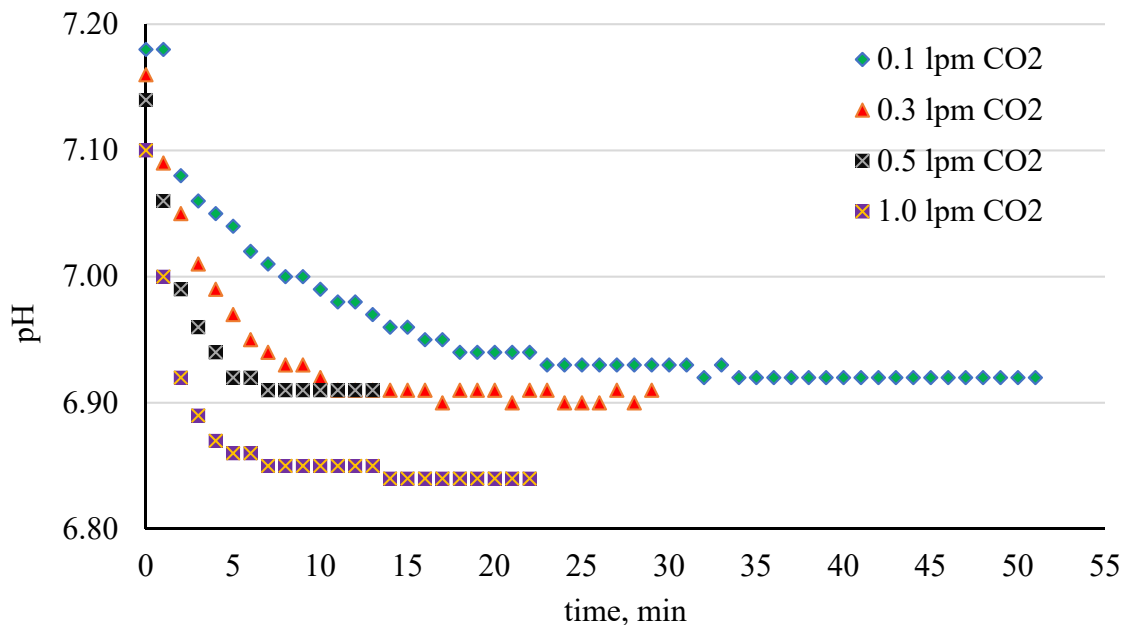


**Figure 47. Changes in pH due to addition of CO<sub>2</sub> at different rates**

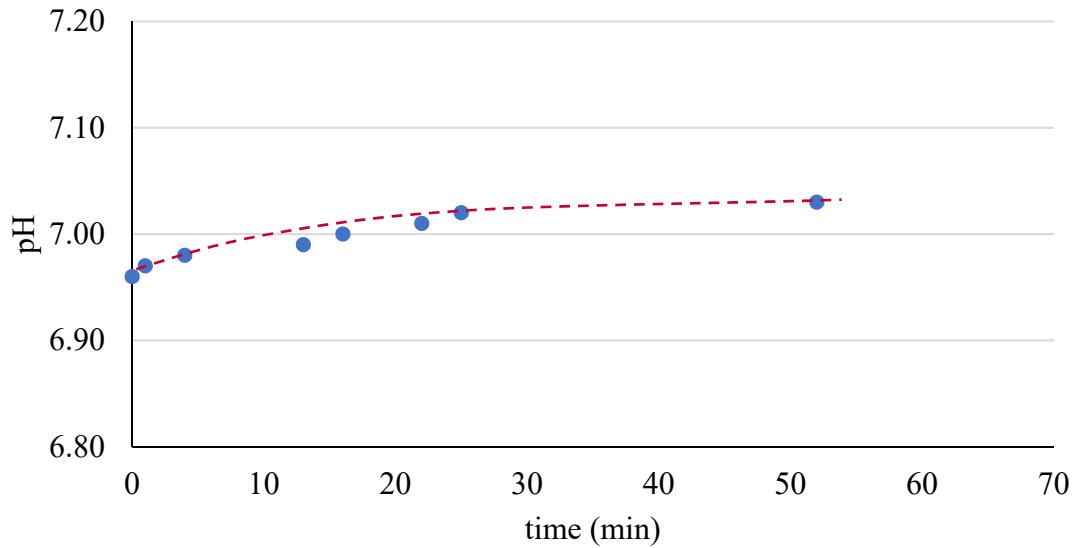


**Figure 48. Changes in pH by exposing leachate to open air**

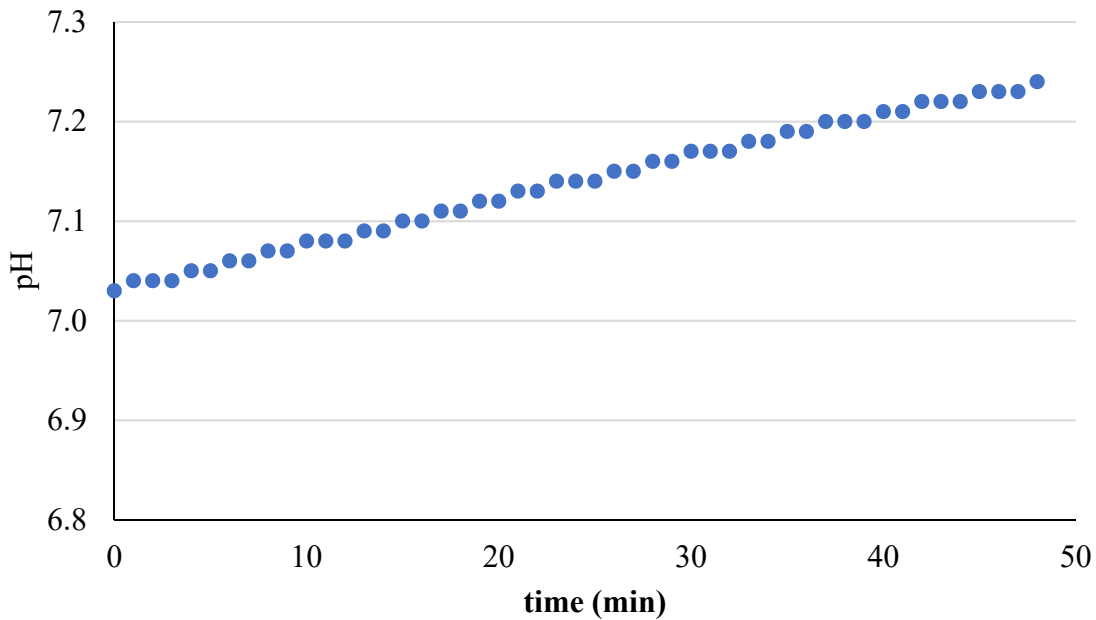


**Figure 49. Changes in pH by external turbulence (500 rpm)**

A set of laboratory experiments was conducted to quantify the impacts of pH change on the overall leachate chemistry and the propensity for scaling. Leachate samples (200 ml) were pH-adjusted using various methods (addition of air or carbon dioxide at different rates) and incubated at 35°C for 7 days to observe calcium carbonate precipitation rates. The initial and final volume of leachate was measured using a 200-mL graduated cylinder to account for the loss of leachate due to evaporation. Leachate water quality parameters (pH, conductivity, TDS, calcium, alkalinity,

sulfate, sulfides, temperature) were measured at day 0 and day 7. Two different types of scale formation were observed during this process: 1) “Loose scale,” which formed a thin, floating layer (Figure 50), and 2) “Hard scale,” which attached to all surfaces of the vessel (Figure 51).

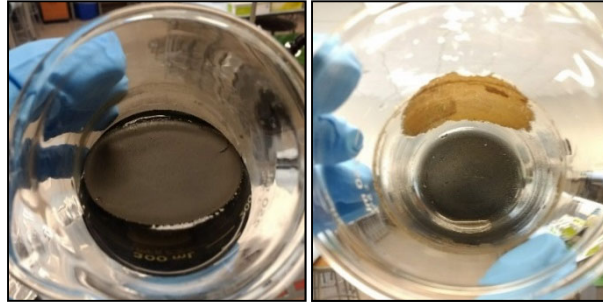


**Figure 50. pH adjustment and the impact on  $\text{CaCO}_3$  precipitation rate: loose scale. A visible floating layer (left) and the layer attached to the beaker surface after pouring out leachate from the beaker (right) (7 days)**

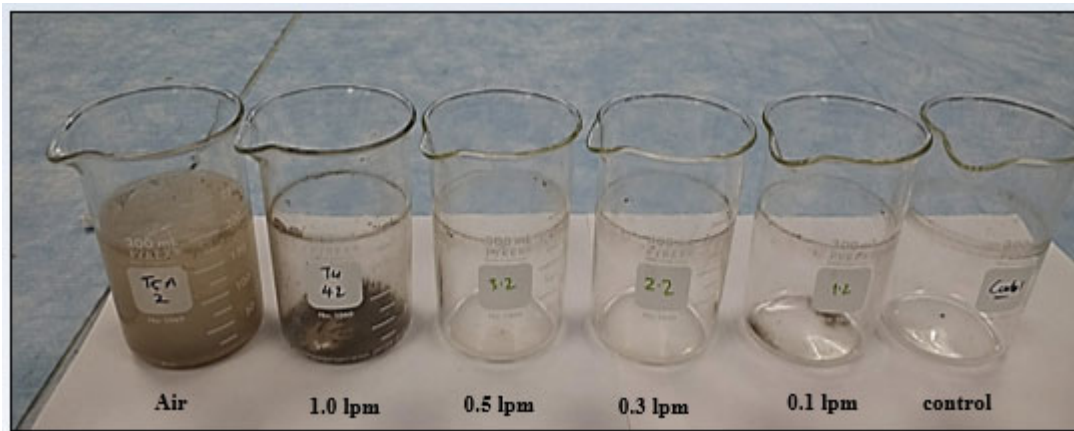


**Figure 51. pH adjustment and the impact on  $\text{CaCO}_3$  precipitation rate: hard scale attached to the surface (7 days)**

During the incubation period, leachate water quality (pH, calcium, alkalinity, sulfides) was measured at day “zero” and day “7”. The changes in water quality parameters are presented in Figure 52, Figure 53, Figure 54, and Figure 55. The pH of leachate after 7 days of incubation stabilizes between 7.5 and 7.8 regardless of initial pH (Figure 52). This happens due to the degasification of carbon dioxide, carbon dioxide and carbonic acid-base equilibria, and biological degradation/photosynthesis involving organic carbon. Calcium and alkalinity reduce in all cases with the precipitation of calcium carbonate resulting in lower ions present in the solution (Figure 53 and Figure 54). Sulfides concentration also reduces during incubation due to the liquid-gas equilibria.

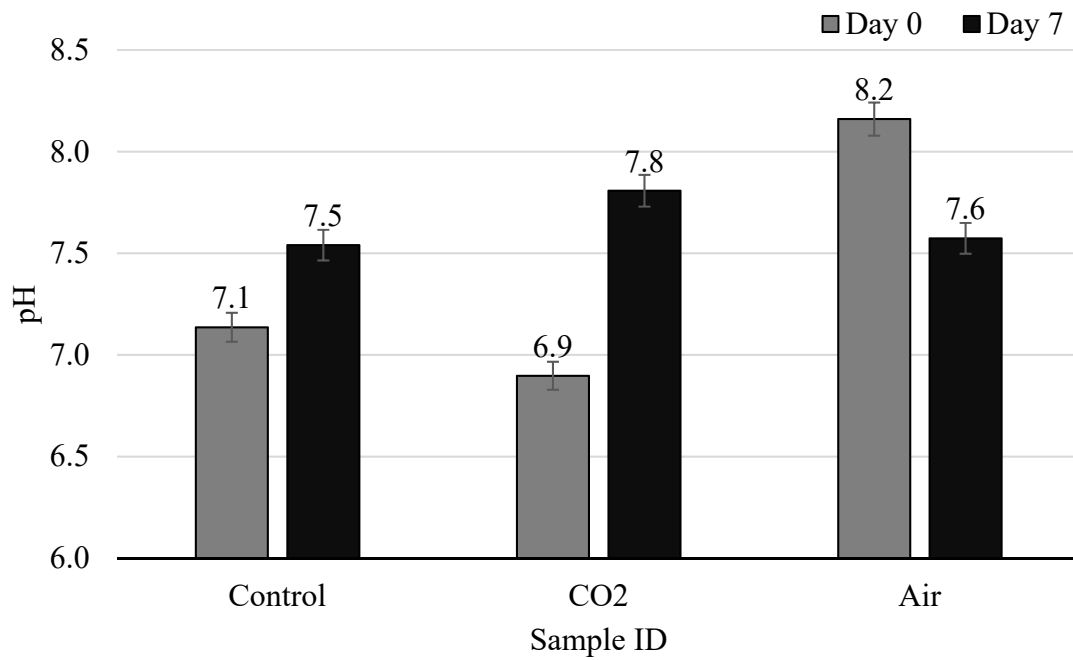


**Figure 52. pH changes during the incubation at 35°C for 7 days**

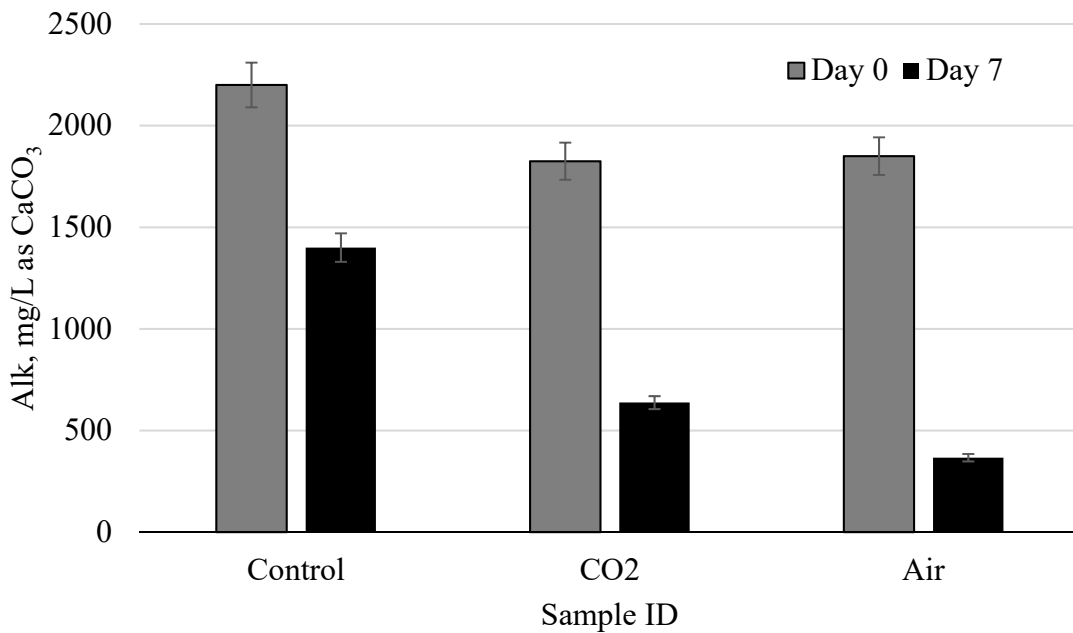


**Figure 53. Changes in alkalinity during the incubation at 35°C for 7 days**

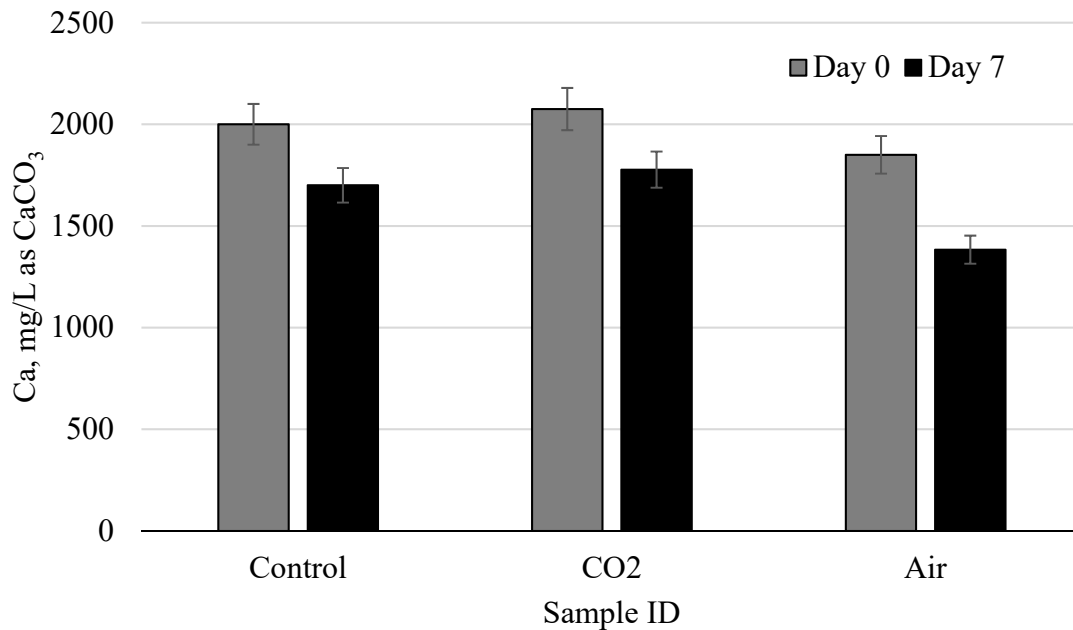


**Figure 54. Changes in dissolved calcium during the incubation at 35°C for 7 days**

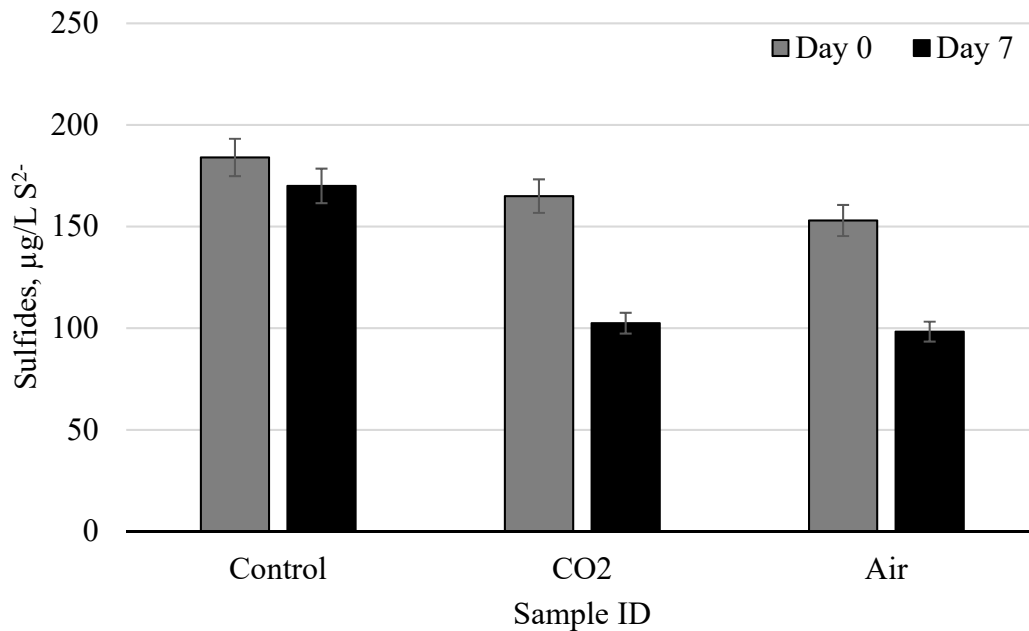


**Figure 55. Changes in dissolved sulfide during the incubation at 35°C for 7 days**

Scale rate was calculated only using the mass of the hard scale attached to the surfaces and expressed in gram per liter of leachate (g/L). **Figure 56** shows the difference in scale formation per 100 mL sample due to the pH adjustment by the addition of carbon dioxide and air into the leachate. It was evident that initial higher pH resulted in a higher ( $\geq 15$  times) “hard” scale formation and was difficult to remove.

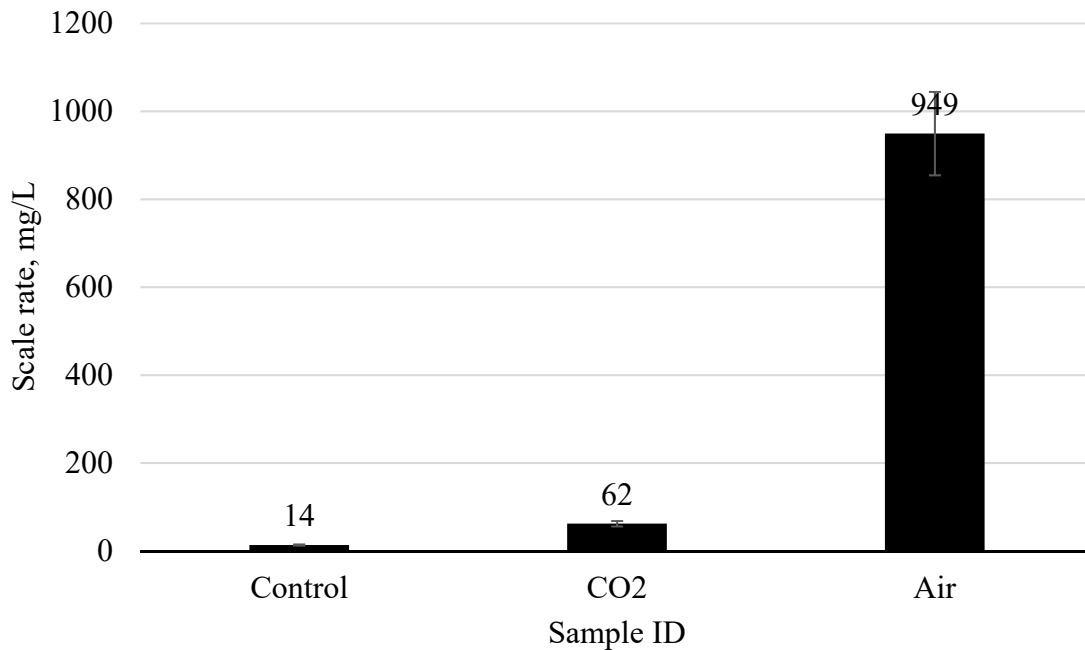


**Figure 56. Impact of initial pH of leachate on scale rate**

A small piece of loose floating scale was magnified 400 times and visualized under a microscope (**Figure 57**).

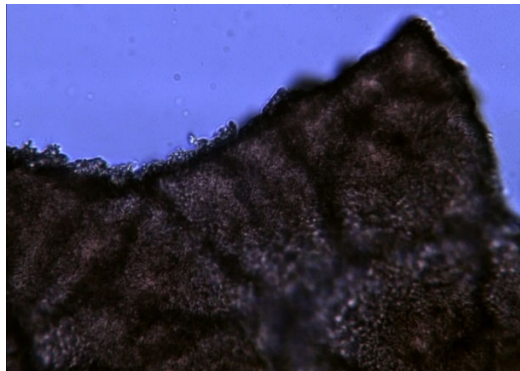


**Figure 57. Loose scale under microscope (x400)**

A set of tests was conducted by increasing the pH of leachate by adding concentrated (1M) NaOH. The first test was conducted on June 21, 2018, using the PS/A leachate, and the results are presented in **Figure 58**, **Figure 59**, and **Figure 60**. Zero “0” in the x-axis indicates the control, and 1, 2, 3, 4, and 5 represent the volume (ml) of NaOH added into the leachate solution. The addition of NaOH spikes the pH and result in instant calcium carbonate precipitation that increases with the volume of NaOH added (**Figure 58**). The difference in dissolved calcium between Day 0 and Day 7 is highest in the control sample and decreases with the addition of NaOH. This indicates that the higher pH shifts the carbonate equilibrium towards the right because of the higher amount

of carbonate present in the solution, resulting in  $\text{CaCO}_3$  precipitation. Alkalinity also reduces with increasing pH (**Figure 59**) due to the addition of NaOH as there are fewer ions in the solution. At approximately neutral pH between 6 and 8, alkalinity is the summation of bicarbonate and carbonate ions present in the solution. As the pH increases, carbonate equilibrium shifts to the right and results in calcium carbonate precipitation and reduces the overall concentration of carbonates in solution. This series of chemical reactions reduces the alkalinity of leachate and enhances the formation of  $\text{CaCO}_3$  precipitation. **Figure 60** shows the saturation index (LSI) of each sample on Day 0 and Day 7. The initial LSI value ranges between +1.93 and +2.04, which indicates the samples are scale forming. After 7 days incubation at  $35^\circ\text{C}$ , the precipitation occurs, the pH stabilizes to normal pH level of leachate, and the LSI values reduce between +0.75 and +1.0, which is still considered scale forming. The major understanding from the experiment is that increased pH enhances immediate precipitation. However, it does not necessarily ensure there will be no further precipitation. As long as the leachate remains supersaturated with respect to calcium carbonate, a small change in the leachate environment that increases the pH results in precipitation.

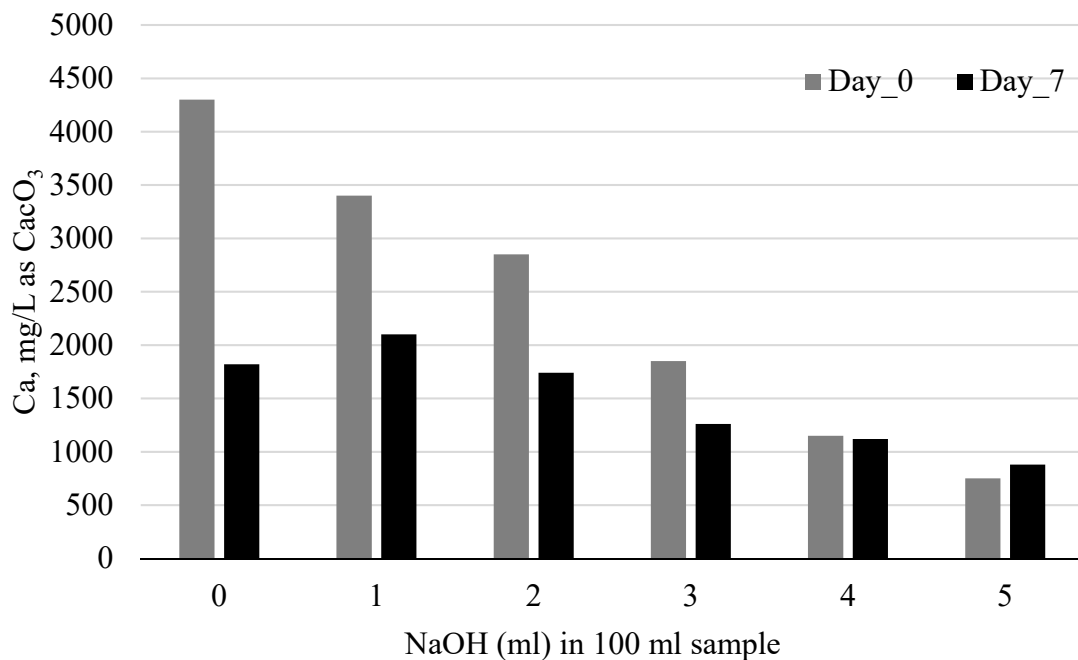


**Figure 58. Impact of increased pH using NaOH on dissolved calcium**

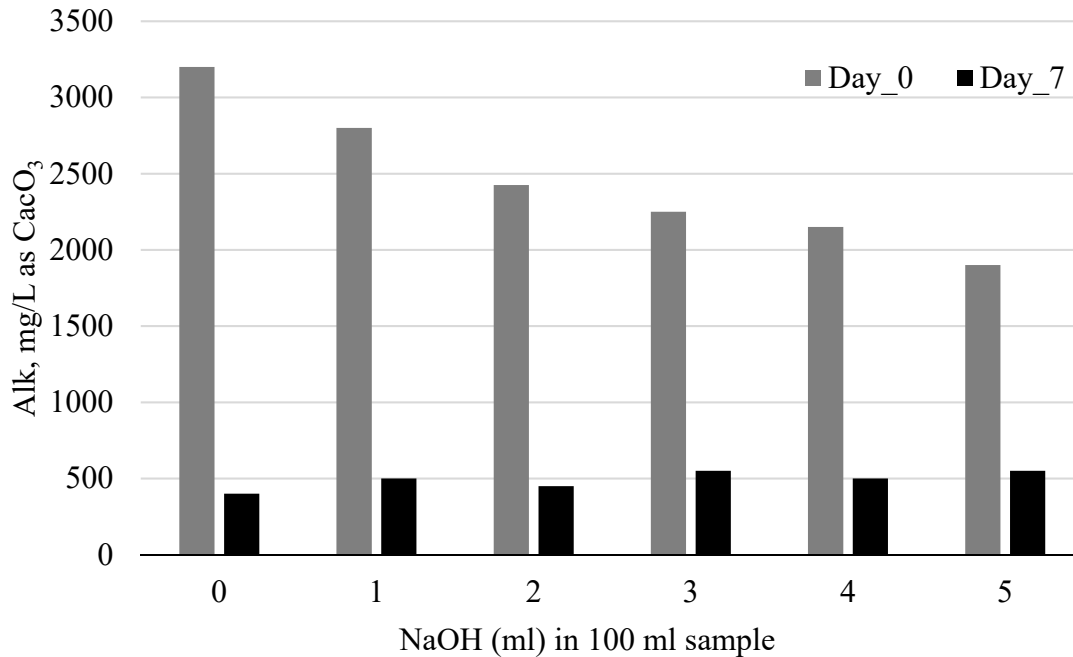


**Figure 59. Impact of increased pH using NaOH on alkalinity**

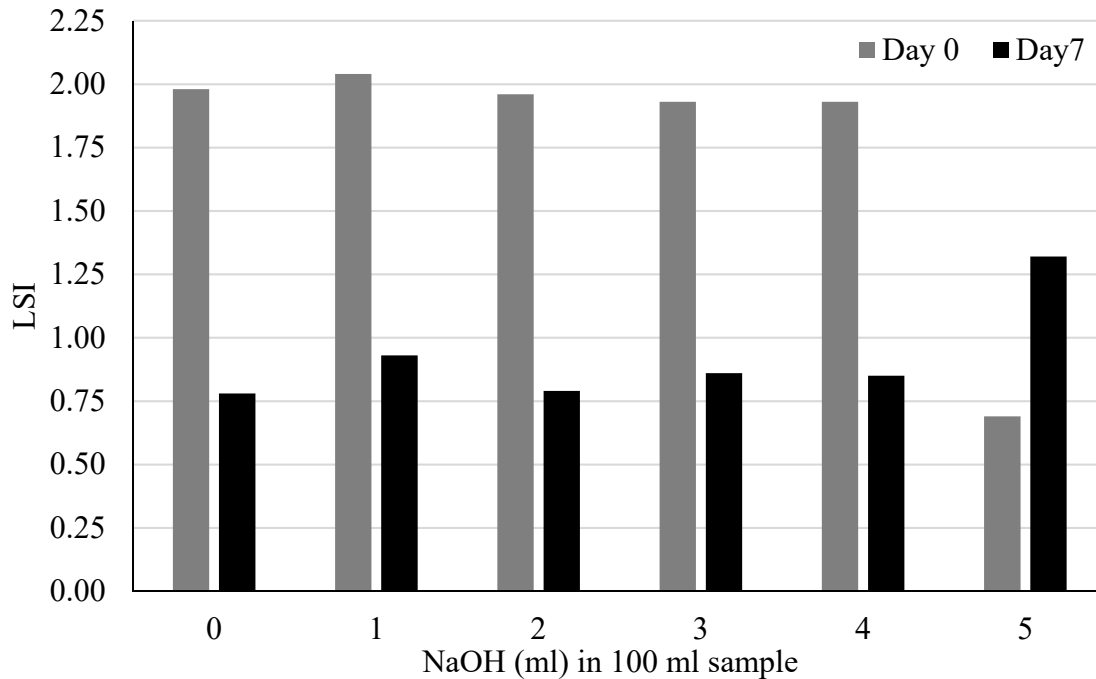


**Figure 60. Saturation index on Day 0 and Day 7**

A second set of pH adjustment experiments was conducted with three different leachates from MH 13, MH 11, and deep well in July 2018. The water quality of leachates is presented in **Table 23**. These three samples have different pH, alkalinity, calcium, and TDS resulting in different LSI values ranging from +1.08 to +1.72. This indicates different precipitation potential of the samples.

**Table 23. Water quality of the three different leachates**

Sample ID	pH	Conductivity μS/cm	Specific Conductance μS/cm	TDS mg/L	Alkalinity mg/L as CaCO <sub>3</sub>	Calcium mg/L as CaCO <sub>3</sub>	Temperature °C	LSI
MH 13	6.6	73.7	78.9	51.3	1,450	7,950	21.6	+1.08
MH 11	7.0	73.7	78.6	51.1	3,000	5,950	21.7	+1.72
Deep well	7.4	13.3	14.2	9.2	1,200	1,050	21.7	+1.22

In this instance, only 3 ml and 5 ml NaOH was added in 100 ml leachate sample. The changes in leachate precipitation potential (LSI) during 7 days incubation period are presented in **Figure 61**, **Figure 62**, and **Figure 63** for the samples from MH 13, MH 11, and deep well, respectively. The initial LSI value increased with the amount of NaOH added for all samples resulting from the increased pH of leachate. Although the immediate precipitation due to the higher pH reduces the calcium and alkalinity of leachate, pH also dictates the LSI calculation, which results in a higher LSI value. After 7 days incubation, the pH of all samples stabilizes towards neutral pH, CaCO<sub>3</sub> precipitates triggered by higher carbonate ions present in the solution results in a lower and more stable LSI value for all the samples. It is important to notice that, even though the precipitation potential reduces by day 7, the leachate samples remain scale forming in nature, and a sudden change in the chemical equilibrium can cause further precipitation.

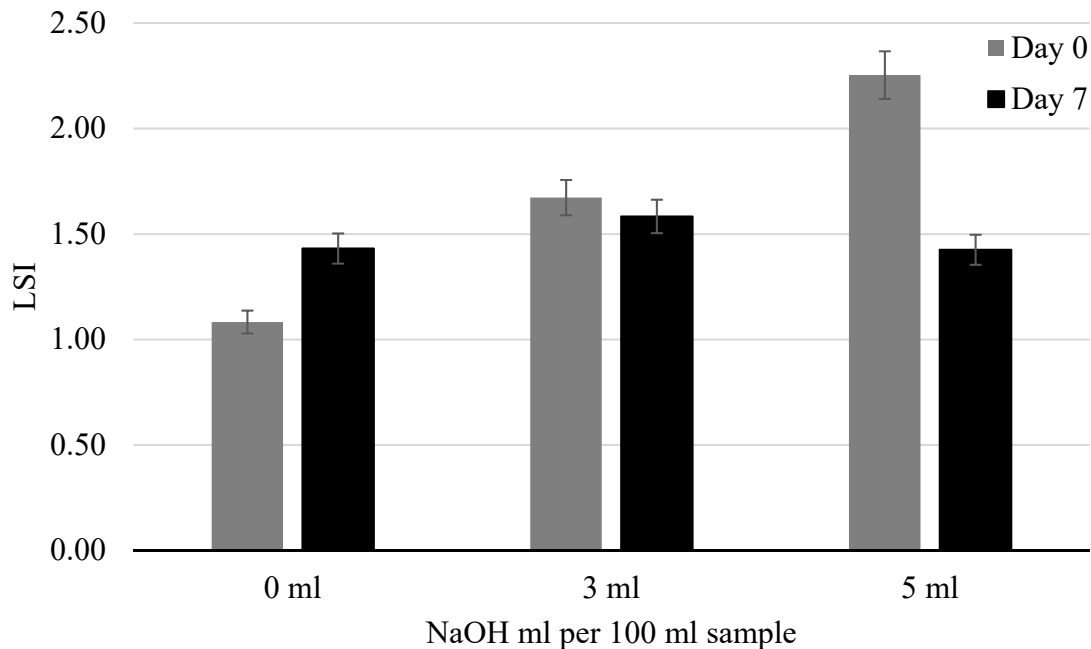


**Figure 61. Saturation index (LSI) at Day 0 and Day 7 for the leachate sample from MH 13**

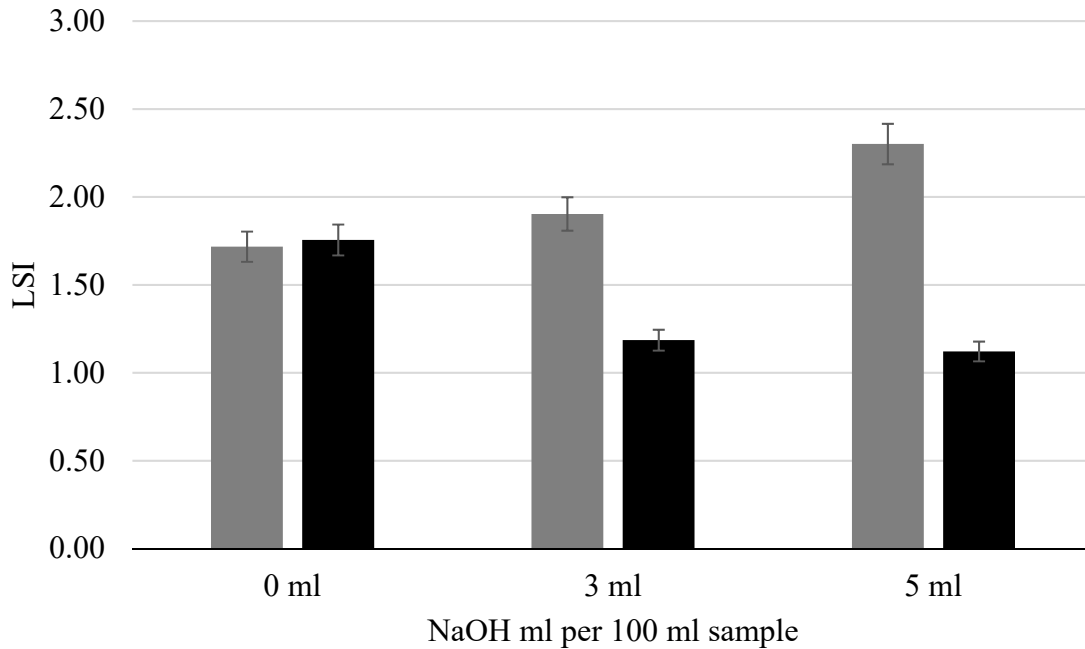


**Figure 62. Saturation index (LSI) at Day 0 and Day 7 for leachate sample from MH 11**

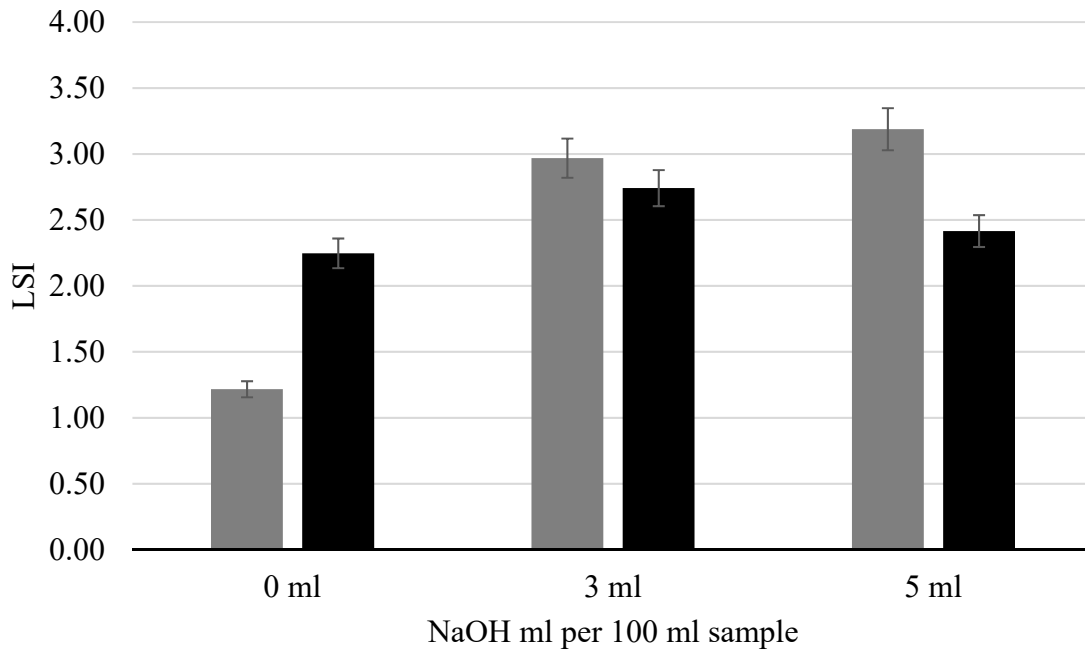


**Figure 63. Saturation index (LSI) at Day 0 and Day 7 for leachate sample from Deep well**

The precipitation of  $\text{CaCO}_3$  initiated by increasing pH using concentrated NaOH was magnified 400 times and photographed under the microscope as shown in **Figure 64**. The loose floating scale (**Figure 57**) have reasonable visual similarity with the scale formed at higher pH (**Figure 64**). XRD/XRF analysis along with Rietveld analysis suggests that the precipitate formed are  $\text{CaCO}_3$ .

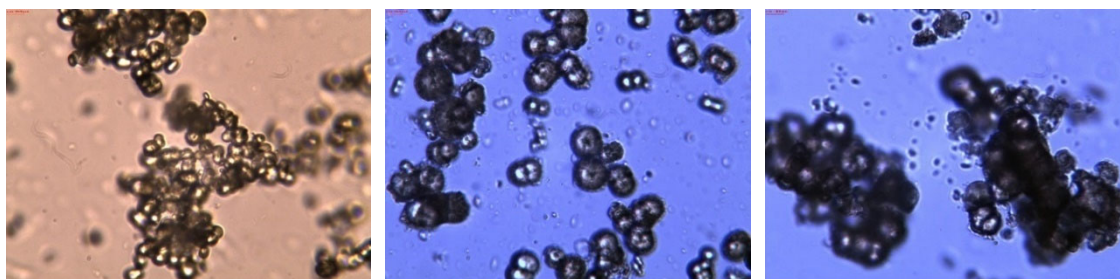


**Figure 64. Enhanced precipitation of calcium carbonate with pH adjustment with the addition of NaOH; 1mL (left), 3mL (middle), and 5 mL (right)**

Precipitates collected during the pH adjustment tests were analyzed using a PXRD unit to obtain a diffraction pattern of each sample, which were then post-processed using MATCH! 3.90 and fullprof suite to identify the components as well as their relative percentages. A summary of the Rietveld refinement results are presented in **Table 24**. It is evident from the analysis that the major component of the precipitates is  $\text{CaCO}_3$  ( $\geq 97.2\%$ ) with some salts and does not depend on the initial pH, method of the pH adjustment, or the type of precipitates (floating or submerged in leachate).

**Table 24. Summary of PXRD analysis and Rietveld refinement**

Sample ID	Compounds	Coefficients	Notes
Control	$\text{CaCO}_3 = 100\%$	Bragg R-factor = 29.5 $\chi^2 = 2.6$	$\chi^2$ is low but the model could be improved if the statistics is good enough
1 mL NaOH	$\text{CaCO}_3 = 100\%$	Bragg R-factor = 5.7 $\chi^2 = 1.9$	Your refinement could still be improved
2 mL NaOH	$\text{CaCO}_3 = 100\%$	Bragg R-factor = 9.6 $\chi^2 = 2.1$	Your refinement could still be improved
9 mL NaOH	$\text{CaCO}_3 = 100\%$	Bragg R-factor = 6.4 $\chi^2 = 1.6$	Your refinement could still be improved
Floating precipitates_trial 1	$\text{CaCO}_3 = 97.2\%$ $\text{NaCl} = 2.8\%$	Bragg R-factor = 9.6 $\chi^2 = 1.8$	Your refinement could still be improved
Floating precipitates_trial 2	$\text{CaCO}_3 = 100\%$	Bragg R-factor = 9.4 $\chi^2 = 1.6$	Your refinement could still be improved
MH 8_ 3 mL NaOH	$\text{CaCO}_3 = 99.7\%$ $\text{NaCl} = 0.3\%$	Bragg R-factor = 8.8 $\chi^2 = 2.0$	$\chi^2$ is low but the high R-factor can be due to a bad structural model and/or a rather poor statistic
MH 11_ 3 mL NaOH	$\text{CaCO}_3 = 100\%$	Bragg R-factor = 7.5 $\chi^2 = 1.6$	Your refinement could still be improved
Mixed Precipitates	$\text{CaCO}_3 = 100\%$	Bragg R-factor = 10.3 $\chi^2 = 2.0$	$\chi^2$ is low but the high R-factor can be due to a bad structural model and/or a rather poor statistic

A pH adjustment test was developed to understand how the calcium and alkalinity changes with pH. Acid (0.1-1.0 M HCl) and base (0.5 M NaOH) were added to 500 mL raw leachate to adjust the pH between 2 and 13, respectively. Alkalinity and calcium were measured at each pH unit and plotted in **Figure 65**. Alkalinity and calcium units were converted to g-moles/L to calculate pAlk and pCa. Where, pY is the negative logarithm of variable Y.

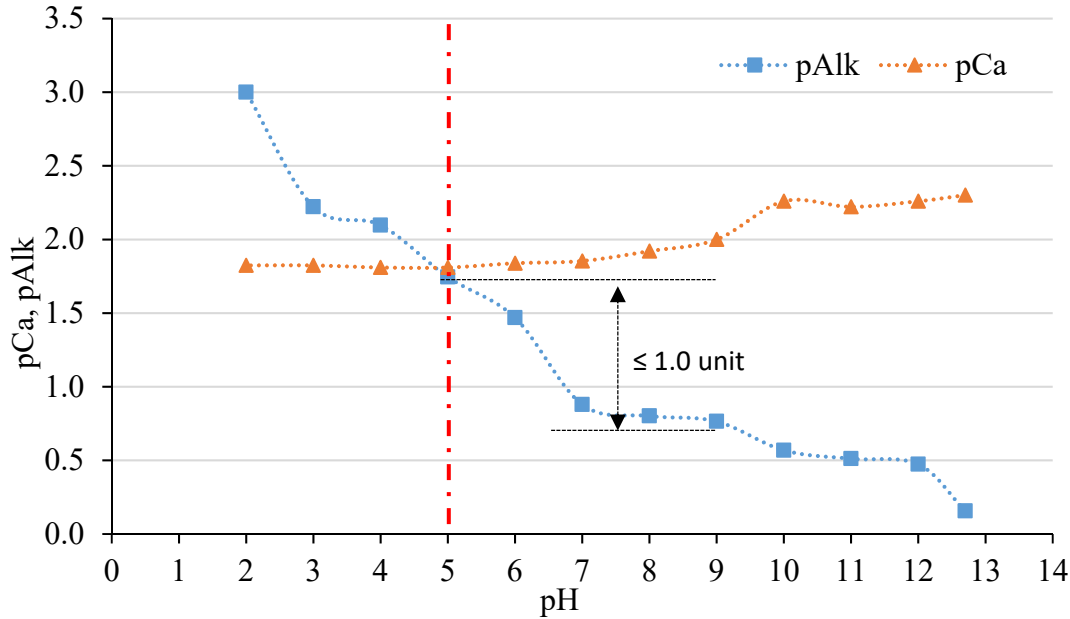


**Figure 65. Alkalinity and calcium concentration changes with pH**

The difference of pH and the  $pH_s$  (saturation pH with respect to  $\text{CaCO}_3$ ) is the Langelier Saturation Index (LSI), a measure of  $\text{CaCO}_3$  precipitation. Calcium concentration and alkalinity are two major influencers in calculating  $pH_s$ . pCa and pAlk are the two additive terms that control the  $pH_s$  and subsequently the LSI considering everything else remains constant. As these two terms increase, the  $pH_s$  increases, which results in a lower LSI value. It is evident from **Figure 65** that, at a pH lower than 5.0,  $pH_s$  is higher and vice versa at a pH higher than 5.0. Therefore, a change in pH from 7.0 to 5.0 results in a  $pH_s$  almost 1 unit lower than that of at pH 7.0 and moves the saturation index towards neutrality ( $0 \leq \text{LSI} \leq 0.4$ ).

### 3.5 Impacts of Microbial Activities on $\text{CaCO}_3$ Scaling

Microbial growth and activities such as production of EPS, biofilm generation, as well as surface adhesion enhance the precipitation of  $\text{CaCO}_3$  in LCS. Disinfection of leachate eliminates the impacts of microbial activities on  $\text{CaCO}_3$  precipitation and thus provides the necessary information to better understand and explain the role of microbial mediation in  $\text{CaCO}_3$  precipitation. Several disinfection methods such as ultraviolet radiation, heat sterilization, and autoclave sterilization were used to disinfect the leachate prior to conducting precipitation experiments in this study. The results are discussed in the following sections.

### 3.5.1 UV Disinfection

To investigate the role of biological activity, UV radiation was tested against water quality impacts (for pH, alkalinity, calcium, total dissolved solids, temperature, sulfides and sulfates to determine LSI/RI) and solids characteristics using the side-by-side leachate loop. To simulate in-situ disinfection conditions, field and laboratory experiments were conducted using a UV disinfection unit to determine the effects of radiation exposure dose on HPC (heterotrophic plate count). A laboratory experiment using a laboratory scale UV source with 2.1 mJ/cm<sup>2</sup>·s achieved an almost 3-log reduction of HPC count within 30 minutes of exposure (**Table 25**).

**Table 25. UV disinfection of leachate using the laboratory setup**

ID	Time, min	DF	Distance, cm	Count (total)	CFU@35°C/48h
C 1:10000		10000	-	88	8,800,000
15/2 Q	15	10	7.55	113	11,300
30/2 Q	30	10	7.55	20	2,000

UV treatment unit with 40 MJ/cm<sup>2</sup>·s fluence to disinfect the leachate was retrofitted in one side of the field scale pipe network in the landfill. An onsite leachate reservoir was set up with about 6-7 ft of head to facilitate gravity flow. In addition, 2 one-inch dia removable pipes were retrofitted in both sides of the outlet to measure the precipitation in both sides (control vs. exposed).

**Table 26** summarizes the leachate quality variation during the field experiment duration (120 minutes), and the leachate quality for the control and treated side remained constant over the experiment duration.

**Table 26. Average water quality parameters from the control and treated side during 120 min experiment**

Parameters	Control		UV treated	
	Average	St. dev	Average	St. dev
pH	7.09	0.05	7.07	0.03
Cond. (mS/cm)	44.01	0.99	44.21	0.44
Sp. Cond. (mS/cm)	40.06	0.28	40.14	0.11
TDS (g/L)	26.05	0.07	26.09	0.07
Temp (°C)	30.17	0.41	30.37	0.41

**Table 27** shows the HPC count of control and disinfected leachate collected at 30, 60, and 90 minutes. It is evident that the UV unit was not performing as expected since no inactivation of

HPC was indicated. Precipitation in the 1-inch dia removable pipe section was also measured and did not follow the expected trend.

**Table 27. HPC count for treated and untreated samples**

Sample ID	HPC/mL
Control	24,000
UV_30 (30 minutes)	20,000
UV_60 (60 minutes)	22,000
UV_90 (90 minutes)	<20,000

A total of three field experiments were conducted, and essentially no disinfection was observed in any of them. This might be related to low transmittance due to high TSS, color, turbidity, and humic/fulvic acid (NOM) content in the leachate.

### 3.5.2 Heat Sterilization

To further investigate the biological trigger, disinfection of leachate using heat sterilization in the laboratory was conducted. The first experiment using heat sterilization was conducted with pump station A leachate, and the initial water quality parameters of the sample are tabulated in **Table 28**. This sample was diluted with groundwater and therefore TDS, alkalinity, and calcium are lower than the typical samples. However, the saturation indices indicate that this sample is still scale forming in nature (LSI > +0.4).

**Table 28. Pump station A leachate water quality parameters and precipitation potential**

Parameter	Control	To be sterilized
pH (standard unit)	7.24	7.25
Temp. (°C)	19.43	19.48
TDS (g/L)	7.756	7.759
Cond. (mS/cm)	10.66	10.68
Sp. Cond. (mS/cm)	11.93	11.93
Ca. hardness (mg/L as CaCO <sub>3</sub> )	650	700
Alkalinity (mg/L as CaCO <sub>3</sub> )	1050	1050
LSI	<b>0.82</b>	<b>0.86</b>
RI	<b>5.60</b>	<b>5.53</b>

**Figure 66** shows the heat sterilized leachate and a visual comparison of control sample and sterilized sample.



**Figure 66. Boiling leachate (left), and visual comparison of sterilized and control leachate (right)**

After 7 days of incubation and water quality measurement, the dry weight of the beaker was measured to estimate the adherent precipitation/scale attached to the beaker surface. **Figure 67** depicts the visual differences between the control samples (from left: 1st and 2nd beaker) and the sterilized samples (from left: 3rd and 4th). It was visible that the sterilized sample had less adherent precipitation. **Figure 68** shows the changes in LSI at different stages of the experiment. It is evident that after 7 days of incubation both the control and sterilized samples reached neutral LSI value ( $0 < \text{LSI} < 0.4$ ). Therefore, the total precipitation during the experiment for both sets of samples was similar. However, the difference observed in **Figure 67** might be attributed to the absence of microbes that may provide the adhesive character.



**Figure 67. Visible adherent scale formation in 250 mL beaker for control (1st and 2nd from left) and sterilized sample (3rd and 4th from left)**

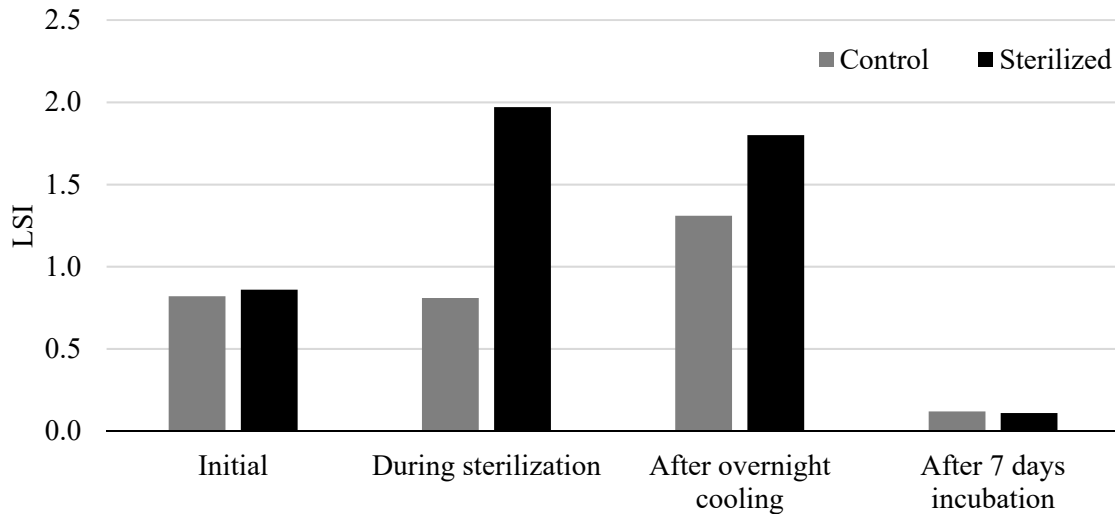


**Figure 68. Changes in Langelier Saturation index (LSI) during different stages of experiment**

Precipitation rate was calculated for both sterilized and control samples. The non-adherent scale is the floating and loose precipitate at the bottom separated by filtration using a 4.5-micron filter. The adherent scale is the precipitate strongly attached to the vessel surface. **Figure 69** shows the comparison of adherent and non-adherent scale formation between control and sterilized sample and confirms that sterilized sample produces less adherent scale/precipitate as observed by visual inspection (**Figure 67**). Although the total precipitation per 100 mL of leachate is a function of the saturation state of the leachate, the observed difference is important to understand the role of microbes in calcium carbonate scale formation.

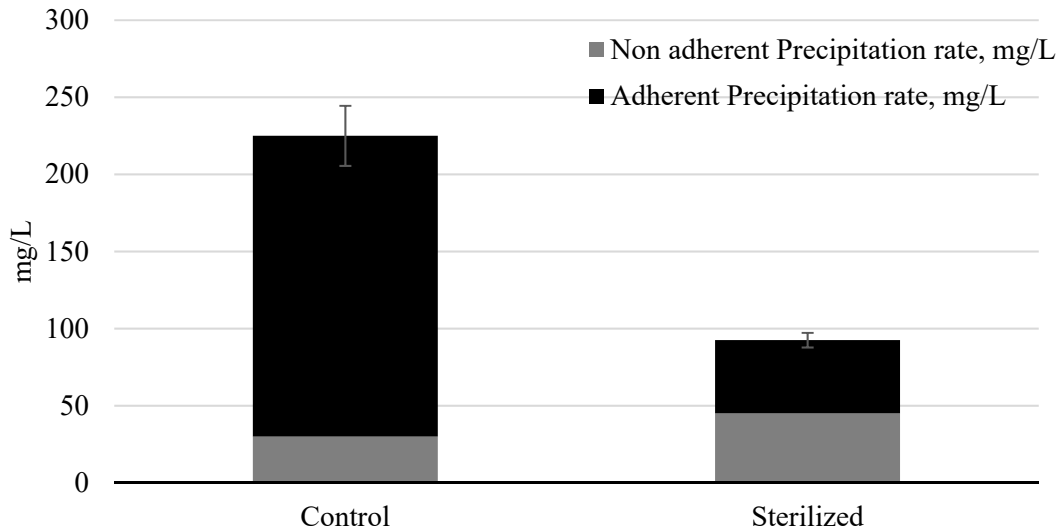


**Figure 69. Precipitation rate obtained from trial 1**

One of the limitations of the first experiment that employed boiling on an open hot plate was the loss of leachate due to evaporation during the sterilization process. For better control of evaporation loss and disinfection efficiency, it was decided to perform autoclaving at 121°C for 30 minutes or sterilizing in an oven at 150°C. To check the disinfection using autoclave and oven, the HPC plate count was measured for samples sterilized both ways. There was no growth in HPC plate for the autoclaved samples (**Figure 70**). However, some growth of bacteria and molds were observed in the oven-sterilized samples at 48-72 hours incubation at 35°C (**Figure 71**). It was suspected that spore formation occurred during the process. In addition, HPC count was also measured after storing the samples in the incubator for 10 days, and HPC count for autoclaved samples was found to be zero, as expected (**Figure 72**). However, oven-sterilized samples showed too numerous to count (TNTC) colonies at 1:1 sample dilution.

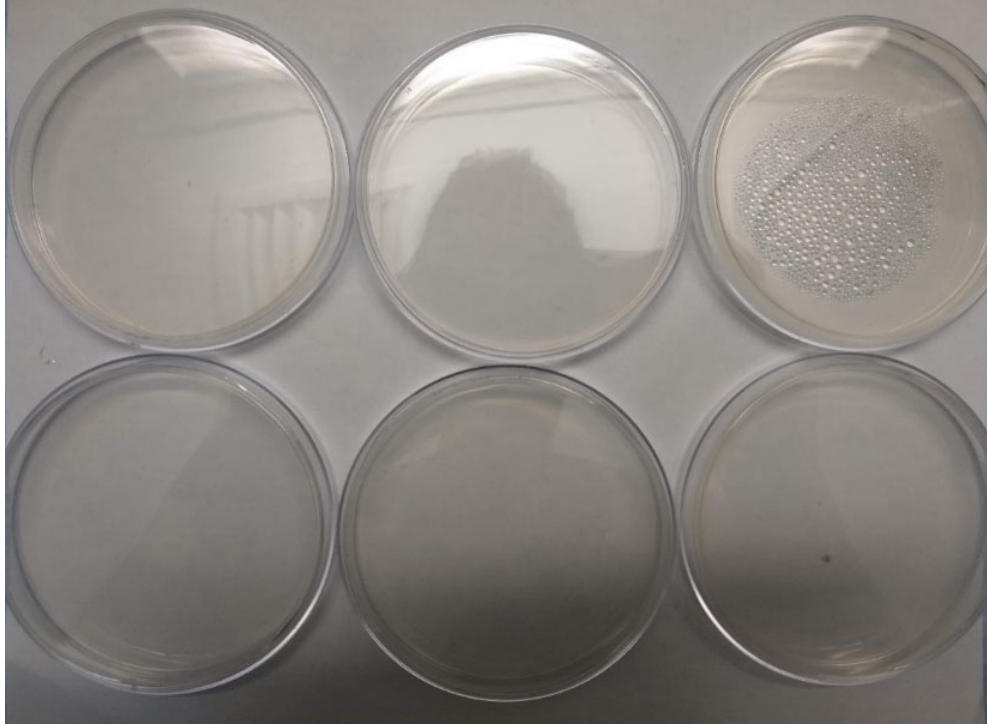


**Figure 70. HPC plates after incubation at 35°C for 48-72 hours (Autoclaved sample)**

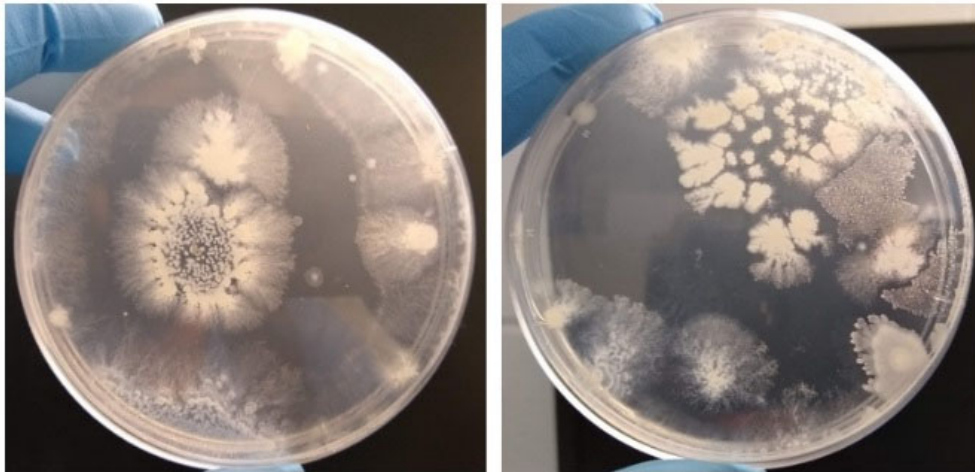


**Figure 71. HPC plates after incubation at 35°C for 48-72 hours (Oven sterilized sample)**

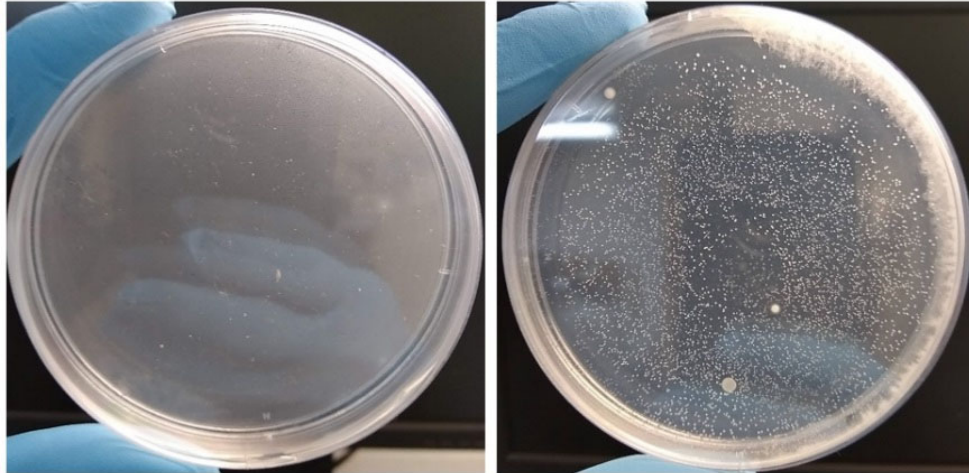


**Figure 72. HPC plates and bacteria growth in 48 hours after with samples stored 10 days at 35°C (Autoclave: left; Oven sterilized: right)**

Visible precipitate formation in the bottle was observed for all samples. However, the adherent scale was visibly less in the case of autoclaved samples (Figure 73).



**Figure 73. Precipitate in the vessel surface and 4.5-micron glass microfiber filters for control, oven sterilized and autoclaved leachate sample from left to right, respectively**

The second trial of sterilization experiments was conducted with higher strength leachate that is more representative of the composite leachates sampled from the SWA historically (TDS: 33,890 mg/L, Ca: 2,750 mg/L as  $\text{CaCO}_3$ , alkalinity: 5,250 mg/L as  $\text{CaCO}_3$ ). The results are presented in **Figure 74**. The total rate of precipitation was lowest (2,390 mg/L) for autoclaved samples; whereas the oven sterilized was the highest (3,460 mg/L) and approximately similar to the control sample (3,300 mg/L). However, average adherent precipitation was maximum for the control sample (2,465 mg/L), which is 2.5 times higher than that of oven sterilized sample (985 mg/L).

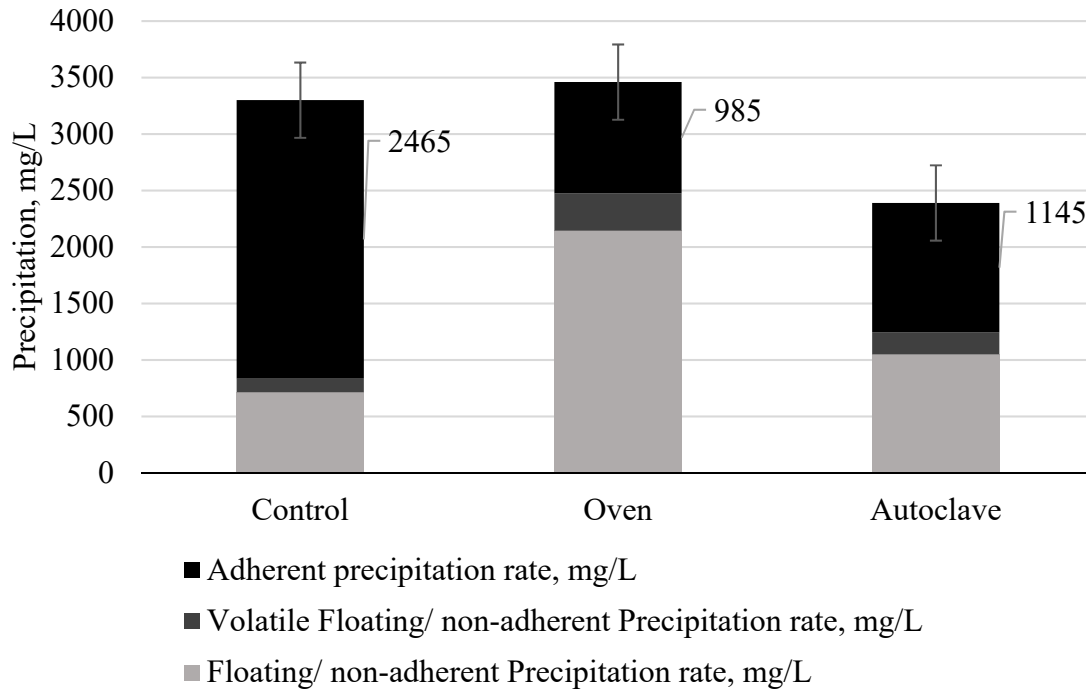


**Figure 74. Precipitation rate obtained from trial 2 with much stronger leachate compared to trial 1.**

In summary, it was evident from the results of trial 1 and trial 2 that the sterilization process reduces the rate of adherent precipitation (which is more difficult to remove). However, further investigation is necessary to better understand the phenomenon.

A further test was developed to understand the importance of aerobic and anaerobic conditions in the formation of adherent precipitation. As observed earlier, pH increases almost two units during the sterilization (autoclave) process due to high temperatures and pressures as well as degasification of carbon dioxide from the leachate. During the aerobic incubation process, the pH stabilizes back towards neutrality with time. During anaerobic incubation, the pH stabilization process is hindered due to the lack of contact with air. Therefore, leachate remains at a higher pH for a longer period and results in a higher amount of adherent precipitate.

Two 100 mL samples were incubated aerobically and two were incubated anaerobically. The result of this experiment is summarized and presented in **Figure 75**. The adherent precipitation with anaerobic incubation was almost three times larger than the samples incubated aerobically.

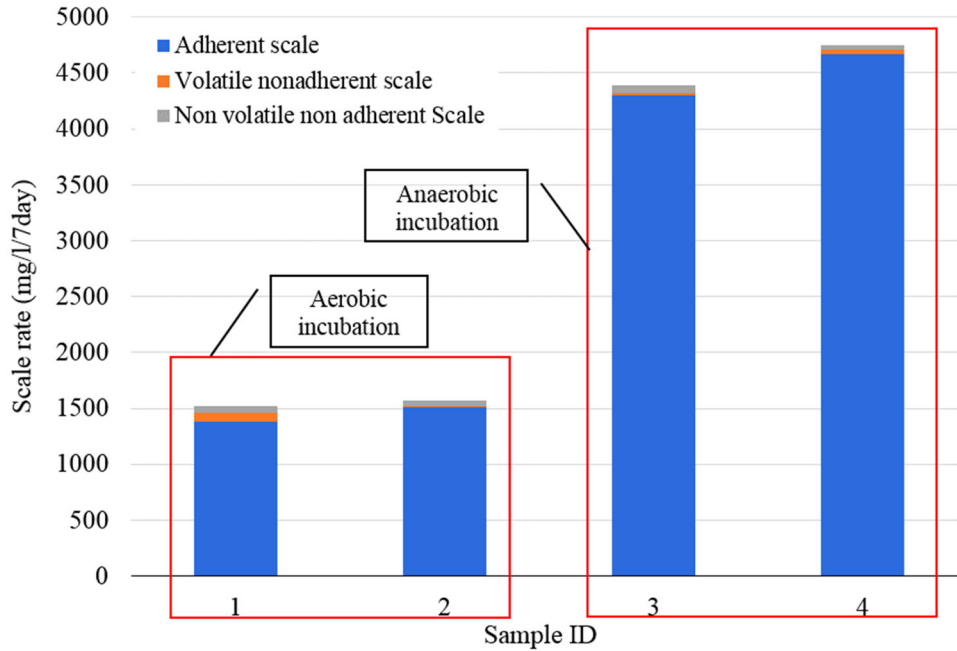


**Figure 75. Precipitation rate of sterilized sample with aerobic and anaerobic incubation**

In this experiment, the incubation period was fixed to 7 days at 35°C. An experiment was conducted for both raw and sterilized leachate with varying incubation periods from 1 to 7 days at 35°C. Results of the experiment are presented in **Figure 76**.

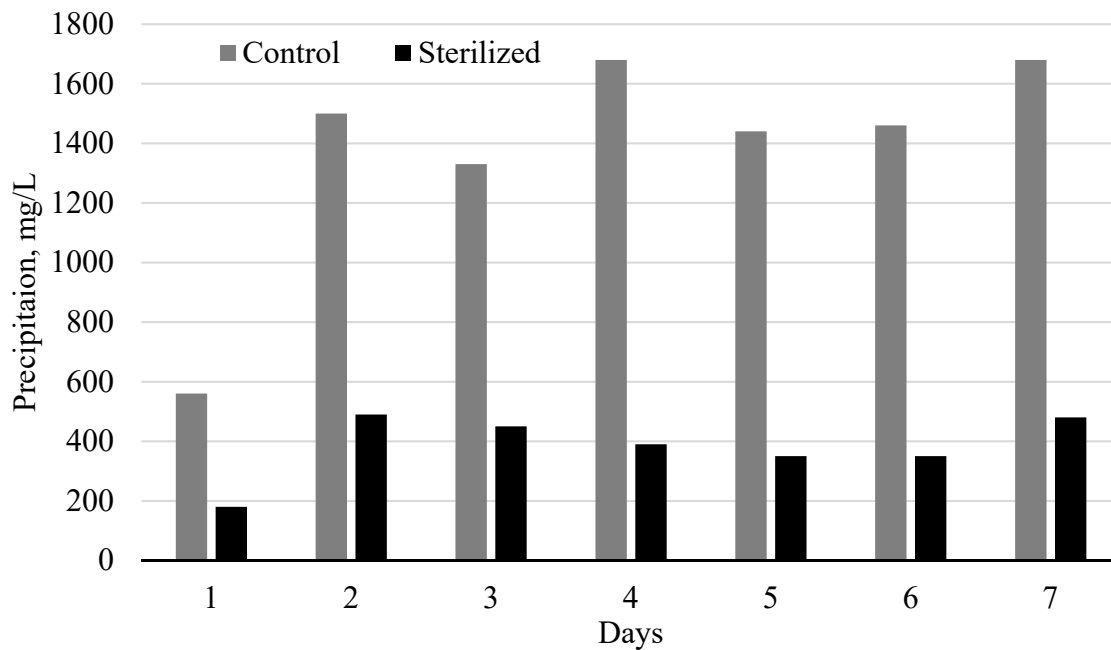


**Figure 76. Precipitation rate of raw and sterilized leachate with different incubation period at 35°C**

In general, larger amounts of precipitation were observed with longer incubation times as expected, However, a clear trend was not observed. It is also evident that 2 days of incubation may be sufficient to record measurable precipitation for further tests. Furthermore, the precipitation rate of sterilized leachate was always lower than that of raw leachate, which is consistent with previous results.

### 3.6 Impacts of Alternate Submerged and Dry Conditions on LCS Clogging

During the UV disinfection experiment using the side by side pipe network, it was observed that a reddish jelly-like layer formed at the pipe surface under submerged conditions. The pipe was kept dry for a week, and the jelly-like layer formed into a hard scale attached to the pipe surface. This leads to the hypothesis that alternating submerged and dry conditions may enhance scale/clog formation in the leachate collection system. This hypothesis was tested in the laboratory. The first trial was started on March 20, 2019, and **Table 29** summarizes the amounts of added leachate required to adjust for the evaporative losses during incubation at different days. Sample 1, which was only adjusted until day 3, corresponds to a two-cycle condition; whereas sample 5 was adjusted until the 19<sup>th</sup> day (six dry and submerge cycle). It was expected that sample 5 will have higher precipitation compared to that of sample 1.

**Table 29. Summary of leachate addition to adjust for the loss due to evapotranspiration**

Sample ID	Initial weight, gram	Additional leachate added, gram					
	Day 0	Day 1	Day 3	Day 5	Day 7	Day 12	Day 19
1	226.38	4.20	10.84	-	-	-	-
2	225.73	5.52	10.87	9.63	-	-	-
3	227.16	6.64	11.97	11.51	12.58	-	-
4	226.75	4.75	13.01	12.19	12.36	32.42	-
5	223.98	5.86	12.11	10.98	10.50	62.42	44.98

The results obtained in the first trial are presented in **Figure 77** (black bars). Sample 1 was exposed to the lowest number of dry and submerged cycles; whereas sample 5 was exposed to the highest number of cycles. The precipitation in sample 5 was expected to be the highest among the samples and that of sample 1 to be the lowest. The result obtained from the first trial generally follows the expected trend except for the precipitation (lower than expected) in sample 3, which could be an anomaly or resulted from the sample handling and preparation during the experiment.

A limitation of the results of this experiment is the addition of leachate to replicate the dry and submerged conditions. The addition of leachate provides more calcium and carbonate to form precipitates, and the result does not provide definitive evidence. Therefore, trial 2 was planned to eliminate this issue and add groundwater instead of leachate to better replicate the dry and submerged conditions.

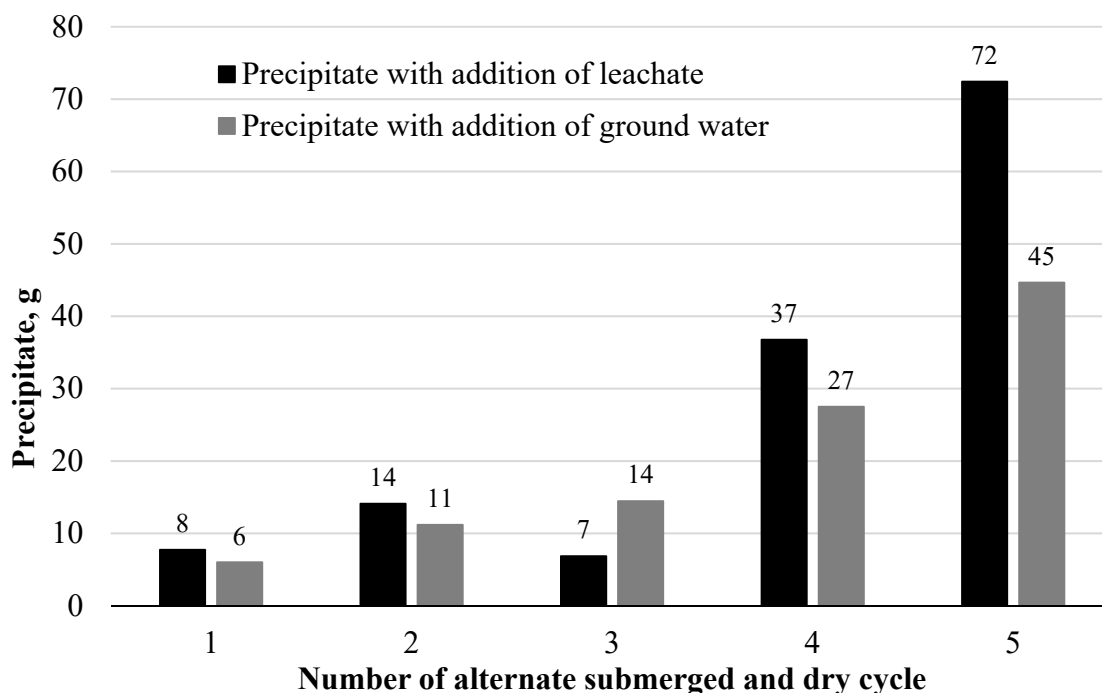


**Figure 77. Precipitation due to submerged and dry cycle in the laboratory**

Moreover, some of the beakers were completely dry and left visible amounts of salt precipitation at the bottom, which was one of the experimental limitations. Therefore, a further test was conducted with a similar setup but with 200 mL of leachate sample in each beaker instead of 100 mL. This next trial was conducted in May 2019. The summary of added groundwater to replicate the dry and submerged conditions is presented in **Table 30**.

**Table 30. Summary of groundwater addition to adjust for the loss due to evapotranspiration**

Sample ID	Initial weight, gram	Additional groundwater added, gram					
	Day 0	Day 1	Day 3	Day 5	Day 7	Day 11	Day 15
1	326.36	4.63	11.21	-	-	-	-
2	325.77	5.62	1.94	10.20	-	-	-
3	327.02	5.74	11.76	11.32	12.36	-	-
4	326.75	4.94	12.95	12.37	12.58	30.26	-
5	324.13	5.58	12.14	10.98	11.63	34.38	46.32

The final dry weights of the precipitates and the beaker were measured, and the amount of precipitation was obtained for each of the samples and presented in **Figure 77** (ash bars). It is evident from the result that cycles of dry and submerged conditions enhance precipitation, which supports the hypothesis. The possible explanation for this outcome is as follows:

1. The initial submerged condition facilitates the initial precipitation of calcium carbonate and the formation of pioneering biofilm attached to the pipe surface due to the microbial activity in leachate
2. The biofilm hardens with the calcium carbonate skeleton inside while dry and forms a thin hard layer on the pipe surface
3. When the next submerged cycle starts, the surface already having a layer acts as a preferred precipitation and biofilm formation zone, and the process continues to deposit layer upon layer of precipitates inside the pipes, over a series of cycles until the growth becomes a clog.

### 3.7 Impacts to the Deep Injection Well

A mass balance analysis was conducted based on the leachate flow data provided from March to July, 2017. A weighted average of each water quality parameter is calculated based on the respective flow to estimate the water quality data and compared with the actual water quality from laboratory analysis. A summary of the mass balance is presented in **Table 31**.

**Table 31. Summary of mass balance analysis based on the flow going to the deepwell in March 2017**

Water Source	AVG monthly Q 2017-2018 MG/month	MIN monthly Q 2017-2018 MG/month	MAX monthly Q 2017-2018 MG/month	pH	TDS	Alk	Ca	Cond	Temp	pHs	LSI	RI
P/S A	2.5	0.9	6.8	7.1	17,400	1,574	3,175	23.3	29.0	5.5	1.6	3.9
P/S B	2.7	1.3	6.9	7.2	15,300	4,810	3,280	30.8	32.6	4.9	2.3	2.6
P/S C	1.1	0.7	1.5	7.6	3,561	1,750	775	7.4	31.1	5.9	1.8	4.1
P/S D	1.1	0.6	1.8	7.0	3,608	2,100	600	8.5	30.0	5.9	1.1	4.8
DYER	4.6	0.6	18.4	7.1	2,303	1,618	565	3.6	28.4	6.0	1.1	4.8
CISW	0.7	0.3	1.1	7.4	600	970	470	1.1	28.7	6.1	1.3	4.8
ISW	1.7	0.2	3.3	7.4	600	970	470	1.1	28.7	6.1	1.3	4.8
Plant water	7.5	6.9	7.9	7.2	3,644	155	1,364	4.6	32.5	6.7	0.9	5.8
NEFCO	6.1	5.1	7.4	5.8	1,970	500	530	7.4	35.1	6.7	-0.6	7.0
AVG	28.0			7.4	5,152	1,252	1,270	9.2	31.6	5.8	1.6	4.3
MIN		16.5		7.3	4,676	915	1,253	8.7	32.7	6.0	1.3	4.6
MAX			55.0	7.5	5,882	1,622	1,336	10.1	30.6	5.7	1.8	4.0
DEEP WELL				7.0	6,200	1,190	1,110	11.70	33.7	5.9	1.1	4.8

Based on the analysis, the calculated saturated indices (LSI and RI) agree with the actual measured indices as sampled in the field. The saturation indices also did not change significantly from 2015-2016 (actual LSI changed from +1.25 to +1.10). According to the calculations, the contribution from P/S B supplies the most scale-forming or lowest water quality for clog formation, which is balanced by the contribution of the NEFCO wastewater, which has the most corrosive water that is least likely to form clogs. The alkalinity for P/S B is higher than the other leachates. Other titratable bases are known to contribute to alkalinity, such as silicates, HS<sup>-</sup>, organic anions, etc.

(Stumm and Morgan, 2012). It is possible that these effects need to be accounted for in order to calculate a more accurate LSI or RI value.

Each flow stream was monitored at the wet well prior to final discharge to the deep injection well. The mass balance chart was updated to compare the estimated LSI based on flow and water quality of each individual streams with actual LSI calculated from the wet well leachate sample. A summary of the mass balance is presented in **Table 32**.

It was found that the actual LSI of wet well mixed leachate matches very closely with the mass balanced LSI (actual LSI = +1.1, mass balanced LSI = +0.9 to +1.0).

**Table 32. A summary of the mass balance based on individual waste streams going to the injection well**

Water Source	AVG monthly Q 2017-2018 MG/month	MIN monthly Q 2017-2018 MG/month	MAX monthly Q 2017-2018 MG/month	pH	TDS mg/L	Alk mg/L as CaCO <sub>3</sub>	Ca mg/L as CaCO <sub>3</sub>	Cond mS/cm	Temp °C	pH <sub>s</sub>	LSI	RI
P/S A	3.0	0.6	6.8	7.04	17,400	1,574	3,330	24.19	28.7	5.46	1.6	3.9
P/S B	3.5	1.3	7.3	6.85	6,670	3,058	630	12.04	34.2	5.76	0.7	5.5
P/S C	1.4	0.7	2.7	7.61	3,561	1,750	775	7.39	31.1	5.85	1.8	4.1
P/S D	1.3	0.6	2.2	7.03	3,608	2,100	600	8.52	30.0	5.90	1.1	4.8
DYER	1.7	0.6	3.8	7.11	2,303	1,618	565	3.55	28.4	5.99	1.1	4.8
CISW	0.8	0.1	1.4	6.95	1,015	371	404	1.29	29.0	6.65	0.3	6.4
ISW	1.8	0.2	3.4	6.95	1,015	371	404	1.29	29.0	6.65	0.3	6.4
Plant water	6.9	5.0	7.9	7.17	3,644	155	1,364	4.57	32.5	6.65	0.9	5.8
NEFCO	5.9	4.6	7.4	5.39	1,153	400	300	4.37	37.5	6.65	-1.3	7.9
AVG	26.2			7.22	4,176	1,010	972	6.82	32.3	6.13	0.9	5.2
MIN		13.7		7.10	3,769	733	984	6.34	33.6	6.15	1.0	5.3
MAX			42.8	7.35	4,721	1,341	986	7.50	31.1	6.05	0.9	4.9
DEEPWELL				7.00	6,200	1,190	1,110	11.70	33.7	5.9	1.1	4.8

In addition, samples were collected along with AECOM/URS during the IW-1 brushing event (**Figure 78**) on February 28, 2018. Three composite samples and duplicates were collected (500 mL each) in 500 mL HDPE sample bottles for water quality analyses at 0-200 ft, 200-1500 ft, and 1500-2900 ft. In addition, two 5-gallon buckets (**Figure 78, d**) were filled with sample from each depth and retained for approximately 10 minutes to allow the brushed particles to settle out. The settled particles were collected from the bottom of the bucket in a 500 mL HDPE sample bottle and transported to the FAU Boca Raton campus for subsequent mineralogical analyses.



**Figure 78. IW-1 brushing and sample collection for mineralogical testing (a. brushing equipment setup (top left), b. a closer view of the setup and the sample port (green flexible hose) (top right), c. sample port assembly (bottom left), and d. 5-gallon sampling bucket filled with sample to collect settled particles.**

To investigate the mineral content of solid samples collected from three depths from the SWA industrial deep injection well, water quality and x-ray diffraction tests were conducted. During collection of each sample, field water quality data (pH, conductivity, water temperature, TDS, DO) were obtained using a calibrated YSI 556 multiparameter meter. Turbidity of each sample was also recorded in the field using a portable Hach 2100Q turbidimeter. The water quality parameters are summarized in **Table 33**.

**Table 33. Field data using YSI 556 multiparameter meter and turbidimeter on February 28, 2018.**

Description	Water quality parameters	Unit	Sample		
			D1 (0-61 m)	D2 (62-457 m)	D3 (458-884 m)
Field parameters*	pH	standard unit	7.98	7.10	7.10
	Sp. Conductance	mS/cm	0.6	9.8	18.8
	Conductivity	mS/cm	0.6	9.9	20.2
	TDS (field)	mg/L	350	6,340	12,210
	Water temperature	°C	25.8	26.0	28.9
	Turbidity	NTU	113	169	162
	Dissolved oxygen	mg/L	2.2	<1.0	<1.0
	ORP	mV	-38	-404	-415
Laboratory parameters#	TDS (gravimetric)	mg/L	390	5,700	11,930
	Calcium (Ca)	mg/L as CaCO <sub>3</sub>	250	1,125	1,600
	Alkalinity	mg/L as CaCO <sub>3</sub>	150	2,175	2,125
	Chloride (Cl <sup>-</sup> )	mg/L	350	2,375	5,575
Saturation Indices	pH <sub>s</sub>	standard unit	7.2	5.8	5.7
	LSI	unitless	0.8	1.4	1.4
	RI	unitless	6.4	4.4	4.3

\*All field parameters presented are the average of three readings recorded during sampling

#All laboratory parameters presented are the average of the sample and the duplicate collected at each depth range

Dissolved oxygen measurements were indicative of an anaerobic (reducing) environment, which was also supported by the negative ORP measurements. The pH observed from the intermediate zone (D2) and also the injection zone (D3) was 7.10, which matches with historical pH reported from similar composite leachate collected from this injection wet well in previous work (Shaha et al. 2019; Shaha 2016; Townsend et al. 2016). However, pH observed for the surface zone sample (D1) was 7.98 and was slightly higher than expected. It is likely that this reading was caused by exposure to air or carbon dioxide degasification, as seen in prior work (Shaha et al. 2019; Shaha 2016) in which pH spikes of up to 1.0-unit were observed in leachates depending on the alkalinity. Briefly, the lower the alkalinity, the more rapidly the pH climbs with exposure to air and subsequent degasification of carbon dioxide. From previous monitoring conducted by the researchers (Shaha et al. 2019; Shaha 2016, Townsend et al. 2016), wet well sampling averaged 1,200 mg/L as CaCO<sub>3</sub> for alkalinity, but for the D1 sample, the alkalinity was measured at only 150 mg/L as CaCO<sub>3</sub>. Saturation carbon dioxide concentrations are proportional to pressure. Therefore, as soon as the pressure changes, so does the available carbon dioxide in the leachate and subsequently the pH.

The water temperature reading recorded at the injection zone (D3) was 28.9°C, which was about 3 degrees higher than the other two samples. This is expected since the temperature increases with

depth in the subsurface such that the water temperature at the borehole depth (610-915 m below surface) of the well is expected to be between 80-90°F (26-32°C) (Loeb and Poupon 1965, McKinley and Thornhill 1994).

The surface zone sample (D1) showed low TDS (390 mg/L), alkalinity (150 mg/L as CaCO<sub>3</sub>), and calcium (250 mg/L as CaCO<sub>3</sub>). In 2017-2018, the average TDS, alkalinity, and calcium in the deep injection wet well samples were found to be 6,200 mg/L, 1,200 mg/L as CaCO<sub>3</sub>, and 1,100 mg/L as CaCO<sub>3</sub>, respectively. This nearly 10-fold dilution may have been a signal of stratification in the injection tubing. Stratification occurs because higher salinity water is denser and sinks to the bottom, while lower salinity water is less dense and tends to rise to the surface. However, this would not have any adverse impact on the mineralogical analysis of the solid samples collected and analyzed by XRD.

The gravimetric solids analysis (TDS) performed in the laboratory matched the field TDS obtained using the YSI 556 multiparameter meter within relative error less than 10%. All other data obtained from the samples collected from the intermediate zone (D2) and from the injection zone (D3) were within the expected ranges, and QA/QC samples were less than 3% error for alkalinity, calcium, and chloride. LSI in the intermediate zone and the injection zone was 1.4, which indicates supersaturation with respect to CaCO<sub>3</sub>. RI values at the same depths were 4.3-4.4, indicating the scale-forming nature of the samples.

A summary of the XRD analysis and Rietveld refinement using MATCH! 3.9 is presented in **Table 34** and **Figure 79**.

**Table 34. Summary of XRD pattern analysis and Rietveld refinement using MATCH! 3.9**

Sample ID	Compounds	Coefficients	Notes
<b>QA/QC</b> (pure calcite)	CaCO <sub>3</sub> = 100%	Bragg R-factor = 5.6 $\chi^2 = 0.9$	Your refinement could still be improved
<b>D1</b> "Surface zone" (0-61 m) 0-200 ft	Calcite, CaCO <sub>3</sub> = 37.7% Quartz, SiO <sub>2</sub> = 33.1% Magnetite, Fe <sub>3</sub> O <sub>4</sub> = 29.2%	Bragg R-factor = 38.5 $\chi^2 = 0.6$	$\chi^2$ is not high but the model could be still improved if the statistics is good enough
<b>D2</b> "Intermediate zone" (62-457 m) 200-1500 ft	Halite, NaCl = 67.7% Calcite, CaCO <sub>3</sub> = 21.8% Sylvite, KCl = 10.6%	Bragg R-factor = 18.8 $\chi^2 = 0.9$	$\chi^2$ is not high but the model could be still improved if the statistics is good enough
<b>D3</b> "Injection Zone" (458-884 m) 1500-2900 ft	Halite, NaCl = 66.5% Calcite, CaCO <sub>3</sub> = 26.6% Sylvite, KCl = 6.9%	Bragg R-factor = 10.1 $\chi^2 = 0.8$	$\chi^2$ is low but the high R-factor can be due to a bad structural model and/or a rather poor statistic

For comparison purposes, a pure calcite ( $\text{CaCO}_3$ ) sample was analyzed using XRD. The search match calculation and Rietveld refinement confirmed the composition to be 100% calcite. For the three depths, it was evident that calcite was present. In addition, the presence of salts (halite -  $\text{NaCl}$  and sylvite -  $\text{KCl}$ ) in the matrix increased with depth as the salinity increased. In the solids collected from the surface zone sample (D1), approximately 33% quartz ( $\text{SiO}_2$ ) was identified. This was expected because  $\text{SiO}_2$  is typically found in sand, which is a common material found in leachate collection systems. Magnetite ( $\text{Fe}_3\text{O}_4$ ) was also present in the D1 sample. This too was expected because of the availability of the dissolved oxygen and also iron are common cations in the injectate.

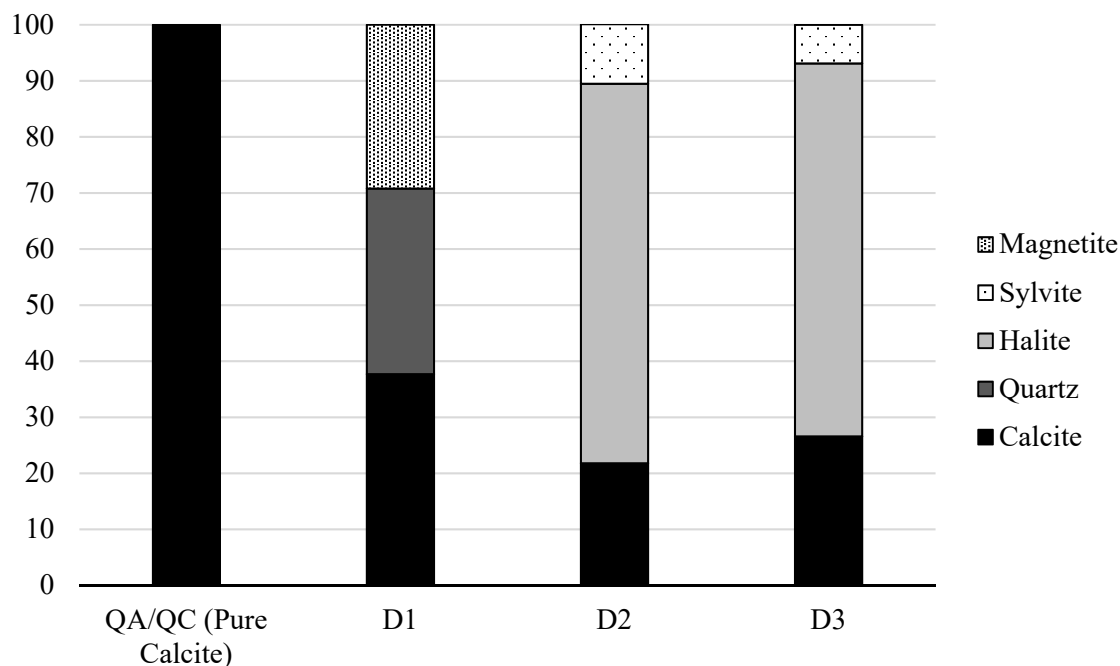


**Figure 79. Stacked bar chart showing the composition of the samples at each depth compared to a pure calcite QA/QC standard**

To determine the possible cause(s) of biofilm formation in the SWA deep injection well, three samples were collected in duplicate from three depths (approximate depth of 0-200 ft, 200-1500 ft, and 1500-2900 ft) for microbial analysis. Quality control standards were also collected and analyzed. Metagenomic DNA samples were subjected to shotgun, deep sequencing protocol and analyzed. Over 75 million genomic reads were obtained after quality filtering, providing sufficient span to capture the most representative members of the microbiota in the injection well.

In terms of microbiological composition, there was no algae found in any of the samples as expected, since no photosynthetic light sources are available inside the injection well. The Chao alpha diversity indices for bacteria, viruses and protozoans were highest at 0-61 m and gradually declined with increasing depth. A combination of factors, including nutrient availability, obligate

anaerobiosis (microbes that require the absence of oxygen to proliferate) and pressure to a lesser extent can explain this. Increasing depth typically means less available electron acceptors and readily biodegradable nutrients, which favors the richness of only a few specialized microbes. The prevalent species at 2900 ft are not barophilic organisms that thrive at high pressures, rather they are sulfate reducing bacteria involved in anaerobic dissimilatory sulfate metabolism. Methanogenic archaea and sulfate-reducing bacteria both of which are anaerobic biofilm producers were the most prevalent members of the prokaryotic community at all depths. *Methanosarcinae* spp. increased with increasing depths unlike other archaea. The principal coordinate analysis plot based on Bray-Curtis index of the relative abundance of the various microbial taxa shows a non-pathogenic biofilm-producing *Entamoeba dispar* was the most prevalent member of this microbial domain (>30%) in all samples but was highest at the 200-1500 ft depth (Meeroff et al. 2019).

## 4 CONCLUSIONS

### 4.1 Summary of Findings

Leachate used in this study to feed the pipe network as well as to conduct the laboratory experiments were collected from PS-A, PS-B, MH 14, MH 13, MH 12, MH 11, MH 10, MH 9, MH 8, MH 6, and MH 5. PS-A leachate consists of leachate from cells 13, 11, 9, 8, and 5 along with gas condensate as well as groundwater used for dilution (west side), whereas PS-B contains leachate from cells 14, 12, 10, and 6 along with other influent and groundwater (east side). Leachate characteristics (average and the range of water quality parameters) in this study are consistent with fairly high conductivity, an indication of high dissolved ion concentration.

X-ray diffraction analysis of six historical clogs/bio rock/precipitates confirms that the major component of the precipitate is calcium carbonate, which agrees with the literature reviewed. Although the samples were different visually, the compositions are more or less similar, which suggests that these precipitates are triggered by different factors and formed in a different chemical environment, giving them different appearances even though the composition remains the same. Alternatively, the different appearance could be related to the highly variable nature of the leachate itself.

Leachate clogging, in other words, calcium carbonate precipitation in LCS, is a complex biogeochemical process that appears to depend on several factors that include but not limited to pH, temperature, chemical strength of leachate/saturated and unsaturated condition, presence of catalysts (e.g., urease or carbonic anhydrase), and the flow regime in LCS.

The flow regime in LCS is the overall leachate flow condition that involves the characteristics of turbulence during leachate flow, aeration, pipe surface irregularity, redox conditions, dilution with groundwater, and stagnation of leachate. During the study period (2017-2019), samples were collected from critical points of the LCS that included manholes, pump stations, injection wet well, and NEFCO wastewater. Water quality analyses of these samples demonstrated that all leachate samples have  $LSI \geq +0.40$ , indicating supersaturation with respect to calcium carbonate precipitation. This was true except for the NEFCO wastewater, which had a negative LSI indicative of undersaturation. The addition of groundwater in the LCS to dilute the leachate reduces the precipitation potential as the leachate flows downstream, which reduces further in the deep well by the addition of NEFCO wastewater. Furthermore, having more flow helps to reduce stagnant conditions in the gravity collection lines upstream of the wet well and pump stations and thus reduces crystal formation. Theoretical mass balance analysis using NEFCO water as an alternative to groundwater in dilution purposes identifies NEFCO water as a potential alternative to neutralize the precipitation potential.

NEFCO wastewater having total suspended (TSS) solids in the range of 400 to 600 mg/L (more than double or even triple in some instances compared to leachate) and the adhesive nature of those

solids is a concern. This amount of solids loading to the gravity collection system requires a solids separation method before contemplating the use of NEFCO water for dilution of leachate. Cyclone separation is a common physical method for solid-liquid separation. Preliminary tests using a custom-built laboratory scale cyclone separator reduced both turbidity and TSS (turbidity reduction  $\geq 32\%$ , TSS reduction  $\geq 69\%$ ) in just 10 minutes. Based on the 6 million gallons/month NEFCO wastewater flow with 500 mg/L of TSS and 70% TSS removal, approximately 580 lb/day of solids would need to be handled if cyclone pretreatment were instituted.

The pH of leachate in the LCS is influenced by several factors including CO<sub>2</sub> equilibria in leachate, exposure to air, mechanical turbulence (500 rpm), as well as aeration with air, which were all investigated in this study. These factors increase leachate pH at variable rates except for the addition of carbon dioxide, which reduces the pH of leachate. Based on the precipitation testing conducted in this study using pH adjusted samples with the aforementioned methods, it is evident that initial higher pH resulted in a higher ( $\geq 15$  times more) “hard” scale formation that was difficult to remove.

Also, a set of pH adjustment tests was conducted by adding NaOH to the leachate, and subsequently, measuring the precipitation per 100 mL and the saturation indices. Although the immediate precipitation due to the higher pH reduces the calcium and alkalinity of leachate, pH also dictates the LSI calculation, which results in a higher LSI value. After 7 days incubation, the pH of all samples stabilizes towards neutral pH, CaCO<sub>3</sub> precipitates triggered by higher concentrations of carbonate ions present in the solution results in a lower and more stable LSI value for all the samples. It is important to notice that even though the precipitation potential reduces in day 7, the leachate samples remain scale-forming in nature, and a sudden change in the chemical equilibrium can cause further precipitation.

The precipitates obtained from the pH adjustment experiments were analyzed using a PXRD unit and post-processed using MATCH! 3.90 and fullprof suite to identify the components as well as their relative percentages. It is evident from the analysis that the major component of the precipitates is CaCO<sub>3</sub> ( $\geq 97.2\%$ ) with some salts and does not depend on the initial pH, method of the pH adjustment, or the type of precipitates that formed (floating or submerged in leachate).

Microbial growth and activities such as the production of EPS, biofilm generation, and surface adhesion favor the precipitation of CaCO<sub>3</sub> in LCS. To eliminate the impacts of microbial activity on CaCO<sub>3</sub> precipitation and characteristics of the precipitate, several disinfection methods such as ultraviolet radiation, heat sterilization, and autoclave sterilization were tested to disinfect the leachate before conducting precipitation experiments. UV disinfection did not perform as expected, and essentially no disinfection was observed in the field. This was likely related to low transmittance due to high TSS, color, turbidity, and humic/fulvic acid (NOM) content in the leachate. Heat sterilization and sterilization using autoclave or oven successfully disinfected the

leachate, which was confirmed by HPC plate count. Two types of scale formed during these experiments; adherent precipitates that stick to the surfaces, and non-adherent or loose scale that either floats along the air-water interface or deposits at the bottom. It is found that the amount of adherent precipitation is approximately 2-3 times lower in sterilized or disinfected leachate compared to that of the control sample. These findings confirm the important role of microorganisms in the formation of problematic precipitates and that the adhesive properties of microbial EPS enhance the adherent characteristics of precipitates, which tend to magnify the clogging issue exponentially.

In general, larger amounts of precipitation were observed with longer incubation times as expected. It is also evident that 2 days of incubation may be sufficient to record measurable precipitation for further tests. Furthermore, the precipitation rate of sterilized leachate was always lower than that of raw leachate, which is consistent with previous results.

The hypothesis that alternating submerged and dry conditions may enhance scale/clog formation in the LCS was tested in the laboratory. Alternating cycles of dry and submerged conditions were observed to enhance the precipitation. The initial submerged condition facilitates the precipitation of calcium carbonate and the formation of biofilm attached to the pipe surface due to the microbial activity in leachate. The biofilm hardens with the calcium carbonate skeleton inside while dry and forms a thin hard layer at the pipe surface. When the next submerged cycle starts, the surface already having a layer acts as preferred precipitation and biofilm formation zone, and the process continues to deposit layer upon layer of precipitates inside the pipes until the structure sloughs off or is removed.

The leachate characteristics in the LCS, operational changes, addition of chemicals, addition of groundwater for dilution purposes, excessive turbulence or aeration, and stagnation in the system also potentially impact the function of the deep injection well. Higher precipitation potential, and/or microbial growth and activity of the injectate (mixed leachate solution from all the sources) reduces the injectivity of the well and results in frequent cleaning or brushing of the well. Based on the leachate water quality and flow data, a mass balance analysis was developed to predict the precipitation potential of mixed leachate. The mass balanced LSI of the wet well sample was found to be consistent with the actual wet well LSI that was measured in the field.

To investigate the mineral content, solid samples collected from three depths; a) surface zone (0-200 ft/D1), b) intermediate zone (200-1500 ft/D2), and c) injection zone (1500-2900 ft/D3) from the SWA industrial deep injection well, water quality and x-ray diffraction tests were conducted. LSI in the intermediate zone and the injection zone was 1.4, which indicates supersaturation with respect to  $\text{CaCO}_3$ . For the three depths, it was evident that calcite was present. Besides, the presence of salts (halite -  $\text{NaCl}$  and sylvite -  $\text{KCl}$ ) in the matrix increased with depth as the salinity increased. Solids collected from the surface zone sample (D1) contained approximately 33%

quartz (SiO<sub>2</sub>). This was expected because SiO<sub>2</sub> is typically found in sand, which is a common material found in leachate collection systems. Magnetite (Fe<sub>3</sub>O<sub>4</sub>) was also present in the D1 sample. This too was expected, because of the availability of the dissolved oxygen and iron in the injectate.

Microbial analysis of the samples collected from the deep injection well showed over 75 million genomic reads using metagenomic DNA samples subjected to a shotgun, deep sequencing protocol, and analysis. In terms of microbiological composition, there were no algae found in any of the samples as expected. The prevalent species at the injection zone are not barophilic organisms that thrive at high pressures, rather they are sulfate-reducing bacteria involved in anaerobic dissimilatory sulfate metabolism. Methanogenic archaea and sulfate-reducing bacteria, both of which are anaerobic biofilm producers, were the most prevalent members of the prokaryotic community at all depths. A non-pathogenic biofilm-producing *Entamoeba dispar* was the most prevalent member of the microbial domain (>30%) in all samples but was highest at the intermediate zone.

#### **4.2 Recommendations**

The main limitation of this study is the number of variabilities from the daily operation and maintenance of the landfill, such as jetting, acid washing, etc., which changes the leachate characteristics significantly and thus affects the reproducibility of experimental data. In addition, sample characteristics from the same location of the landfill vary notably between the sampling events. Also, several new ideas and hypotheses were introduced and tested in this study. Further confirmation of the findings need to be replicated with a similar setup to provide more robust evidence from a wider range of samples to support the conclusions.

The sample collection and preparation methods have a strong effect on XRD/XRF analysis and Rietveld refinement. The solids can be analyzed with Inductively Coupled Plasma with Optical Emission Spectroscopy (ICP-OES) or Mass Spectrometry (ICP-MS) to confirm the elemental analysis. ICP-MS has very high sensitivity (0.1 µg/L) which enables it to identify minor impurities ignored in this study and may help to better understand the clogging mechanism and thus help to pinpoint the most effective control methods.

The flow regime in the LCS plays a vital role in the leachate clogging and its control strategies. The variability in the flow regime is one of the important causes of the clogging issue. Any operational changes or unavoidable circumstances that impact the flow regime can imbalance the local or overall chemical and biological equilibrium of leachate and thus enhance precipitation. Therefore, it is recommended to assess the impacts of any operational changes in the LCS carefully for subsequent impact on the clogging potential of leachate.

Additionally, pipe surface characteristics and materials can have an important impact on the flow near the air-water interface and the pipe walls, which can influence the precipitation. Literature review on the application of hydrophilic and hydrophobic materials in pipe surfaces suggests that these treatments impact the interaction between fluids and the flow surfaces. There is no evidence found regarding the application of surface treatment in the leachate collection system to control fouling. However, a laboratory test with treated pipe surfaces is recommended to provide valuable information on the effectiveness of such treatments.

From empirical evidence, the addition of dilution water is found to be beneficial in limiting clogging of the leachate collection system; however, the saturation indices do not indicate sufficient improvement to actually prevent scale formation. The calculated LSI value of the diluted leachate was in the range of +1.5 to +1.9, which is substantially above the target LSI of +0.4 that would essentially eliminate scaling. Therefore, the observed improvements of dilution may be related more to the increased flow (and less stagnation) in the pipes than its impact on water quality. This finding may suggest that additional flows regardless of water quality may be beneficial in limiting clogging impacts in the LCS.

NEFCO wastewater that has negative LSI (undersaturated) can be considered as an alternative or a supplement to the groundwater used for dilution purposes. Theoretical mass balance analysis using NEFCO wastewater in dilution purposes identifies NEFCO water as a potential alternative to neutralize the precipitation potential. This also eliminates the limitation of the maximum allowable groundwater flow rate (100 gpm), which is insufficient to dilute the combined leachate from a water quality perspective. It also helps to reduce the overall leachate flow going down the deep injection well by reducing the addition of groundwater. However, NEFCO wastewater having total suspended (TSS) solids in the range of 400 to 600 mg/L (more than double or even triple in some instances compared to leachate) and the adhesive nature of those solids is a concern. A proper solid separation method (mechanical or chemical) needs to be implemented before considering NEFCO wastewater as an alternative. Besides, the adhesive nature of the solids and the microbial community of NEFCO wastewater should also be taken into consideration, as these may create an unintended imbalance in the leachate chemistry and potentially worsen the clogging instead of controlling it.

The pH of leachate in the LCS is influenced by several factors including CO<sub>2</sub> equilibria in leachate, exposure to air, turbulence, as well as aeration. It is evident from the results that higher pH results in higher scale formation. Acid addition to lower the pH significantly improved the saturation indices (LSI and RI) towards neutrality and thus would contribute positively to eliminating the clogging issues. Adding enough acid to drop the pH by one full pH unit helps to achieve near neutral LSI of +0.4 and it also lowers the dilution water requirement, theoretically. If an acid addition system is planned, it should be set up with an injection point as far upstream in the LCS as possible.

Microbial growth and activities such as the production of EPS, biofilm generation, and surface adhesion enhance the precipitation of  $\text{CaCO}_3$  in LCS. Experimental results suggest that microbial EPS enhance the adherent characteristics of precipitates and thus magnify the clogging issue. Further evaluation of these findings is necessary. It is extremely difficult to control the microbial activity in the LCS; therefore, it is recommended to maintain the appropriate operational activities, conduct periodic evaluation of the LCS pipes, reduce stagnation in the system if any, reduce the pH, etc.

Microbial activities along with  $\text{CaCO}_3$  precipitation and other solids deposition can reduce the injectivity of the deep injection well by reducing the effective diameter of the pipe or clogging the injection zone. This results in frequent brushing or cleaning of the well. Once biofouling has begun, little can be done to eliminate it permanently except for replacing the tubing completely. To avoid replacement, control of the microbial biofilm colonies is the preferred strategy. Options for management of biofouling on deep injection well tubing include pre-treatment of the injectate and/or tailored well rehabilitation strategies. Pre-treatment can take the form of aeration, acidification, and/or disinfection (chlorination or shock chlorination) before injection. Well rehabilitation efforts must be tailored to and designed around the site-specific characteristics and chemistry of the receiving water and the injectate and must be compatible with the construction and use patterns of the injection well itself. Chlorine and various acids, surfactants, and dispersants have been used for decades, often with mixed success due to the uncertainty of solution strength, mixture uniformity/distribution, and penetration. It should be noted that any attempt to control the population of the current microcosm could bring about an imbalance that would favor other fast-growing microbes that may or may not be more problematic for biofilm issues in the well than the current population.

Clogging in LCS pipe can be controlled if not eliminated by frequent high-pressure water jetting and cleaning of the LCS, cutters and milling machines attached to the jetting hose, and chemical treatment (recirculation or resurgence of chemical). The performance of each of these methods depends on the severity of the problem. With routine monitoring of the LCS pipes for clogs and microbial activities, landfill owners and operators can develop a better understanding of biogeochemical deposits that clog collection systems and develop optimum interval of control activities.

## BIBLIOGRAPHY

- Abu Amr, S. S., and Aziz, H. A., (2012). New treatment of stabilized leachate by ozone/Fenton in the advanced oxidation process. *Waste Management*.
- Adlan, M.N., Palaniandy, P., Aziz, H.A. (2011). Optimization of coagulation and dissolved air flotation (DAF) treatment of semi-aerobic landfill leachate using response surface methodology (RSM). *Desalination 277*: 74-82.
- Ahmad, Z. U. (2019). Synthesis and Characterization of Novel Functionalized Ordered Mesoporous Carbon (OMC) for Resorcinol and Sunset Yellow Removal. University of Louisiana at Lafayette.
- Ahmad, Z.U., Chao, B., Konggidinata, M.I., Lian, Q., Zappi, M.E., Gang, D.D., 2018. "Molecular Simulation and Experimental Validation of Resorcinol Adsorption on Ordered Mesoporous Carbon (OMC)." *Journal of Hazardous Materials*. 354, 258–265. <https://doi.org/10.1016/j.jhazmat.2018.04.072>.
- Ahmad, Z.U., Lian, Q., Zappi, M.E., Buchireddy, P.R., Gang, D.D., 2019. "Adsorptive Removal of Resorcinol onto Surface Modified Ordered Mesoporous Carbon (OMC): Kinetics and Equilibrium Study." *Environmental Progress and Sustainable Energy*. 38 (S1), S386–S397. <https://doi.org/10.1002/ep.13070>.
- Ahmad, Z.U., Lian, Q., Zappi, M.E., Buchireddy, P.R., Gang, D.D., 2019. "Adsorptive Removal of Resorcinol on a Novel Ordered Mesoporous Carbon (OMC) Employing COK-19 Silica Scaffold: Kinetics and Equilibrium Study." *Journal of Environmental Sciences*. 75, 307–317. <https://doi.org/10.1016/j.jes.2018.04.014>.
- Ahmad, Z.U., Yao, L., Wang, J., Gang, D. D., Islam, F., Lian, Q., Zappi, M. E., 2019. "Neodymium Embedded Ordered Mesoporous Carbon (OMC) for Enhanced Adsorption of Sunset Yellow: Characterizations, Adsorption Study and Adsorption Mechanism". *Chemical Engineering Journal*. 359, 814–826. <https://doi.org/10.1016/j.cej.2018.11.174>.
- Anglada, A., Urtiaga, A., Ortiz, I., Mantzavinos, D., Diamadopoulos, E. (2011). Treatment of municipal landfill leachate by catalytic wet air oxidation: Assessment of the role of operating parameters by factorial design. *Waste Management* 31: 1833–1840.
- Apha, A. WPCF (1995) Standard methods for the examination of water and waste water. American Public Health Association, Washington, DC, 456.
- Arias JL, Fernandez M.S. (2008). Polysaccharides and proteoglycans in calcium carbonate-based biomineralization. *Chem Rev* 108:4475–4482
- Armstrong, M.D. (1998). Laboratory program to study clogging in a leachate collection system. M.E.Sc. thesis, The University of Western Ontario, London, Ontario, CANADA.
- Arp G, Thiel V, Reimer A et al. (1999). Biofilm exopolymers control microbialite formation at thermal spring discharging into the alkaline Pyramid Lake, Nevada, USA. *Sediment Geology*, 126, 159-176.
- Aziz, H.A., Ling, T.J., Haque, A.A.M., Umar, M., Adlan, M.N. (2011). Leachate treatment by swim-bed bio fringe technology. *Desalination* 276: 278–286.

- Bashir, M.J.K., Aziz, H.A., Yusoff, M.S., Aziz, S.Q., Mohajeri, S. (2010). Stabilized sanitary landfill leachate treatment using anionic resin: Treatment optimization by response surface methodology. *Journal of Hazardous Materials* 182: 115–122.
- Bass, J. M. (1985). Avoiding failure of leachate collection systems. *Waste management & research*, 3(3), 233-243.
- Baveye, P., Vandevivere, P., Hoyle, B. L., DeLeo, P. C., & de Lozada, D. S. (1998). Environmental impact and mechanisms of the biological clogging of saturated soils and aquifer materials. *Critical reviews in environmental science and technology*, 28(2), 123-191.
- Bekbolet, M. and Araz, C.V. (1996). Inactivation of *Escherichia coli* by photocatalytic oxidation. *Chemosphere* 32: 959-965.
- Benzerara, K., Miot, J., Morin, G., Ona-Nguema, G., Skouri-Panet, F., & Ferard, C. (2011). Significance, mechanisms and environmental implications of microbial biomineralization. *Comptes Rendus Geoscience*, 343(2-3), 160-1
- Betzel, C., Dauter, Z., Dauter, M., Ingelman, M., Papendorf, G., Wilson, K. S., & Branner, S. (1988). Crystallization and preliminary X-ray diffraction studies of an alkaline protease from *Bacillus lentus*. *Journal of molecular biology*, 204(3), 803-804.
- Booker, J. R., Brachman, R., Quigley, R. M., & Rowe, R. K. (2004). *Barrier systems for waste disposal facilities*. CRC Press.
- Bosak, T., & Newman, D. K. (2005). Microbial kinetic controls on calcite morphology in supersaturated solutions. *Journal of Sedimentary Research*, 75(2), 190-199.
- Bouchez, T., Munoz, M. L., Vessigaud, S., Bordier, C., Aran, C., & Duquennoi, C. (2003, October). Clogging of MSW landfill leachate collection systems: prediction methods and in situ diagnosis. In *Proceedings, Sardinia*.
- Bouhezila, F., Hariti, M., Lounici, H., Mameri, N. (2011). Treatment of the OUED SMAR town landfill leachate by an electrochemical reactor. *Desalination* 280: 347–353.
- Braissant, O., Decho, A. W., Dupraz, C., Glunk, C., Przekop, K. M., & Visscher, P. T. (2007). Exopolymeric substances of sulfate-reducing bacteria: interactions with calcium at alkaline pH and implication for formation of carbonate minerals. *Geobiology*, 5(4), 401-411.
- Brune, M., Ramke, H. G., Collins, H. J., & Hanert, H. H. (1991, October). Incrustation processes in drainage systems of sanitary landfills. In *Proc. 3rd Int. Landfill Symp., Cagliari* (pp. 999-1035).
- Bryers, J., & Characklis, W. (1981). Early fouling biofilm formation in a turbulent flow system: overall kinetics. *Water Research*, 15(4), 483-491.
- Burbank, M. B., Weaver, T. J., Williams, B. C., & Crawford, R. L. (2012). Urease activity of ureolytic bacteria isolated from six soils in which calcite was precipitated by indigenous bacteria. *Geomicrobiology Journal*, 29(4), 389-395.
- Burne, R. A., & Chen, Y. Y. M. (2000). Bacterial ureases in infectious diseases. *Microbes and Infection*, 2(5), 533-542.
- C. Cañveras, S. Sanchez-Moral, V. Sloer, C. Saiz-Jimenez, J. (2001). Microorganisms and microbially induced fabrics in cave walls. *Geomicrobiology journal*, 18(3), 223-240.

- Castanier, S., Le Métayer-Levrel, G., & Perthuisot, J. P. (1999). Ca-carbonates precipitation and limestone genesis—the microbiogeologist point of view. *Sedimentary geology*, 126(1-4), 9-23.
- Chevrefils, G., Caron, É., Wright, H., Sakamoto, G., Payment, P., Barbeau, B., & Cairns, B. (2006). UV dose required to achieve incremental log inactivation of bacteria, protozoa and viruses. *IUVA News*, 8(1), 38-45.
- Cho, Y. I., & Choi, B. G. (1999). Validation of an electronic anti-fouling technology in a single-tube heat exchanger. *International Journal of Heat and Mass Transfer*, 42(8), 1491-1499.
- Cho, Y. I., Fan, C., & Choi, B. G. (1997). Theory of electronic anti-fouling technology to control precipitation fouling in heat exchangers. *International communications in heat and mass transfer*, 24(6), 757-770.
- Cho, Y. I., Lane, J., & Kim, W. (2005). Pulsed-power treatment for physical water treatment. *International communications in heat and mass transfer*, 32(7), 861-871.
- Cooke, A. J., Rowe, R. K., Rittmann, B. E., & Fleming, I. R. (1999). Modeling biochemically driven mineral precipitation in anaerobic biofilms. *Water Science and Technology*, 39(7), 57.
- Cooke, A.J., Rowe, R.K., Rittmann, B.E. (2005). Modeling species fate and porous media effects for landfill leachate flow. *Canadian Geotechnical Journal*, 42(9), 1116-1132.
- Cooke, A.J., Rowe, R.K., Rittmann, B.E., VanGulck, J.F. and Millward, S.C. (2001). Biofilm growth and mineral precipitation in synthetic leachate columns. *Journal of Geotechnical and Geoenvironmental Engineering*, ASCE 127(10), 949-856.
- De Moel, P. J., Van der Helm, A. W. C., Van Rijn, M., Van Dijk, J. C., & Van der Meer, W. G. J. (2013). Assessment of calculation methods for calcium carbonate saturation in drinking water for DIN 38404-10 compliance. *Drinking water engineering and science*, 6(2), 115-124.
- De Muynck, W., Cox, K., De Belie, N., & Verstraete, W. (2008). Bacterial carbonate precipitation as an alternative surface treatment for concrete. *Construction and Building Materials*, 22(5), 875-885.
- De Muynck, W., De Belie, N., & Verstraete, W. (2010). Microbial carbonate precipitation in construction materials: a review. *Ecological Engineering*, 36(2), 118-136.
- De Muynck, W., De Belie, N., & Verstraete, W. (2010). Microbial carbonate precipitation in construction materials: a review. *Ecological Engineering*, 36(2), 118-136.
- Declat, A., Reyes, E., & Suárez, O. M. (2016). Calcium carbonate precipitation: a review of the carbonate crystallization process and applications in bioinspired composites. *Reviews on Advanced Materials Science*, 44(1).
- DeJong, J. T., Mortensen, B. M., Martinez, B. C., & Nelson, D. C. (2010). Bio-mediated soil improvement. *Ecological Engineering*, 36(2), 197-210.
- Deng, Y., and Ezyske, C. M. (2011). Sulfate radical-advanced oxidation process (SR-AOP) for simultaneous removal of refractory organic contaminants and ammonia in landfill leachate. *Water Research* 45: 6189-6194.

- Douglas, S., & Beveridge, T. J. (1998). Mineral formation by bacteria in natural microbial communities. *FEMS microbiology ecology*, 26(2), 79-88.
- Dupraz, C., & Visscher, P. T. (2005). Microbial lithification in marine stromatolites and hypersaline mats. *Trends in microbiology*, 13(9), 429-438.
- Fan, C., & Cho, Y. I. (1997). Microscopic observation of calcium carbonate particles: validation of an electronic anti-fouling technology. *International communications in heat and mass transfer*, 24(6), 747-756.
- Federation, W. E., & American Public Health Association. (2005). *Standard methods for the examination of water and wastewater*. American Public Health Association (APHA): Washington, DC, USA.
- Fleming, I. R., Rowe, R. K., & Cullimore, D. R. (1999). Field observations of clogging in a landfill leachate collection system. *Canadian Geotechnical Journal*, 36(4), 685-707.
- Fleming, I.R. and Rowe, R.K. (2004). Laboratory studies of clogging of landfill leachate collection and drainage systems. *Canadian Geotechnical Journal* 41, 134-153.
- Fujita, Y., Taylor, J. L., Gresham, T. L., Delwiche, M. E., Colwell, F. S., McLing, T. L., ... & Smith, R. W. (2008). Stimulation of microbial urea hydrolysis in groundwater to enhance calcite precipitation. *Environmental science & technology*, 42(8), 3025-3032.
- Gabrielli, C., Maurin, G., Poindessous, G., & Rosset, R. (1999). Nucleation and growth of calcium carbonate by an electrochemical scaling process. *Journal of crystal growth*, 200(1-2), 236-250.
- Goddette, D. W., Paech, C., Yang, S. S., Mielenz, J. R., Bystroff, C., Wilke, M. E., & Fletterick, R. J. (1992). The crystal structure of the *Bacillus lentus* alkaline protease, subtilisin BL, at 1.4 Å resolution. *Journal of molecular biology*, 228(2), 580-595.
- González-Muñoz, M. T., Rodríguez-Navarro, C., Martínez-Ruiz, F., Arias, J. M., Merroun, M. L., & Rodríguez-Gallego, M. (2010). Bacterial biomineralization: new insights from *Myxococcus*-induced mineral precipitation. *Geological Society, London, Special Publications*, 336(1), 31-50.
- Groth, P. Schumann, L. Laiz, S. Sanchez-Moral, JC Cañveras, C. Saiz-Jimenez, I. (2001). Geomicrobiological study of the grotta dei cervi, Porto Badisco, Italy. *Geomicrobiology Journal*, 18(3), 241-258.
- Hammes, F., Boon, N., de Villiers, J., Verstraete, W., & Siciliano, S. D. (2003). Strain-specific ureolytic microbial calcium carbonate precipitation. *Appl. Environ. Microbiol.*, 69(8), 4901-4909.
- Iaconi, C. D., Pagano, M., Ramadori, R., Lopez, A. (2010). Nitrogen recovery from a stabilized municipal landfill leachate. *Bioresource Technology* 101: 1732–1736.
- Jansson, C., & Northen, T. (2010). Calcifying cyanobacteria—the potential of biomineralization for carbon capture and storage. *Current Opinion in Biotechnology*, 21(3), 365-371.
- Jha, B. K., Pragash, M. G., Cletus, J., Raman, G., & Sakthivel, N. (2009). Simultaneous phosphate solubilization potential and antifungal activity of new fluorescent pseudomonad strains,

- Pseudomonasaeruginosa*, *P. plecoglossicida* and *P. mosselii*. *World Journal of Microbiology and Biotechnology*, 25(4), 573-581.
- Jia, C., Wang, Y., Zhang, C., Qin, Q. (2011). UV-TiO<sub>2</sub> Photocatalytic Degradation of Landfill Leachate. *Water Air Soil Pollution* 217:375–385.
- Jørgensen, P. L., Tangney, M., Pedersen, P. E., Hastrup, S., Diderichsen, B., & Jørgensen, S. T. (2000). Cloning and sequencing of an alkaline protease gene from *Bacillus lentus* and amplification of the gene on the *B. lentus* chromosome by an improved technique. *Appl. Environ. Microbiol.*, 66(2), 825-827.
- Kawaguchi, T., & Decho, A. W. (2002). A laboratory investigation of cyanobacterial extracellular polymeric secretions (EPS) in influencing CaCO<sub>3</sub> polymorphism. *Journal of Crystal Growth*, 240(1-2), 230-235.
- Kim, W. T., Cho, Y. I., & Bai, C. (2001). Effect of electronic anti-fouling treatment on fouling mitigation with circulating cooling-tower water. *International Communications in Heat and Mass Transfer*, 28(5), 671-680.
- Koerner, G. R., Koerner, R. M., & Martin, J. P. (1994). Design of landfill leachate-collection filters. *Journal of Geotechnical Engineering*, 120(10), 1792-1803.
- Koerner, R. M. (2008). *Results of a Worldwide Regulatory Survey on Allowable Hydraulic Head*. Folsom, PA 19033 USA: Geosynthetic Institute.
- Levine, A. D., Cardoso, A. J., Nayak, B., Rhea, L. R., Dodge, B. M., & Harwood, V. J. (2005). Assessment of biogeochemical deposits in landfill leachate drainage systems. Project Final Rep.
- Li, H., Zhou, S., Sun, Y., Feng, P., Li, J. (2009). Advanced treatment of landfill leachate by a new combination process in a full-scale plant. *Journal of Hazardous Materials* 172: 408–415.
- Lian, Q., Ahmad, Z. U., Gang, D. D., Zappi, M. E., Fortela, D. L. B., Hernandez, R., 2020. “The Effects of Carbon Disulfide Driven Functionalization on Graphene Oxide for Enhanced Pb(II) Adsorption: Investigation of Adsorption Mechanism.” *Chemosphere*, 248, 126078. <https://doi.org/10.1016/j.chemosphere.2020.126078>.
- Lian, Q., Yao, L., Ahmad, Z. U., Konggidinata, M. I., Zappi, M. E., Gang, D. D., 2019. “Modelling Mass Transfer for Adsorptive Removal of Pb(II) onto Phosphate Modified Ordered Mesoporous Carbon (OMC).” *Journal of Contaminant Hydrology*, 228, 103562. <https://doi.org/10.1016/j.jconhyd.2019.103562>.
- Limoli, D. H., Jones, C. J., & Wozniak, D. J. (2015). Bacterial extracellular polysaccharides in biofilm formation and function. *Microbial Biofilms*, 223-247.
- Liu, Y., & Tay, J. H. (2002). The essential role of hydrodynamic shear force in the formation of biofilm and granular sludge. *Water research*, 36(7), 1653-1665.
- Lowenstam, H. A., & Weiner, S. (1989). *On biomineralization*. Oxford University Press on Demand.
- Lozeczniak, S. (2010). Occurrence and remediation of pipe clogging in landfill leachate recirculation systems.

- Mahmud, K., Hossain, Md. D., Shams, S. (2011). Different treatment strategies for highly polluted landfill leachate in developing countries. *Waste Management*.
- Malayeri, A. H., Mohseni, M., Cairns, B., Bolton, J. R., Chevrefils, G., Caron, E., ... & Linden, K. G. (2016). Fluence (UV dose) required to achieve incremental log inactivation of bacteria, protozoa, viruses and algae. *IUVA News*, 18(3), 4-6.
- Maliva, R. G., Missimer, T. M., Leo, K. C., Statom, R. A., Dupraz, C., Lynn, M., & Dickson, J. A. D. (2000). Unusual calcite stromatolites and pisoids from a landfill leachate collection system. *Geology*, 28(10), 931-934.
- Malusa, J., Overby, S. T., & Parnell, R. A. (2003). Potential for travertine formation: fossil Creek, Arizona. *Applied Geochemistry*, 18(7), 1081-1093.
- MATCH!, Version 3.9, CRYSTAL IMPACT, Kreuzherrenstr. 102, 53227 Bonn, Germany. (URL: <http://www.crystalimpact.com/match>)
- Mayer, N. P., M. J. Hernandez, A. M. Saleh, S. S. Carl, and R. Calistri. 2014. "Biogeochemical clogging of landfill leachate collection systems: Why is it occurring, how can it be cleaned and what can be done to prevent it Part II." *Waste Advantage Magazine*, September 22, 2014
- Mayer, Nathan P. et al. (2013). "Biogeochemical clogging of landfill leachate collection systems. Why is it occurring. How can it be cleaned? What can be done to prevent it?"
- McConnaughey, T. A., & Whelan, J. F. (1997). Calcification generates protons for nutrient and bicarbonate uptake. *Earth-Science Reviews*, 42(1-2), 95-117.
- McIsaac, R. and Rowe, R.K. (2005). Change in leachate chemistry and porosity as leachate permeates through tire shreds and gravel. *Canadian Geotechnical Journal*, 42(4), 1173-1188.
- McIsaac, R., Rowe, R.K., Fleming, I.R. and Armstrong, M.D. (2000). Leachate collection system design and clog development. *Proceedings 6th Canadian Environmental Engineering Conference*, London, Ontario, 66-73.
- McLean, R.J.C., Fuqua, C., Siegele, D.A., Kirkland, B.L., Adams, J.L. and Whiteley, M. (1999). Biofilm growth and illustrations of its role in mineral formation. *Proceedings of the 8th International Symposium on Microbial Ecology*, Halifax, CANADA.
- Metcalf & Eddy (2003). *Wastewater Engineering. Treatment, Disposal, and Reuse*. McGraw-Hill, 4rd Edition.
- Mobley, H. L., & Hausinger, R. P. (1989). Microbial ureases: significance, regulation, and molecular characterization. *Microbiology and Molecular Biology Reviews*, 53(1), 85-108.
- Mohajeri, S., Aziz, H.A., Isa, M.H., Zaheda, M.A., Adlana, M.N. (2010). Statistical optimization of process parameters for landfill leachate treatment using electro-Fenton technique. *Journal of Hazardous Materials* 176: 749–758.
- Palm Beach Renewable Energy Facility 1. (2016, May 10). Retrieved from Solid Waste Authority: <http://www.swa.org/161/Palm-Beach-Renewable-Energy-Facility-1>

- Phillips, A. J., Gerlach, R., Lauchnor, E., Mitchell, A. C., Cunningham, A. B., & Spangler, L. (2013). Engineered applications of ureolytic biomineralization: a review. *Biofouling*, 29(6), 715-733.
- Poblete, R., Prieto-Rodríguez, L., Oller, I., Maldonado, M.I., Malato, S., Ota, E., Vilches, L.F., Fernández-Pereira, C. (2012). Solar photocatalytic treatment of landfill leachate using a solid mineral by-product as a catalyst. *Chemosphere* 88: 1090–1096.
- Prisyazhniuk, V. A. (2007). Prognosticating scale-forming properties of water. *Applied Thermal Engineering*, 27(8-9), 1637-1641.
- Qian, X., Koerner, R. M., & Gray, D. H. (2001). *Geotechnical aspects of landfill construction and design*. Prentice Hall.
- Raghab, S. M., El Meguid, A. M. A., & Hegazi, H. A. (2013). Treatment of leachate from municipal solid waste landfill. *HBRC Journal*, 9(2), 187-192.
- Reddy, M. S. (2013). Biomineralization of calcium carbonates and their engineered applications: a review. *Frontiers in microbiology*, 4, 314.
- Renou, S., Givaudan, J.G., Poulain, S., Dirassouyan, F., Moulin, P. (2008). Landfill leachate treatment: Review and opportunity. *Journal of Hazardous Materials* 150: 468–493.
- Rittmann, B. E., Fleming, I. R., & Rowe, R. K. (1996). Leachate chemistry: its implications for clogging. In *North American water and Environment Congress & destructive water* (pp. 28-33). ASCE.
- Rodríguez-Navarro, C., Jroundi, F., Schiro, M., Ruiz-Agudo, E., & González-Muñoz, M. T. (2012). Influence of substrate mineralogy on bacterial mineralization of calcium carbonate: implications for stone conservation. *Appl. Environ. Microbiol.*, 78(11), 4017-4029.
- Rodríguez-Navarro, C., Rodríguez-Gallego, M., Chekroun, K. B., & Gonzalez-Munoz, M. T. (2003). Conservation of ornamental stone by *Myxococcus xanthus*-induced carbonate biomineralization. *Appl. Environ. Microbiol.*, 69(4), 2182-2193.
- Rowe, R. K. (1998). *Geosynthetics and the minimization of contaminant migration through barrier systems beneath solid waste*.
- Rowe, R. K. (2009). Long-term performance of leachate collections systems and geomembrane liners for MSW landfills. Keynote lecture, *GeoAfrica*.
- Rowe, R. K., & VanGulck, J. (2001). Clogging of leachate collection systems: from laboratory and field study to modelling and prediction. In *Proceedings 2nd ANZ Conference on Environmental Geotechnics*, Australian Geomechanics Society, Newcastle (pp. 1-22).
- Rowe, R. K., & Yu, Y. (2010, November). Factors affecting the clogging of leachate collection systems in MSW landfills. In *Proc. of the 6th International Congress on Environmental Geotechnics*, New Delhi (Vol. 1, pp. 3-23).
- Rowe, R. K., Armstrong, M. D., & Cullimore, D. R. (2000). Mass loading and the rate of clogging due to municipal solid waste leachate. *Canadian Geotechnical Journal*, 37(2), 355-370.
- Rowe, R. K., Armstrong, M. D., & Cullimore, D. R. (2000). Particle size and clogging of granular media permeated with leachate. *Journal of Geotechnical and Geoenvironmental Engineering*, 126(9), 775-786.

- Rowe, R. K., Quigley, R. M., Brachman, R. W., & Booker, J. R. (2004). Barrier systems for waste disposal facilities (No. Ed. 2). spon Press.
- Rowe, R. K., VanGulck, J. F., & Millward, S. C. (2002). Biologically induced clogging of a granular medium permeated with synthetic leachate. *Journal of Environmental Engineering and Science*, 1(2), 135-156.
- Rowe, R. K., VanGulck, J. F., & Millward, S. C. (2002). Biologically induced clogging of a granular medium permeated with synthetic leachate. *Journal of Environmental Engineering and Science*, 1(2), 135-156.
- Salem, Z., Hamouri, K., Djemaa, R., Allia, K. (2008). Evaluation of landfill leachate pollution and treatment. *Desalination* 220: 108–114.
- Sánchez-Román, M., Romanek, C. S., Fernández-Remolar, D. C., Sánchez-Navas, A., McKenzie, J. A., Pibernat, R. A., & Vasconcelos, C. (2011). Aerobic biomineralization of Mg-rich carbonates: Implications for natural environments. *Chemical Geology*, 281(3-4), 143-150.
- Shaha, B. N. (2016). Effect of electronic water treatment system on calcium carbonate scaling. Florida Atlantic University.
- Shaha, B. N., Meeroff, D. E., & Kohn, K. Effect of an Electronic Water Treatment System on Calcium Carbonate Scaling: A Case Study. In *World Environmental and Water Resources Congress 2016* (pp. 41-50).
- Shaha, B. N., Meeroff, D. E., Kohn, K., Townsend, T. G., Schert, J. D., Mayer, N., ... & Telson, J. (2019). Effect of Electronic Water Treatment System on Calcium Carbonate Scale Formation in Landfill Leachate Collection Piping. *Journal of Environmental Engineering*, 145(9), 04019052.
- Stabnikov, V., Jian, C., Ivanov, V., & Li, Y. (2013). Halotolerant, alkaliphilic urease-producing bacteria from different climate zones and their application for biocementation of sand. *World Journal of Microbiology and Biotechnology*, 29(8), 1453-1460.
- Stocks-Fischer, S., Galinat, J. K., & Bang, S. S. (1999). Microbiological precipitation of CaCO<sub>3</sub>. *Soil Biology and Biochemistry*, 31(11), 1563-1571.
- Stoodley, P., Lewandowski, Z., Boyle, J. D., & Lappin-Scott, H. M. (1999). Structural deformation of bacterial biofilms caused by short-term fluctuations in fluid shear: An in-situ investigation of biofilm rheology. *Biotechnology and bioengineering*, 65(1), 83-92.
- Thompson, J. B., & Ferris, F. G. (1990). Cyanobacterial precipitation of gypsum, calcite, and magnesite from natural alkaline lake water. *Geology*, 18(10), 995-998.
- Tijing, L. D., Lee, D. H., Kim, D. W., Cho, Y. I., & Kim, C. S. (2011). Effect of high-frequency electric fields on calcium carbonate scaling. *Desalination*, 279(1-3), 47-53.
- VanGulck, J. F., & Rowe, R. K. (2004). Influence of landfill leachate suspended solids on clog (biorock) formation. *Waste Management*, 24(7), 723-738.
- VanGulck, J. F., Rowe, R. K., Rittmann, B. E., & Cooke, A. J. (2003). Predicting biogeochemical calcium precipitation in landfill leachate collection systems. *Biodegradation*, 14(5), 331-346.

- VanGulck, J.F. and Rowe, R.K., (2004b). Evolution of clog formation with time in column permeated with synthetic landfill leachate. *Journal of Contaminant Hydrology*, 75, 115-135.
- Vu, B., Chen, M., Crawford, R. J., & Ivanova, E. P. (2009). Bacterial extracellular polysaccharides involved in biofilm formation. *Molecules*, 14(7), 2535-2554.
- Warthmann, R., Van Lith, Y., Vasconcelos, C., McKenzie, J. A., & Karpoff, A. M. (2000). Bacterially induced dolomite precipitation in anoxic culture experiments. *Geology*, 28(12), 1091-1094.
- Wei, S., Cui, H., Jiang, Z., Liu, H., He, H., & Fang, N. (2015). Biomineralization processes of calcite induced by bacteria isolated from marine sediments. *Brazilian Journal of Microbiology*, 46(2), 455-464.
- Xiaokai, X. (2008). Research on the electromagnetic anti-fouling technology for heat transfer enhancement. *Applied Thermal Engineering*, 28(8-9), 889-894.
- Xiaokai, X., Chongfang, M., & Yongchang, C. (2005). Investigation on the electromagnetic anti-fouling technology for scale prevention. *Chemical Engineering & Technology: Industrial Chemistry-Plant Equipment-Process Engineering-Biotechnology*, 28(12), 1540-1545.

## Appendix A: Water Quality Analyses

Table A. RAW Data for Figure 46

Time, min	pH			Sp. Conductance, $\mu\text{S}/\text{cm}$			Conductivity, $\mu\text{S}/\text{cm}$		
	Control (N <sub>2</sub> )	Test (CO <sub>2</sub> )	Air	Control (N <sub>2</sub> )	Test (CO <sub>2</sub> )	Air	Control (N <sub>2</sub> )	Test (CO <sub>2</sub> )	Air
0	7.35	7.37	7.46	10.55	10.54	10.67	9.22	9.23	8.80
5	7.49	7.06	7.75	10.58	10.50	10.59	9.62	9.48	9.11
10	7.57	7.00	7.91	10.42	10.58	10.54	9.55	9.57	9.16
15	7.62	6.95	7.98	10.34	10.40	10.48	9.51	9.44	9.18
20	7.71	6.88	8.06	10.35	10.40	10.43	9.54	9.51	9.21
30	7.87	6.91	8.15	10.53	10.48	10.41	9.78	9.73	9.30
45	7.81	6.90	8.22	10.30	10.60	10.37	9.68	9.85	9.41
60	7.78	6.85	8.27	10.38	10.57	10.32	9.75	9.83	9.46
90	7.79	6.87	8.35	9.32	10.62	10.27	8.85	10.05	9.56

Table B. RAW Data for Figure 46

Time, min	Alkalinity, mg/L as CaCO <sub>3</sub>			TDS (YSI), g/L			Temp. °C		
	Control (N <sub>2</sub> )	Test (CO <sub>2</sub> )	Air	Control (N <sub>2</sub> )	Test (CO <sub>2</sub> )	Air	Control (N <sub>2</sub> )	Test (CO <sub>2</sub> )	Air
0	1,233	1,267	1,600	6.86	6.85	6.94	18.37	18.50	15.82
5	1,267	1,333	1,300	6.88	6.83	6.88	20.24	19.88	17.71
10	1,367	1,350	1,150	6.80	6.88	6.85	20.55	19.98	18.14
15	1,300	1,333	1,400	6.72	6.76	6.81	20.74	20.14	18.48
20	1,267	1,317	1,300	6.73	6.76	6.78	20.86	20.51	18.90
30	1,267	1,283	1,150	6.85	6.81	6.77	21.27	21.24	19.43
45	1,283	1,283	1,100	6.70	6.89	6.75	21.82	21.27	20.10
60	nr	nr	nr	6.76	6.87	6.71	21.76	21.58	20.61
90	nr	nr	nr	6.66	6.90	6.67	22.36	22.20	21.41

Table C. Processed Data for Figure 46

Time, min	pH	TDS field, g/L	Alk, mg/L as CaCO <sub>3</sub>	Ca, mg/L as CaCO <sub>3</sub>	Temp., °C	pHs	LSI	RI
<b>Control</b>								
0	7.35	6.86	1,230	1,900	18.37	5.9	1.5	4.4
30	7.87	6.81	1,300	1,700	21.27	5.9	2.0	3.9
60	7.78	6.76	1,270	1,750	21.76	5.9	1.9	3.9
90	7.79	6.66	1,280	1,750	22.36	5.8	1.9	3.9
<b>Test</b>								
0	7.37	6.85	1,270	1,750	18.5	5.9	1.5	4.4
30	6.91	6.81	1,330	1,900	21.24	5.8	1.1	4.7
60	6.85	6.87	1,280	1,800	21.58	5.8	1.0	4.8

Time, min	pH	TDS field, g/L	Alk, mg/L as CaCO <sub>3</sub>	Ca, mg/L as CaCO <sub>3</sub>	Temp., °C	pHs	LSI	RI
90	6.87	6.9	1,280	1,800	22.2	5.8	1.0	4.8
<b>Air</b>								
0	7.46	6.94	1,600	1,350	15.82	6.0	1.5	4.5
30	8.15	6.77	1,400	1,650	19.43	5.9	2.3	3.6
60	8.27	6.71	1,150	1,600	20.61	6.0	2.3	3.6
90	8.35	6.67	1,150	1,600	21.41	5.9	2.4	3.5

Table D. Raw Data for Figure 52-55

ID	Day 0			Day 7		
	pH	Alk, mg/L as CaCO <sub>3</sub>	Ca, mg/L as CaCO <sub>3</sub>	pH	Alk, mg/L as CaCO <sub>3</sub>	Ca, mg/L as CaCO <sub>3</sub>
Control	7.14	2200	2000	7.54	1400	1700
0.1 lpm CO <sub>2</sub>	6.92	1750	2150	7.82	717	1825
0.3 lpm CO <sub>2</sub>	6.91	1925	2000	7.85	617	1683
0.5 lpm CO <sub>2</sub>	6.91	1750	2100	7.77	733	1717
1 lpm CO <sub>2</sub>	6.85	1875	2050	7.79	483	1883
Air 1	8.16	1850	1850	7.57	367	1383

Table E. Processed Data for Figure 52-55

ID	Day 0			Day 7		
	pH	Alk, mg/L as CaCO <sub>3</sub>	Ca, mg/L as CaCO <sub>3</sub>	pH	Alk, mg/L as CaCO <sub>3</sub>	Ca, mg/L as CaCO <sub>3</sub>
<b>Control</b>	7.1	2200	2000	7.5	1400	1700
<b>CO<sub>2</sub></b>	6.9	1825	2075	7.8	638	1777
<b>Air</b>	8.2	1850	1850	7.6	367	1383

Table F. Processed Data for Figure 56

Sample ID	Scale, g	volume, mL	Scale, mg/L
Control	0.0027	200	13.5
0.1 lpm CO <sub>2</sub>	0.0168	200	84.2
0.3 lpm CO <sub>2</sub>	0.0144	200	72.0
0.5 lpm CO <sub>2</sub>	0.0060	200	29.8
1 lpm CO <sub>2</sub>	0.1204	200	601.8
Air 1	0.1899	200	949.3

Table G. Processed Data for Figure 58-59

ID	Ca. at Day 0, mg/L as CaCO <sub>3</sub>	Ca. at day 7, mg/L as CaCO <sub>3</sub>	Alk. at Day 0, mg/L as CaCO <sub>3</sub>	Alk. at Day 7, mg/L as CaCO <sub>3</sub>
0	4,300	1,820	3,200	400
1	3,400	2,100	2,800	500
2	2,850	1,740	2,425	450
3	1,850	1,260	2,250	550
4	1,150	1,120	2,150	500
5	750	880	1,900	550

Table H. Processed Data for Figure 60

ID	Initial	1mL NaOH	2mL NaOH	3mL NaOH	4mL NaOH	5mL NaOH
LSI at Day 0	1.98	2.04	1.96	1.93	1.93	0.69
LSI at Day 7	0.78	0.93	0.79	0.86	0.85	1.32

Table I. Processed Data for Figure 61

LSI	Day 0			Day 7		
ID	0 ml NaOH	3 ml NaOH	5 ml NaOH	0 ml NaOH	3 ml NaOH	5 ml NaOH
MH 13	1.08	1.67	2.25	1.43	1.58	1.43
MH 11	1.72	1.90	2.30	1.76	1.19	1.12
Deep well	1.22	2.97	3.19	2.25	2.74	2.42

Table J. Data for Figure 65, Trial 1

pH	Alk. mg/L as CaCO <sub>3</sub>	Ca. Mg/L as CaCO <sub>3</sub>	Alk, g-moles/L	Ca, g-moles/L	pALK	pCa
12.7	34,900	500	6.98E-01	5.00E-03	0.2	2.3
12.0	16,800	550	3.36E-01	5.50E-03	0.5	2.3
11.0	15,400	600	3.08E-01	6.00E-03	0.5	2.2
10.0	13,500	550	2.70E-01	5.50E-03	0.6	2.3
9.0	8,600	1,000	1.72E-01	1.00E-02	0.8	2.0
8.0	7,900	1,200	1.58E-01	1.20E-02	0.8	1.9
7.0	6,600	1,400	1.32E-01	1.40E-02	0.9	1.9
6.0	1,700	1,450	3.40E-02	1.45E-02	1.5	1.8
5.0	900	1,550	1.80E-02	1.55E-02	1.7	1.8
4.0	400	1,550	8.00E-03	1.55E-02	2.1	1.8
3.0	300	1,500	6.00E-03	1.50E-02	2.2	1.8
2.0	50	1,500	1.00E-03	1.50E-02	3.0	1.8

Table K. Data for Figure 65, Trial 2

pH	Temp. °C	Sp. Cond., μS/cm	Cond. μS/cm	TDS, g/L	Alk. mg/L as CaCO <sub>3</sub>	Ca, mg/L as CaCO <sub>3</sub>	Alk, g-moles/L	Ca, g-moles/L	pALK	pCa
12.0	20.85	39.01	35.92	25.35	21,700	900	4.34E-01	9.00E-03	0.4	2.0
11.0	20.8	35.76	32.88	23.24	18,200	800	3.64E-01	8.00E-03	0.4	2.1
10.0	20.36	33.74	30.75	21.93	15,200	900	3.04E-01	9.00E-03	0.5	2.0
9.0	19.92	33.29	30.06	21.64	8,700	950	1.74E-01	9.50E-03	0.8	2.0
8.0	19.79	34.07	30.68	22.15	7,200	1000	1.44E-01	1.00E-02	0.8	2.0
7.6	19.75	34.07	30.66	22.15	6,100	1050	1.22E-01	1.05E-02	0.9	2.0
7.0	nr	nr	nr	nr	5,200	1150	1.04E-01	1.15E-02	1.0	1.9
6.0	20.32	35.95	32.72	23.38	1,600	1000	3.20E-02	1.00E-02	1.5	2.0
5.0	20.45	37.4	34.18	24.35	750	1000	1.50E-02	1.00E-02	1.8	2.0
4.0	20.51	35.58	32.52	23.13	100	900	2.00E-03	9.00E-03	2.7	2.0
3.0	20.53	36.18	33.09	23.52	50	800	1.00E-03	8.00E-03	3.0	2.1
2.0	20.48	41.23	37.7	26.79	1	1700	2.00E-05	1.70E-02	4.7	1.8

Table L. Processed Data for Figure 68

YSI	Initial		After sterilization and 1-hour cooling		Overnight cooling		After 7-day incubation	
	Control	To be sterilized	Control	Sterilized	Control	Sterilized	Control	Sterilized
pH (st unit)	7.24	7.25	7.20	8.36	7.70	8.59	7.40	7.20
Temp. (°C)	19.43	19.48	21.89	39.02	21.61	21.54	22.62	22.5
TDS (g/L)	7.756	7.759	7.738	8.788	7.674	8.52	6.30	7.80
Cond. (mS/cm)	10.66	10.68	11.20	17.11	11.04	12.24	9.20	11.4
Sp. Cond. (mS/cm)	11.93	11.93	11.90	13.48	11.8	13.11	9.70	12
Ca. hardness (mg/L as CaCO <sub>3</sub> )	650	700	500	650/510	550	650/510	850	1,250
Alkalinity (mg/L as CaCO <sub>3</sub> )	1,050	1,050	1,050	800/630	1,050	650/510	90	110
LSI	0.8	0.9	0.8	2.0	1.3	5.1	0.1	0.1
RI	5.6	5.5	5.6	4.4	1.8	5.0	7.2	7.0

Table M. Processed Data for Figure 69

Remaining sample volume	Non-adherent Precipitate	Non-adherent Precipitation rate	Adherent Precipitate	Adherent Precipitation rate
g	g	mg/L		mg/L
81.88	0.005	25	0.038	190
85.70	0.007	35	0.040	200
<b>83.79</b>	<b>Average</b>	<b>30</b>	<b>Average</b>	<b>195</b>
81.09	0.010	50	0.008	40
88.18	0.008	40	0.011	55
<b>84.64</b>	<b>Average</b>	<b>45</b>	<b>Average</b>	<b>47.5</b>

Table N. Processed Data for Figure 74

ID	Floating/ non-adherent Precipitation, mg/L	Volatile Floating/ non-adherent Precipitation, mg/L	Adherent precipitation, mg/L	Scale, mg/L
Control	715	120	2,465	3,300
Oven	2,145	330	985	3,460
Autoclave	1,050	195	1,145	2,390

Table O. Processed Data for Figure 75

Sample ID	Adherent scale, mg/L	Volatile non-adherent scale, mg/L	Nonvolatile non-adherent Scale, mg/L
1	1380	80	60
2	1510	10	50
3	4300	20	70
4	4670	40	40

Table P. Processed Data for Figure 76

Sample ID	Control			Sterilized			Control mg/L	Sterilized mg/L
	W0, g	Wi, g	Precipitate, g	W0, g	Wj, g	Precipitate, g		
1	126.44	126.50	0.056	123.84	123.86	0.018	560	180
2	125.85	126.00	0.150	127.81	127.86	0.049	1,500	490
3	127.63	127.76	0.133	125.23	125.27	0.045	1,330	450
4	127.27	127.44	0.168	127.97	128.01	0.039	1,680	390
5	128.49	128.64	0.144	126.72	126.75	0.035	1,440	350
6	124.23	124.38	0.146	124.12	124.15	0.035	1,460	350
7	126.61	126.78	0.168	125.26	125.30	0.048	1,680	480

Table Q. Processed Data for Figure 77

Sample ID	Addition of Leachate			Addition of Groundwater		
	Dry beaker weight, Day 0 (g)	Dry beaker weight, Day 21 (g)	Precipitate, (g)	Dry beaker weight, Day 0 (g)	Dry beaker weight, Day 21 (g)	Precipitate, (g/100 ml)
1	126.63	134.35	7.72	126.36	132.35	6.00
2	125.85	139.95	14.09	125.77	136.95	11.17
3	127.63	134.47	6.84	127.02	141.47	14.45
4	127.48	164.24	36.76	126.75	154.24	27.49
5	124.39	196.79	72.40	124.13	168.79	44.65

## Appendix B: PXRD/XRF Diffraction Pattern Analyses and Refinement

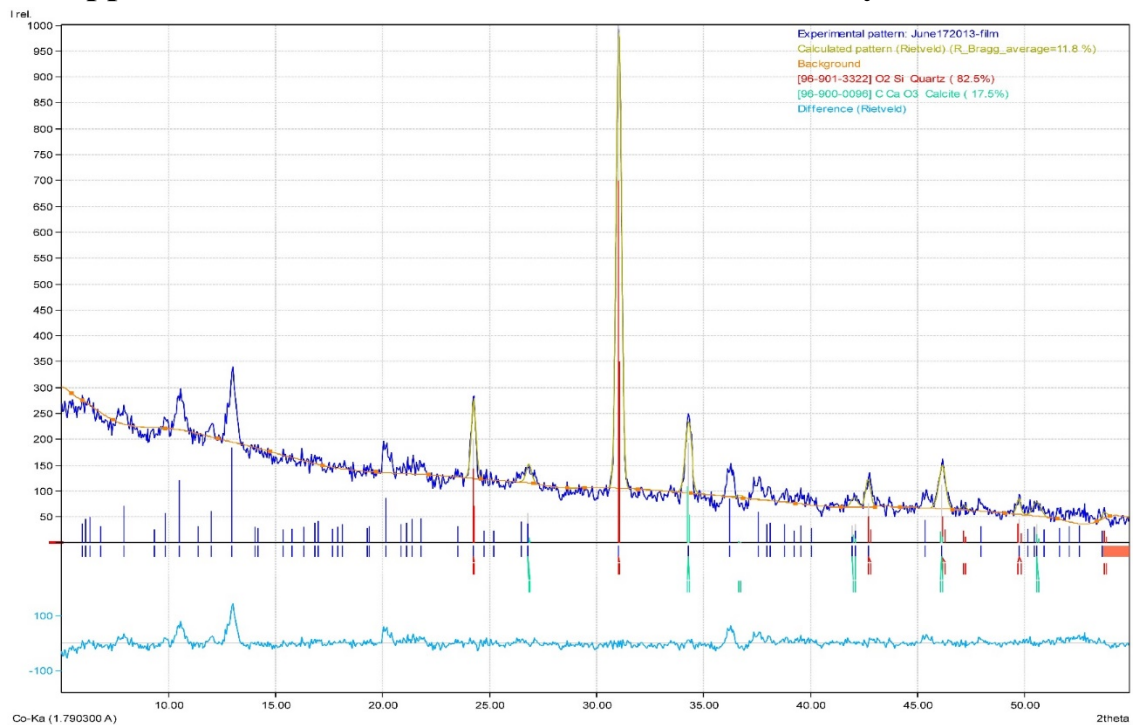


Figure A. Rietveld refinement of June 17, 2013 sample

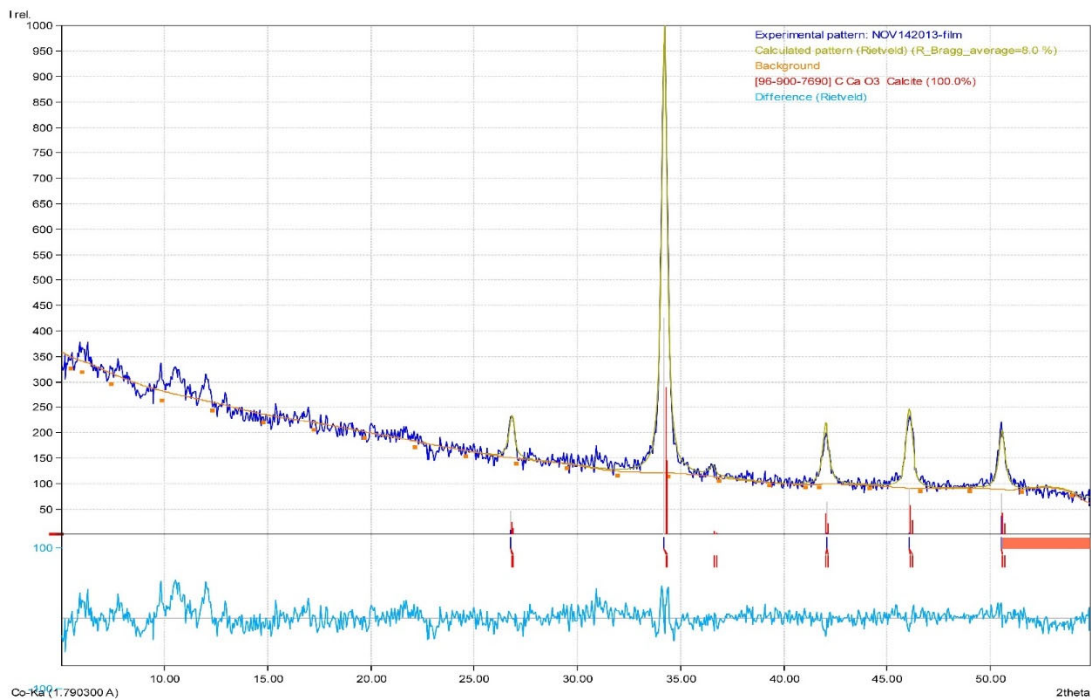


Figure B. Rietveld refinement of November 14, 2013 sample

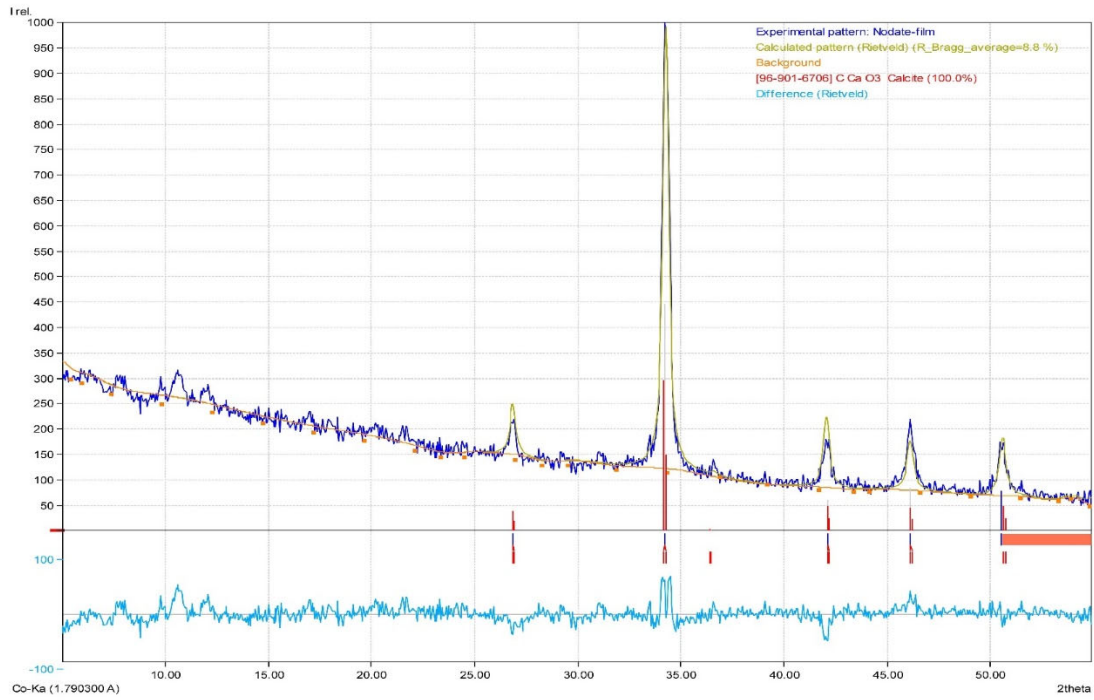


Figure C. Rietveld refinement of sample with no date

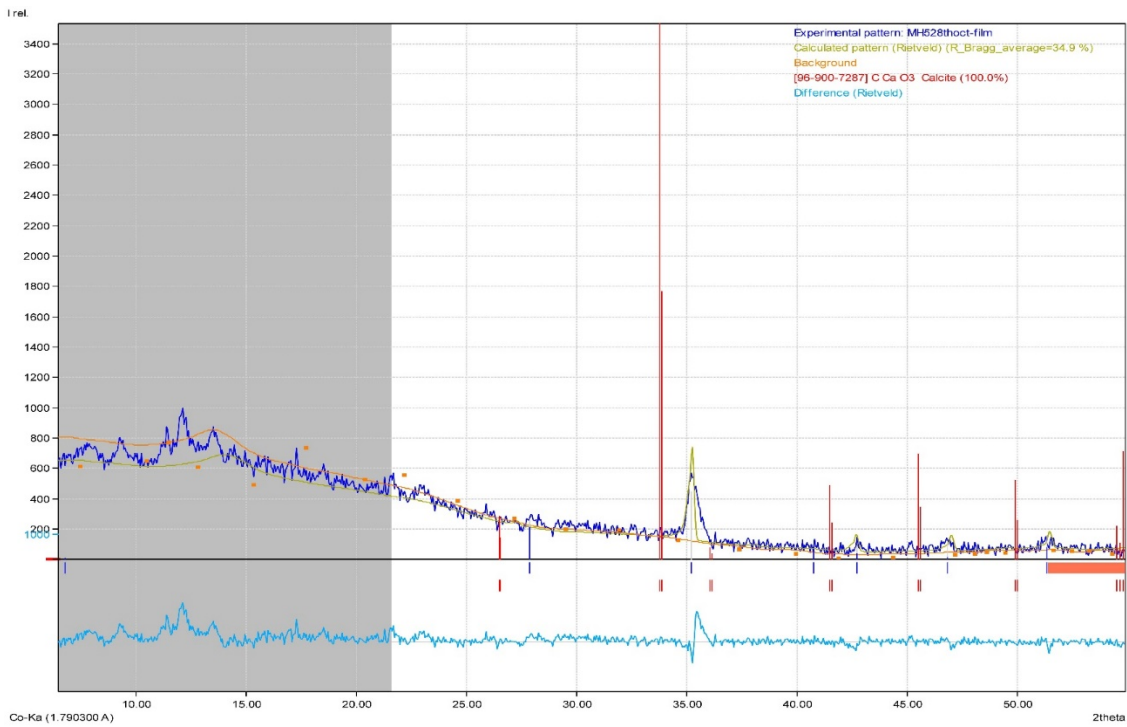


Figure D. Rietveld refinement of preexisting clog sample collected in October 28, 2015 (MH 5)

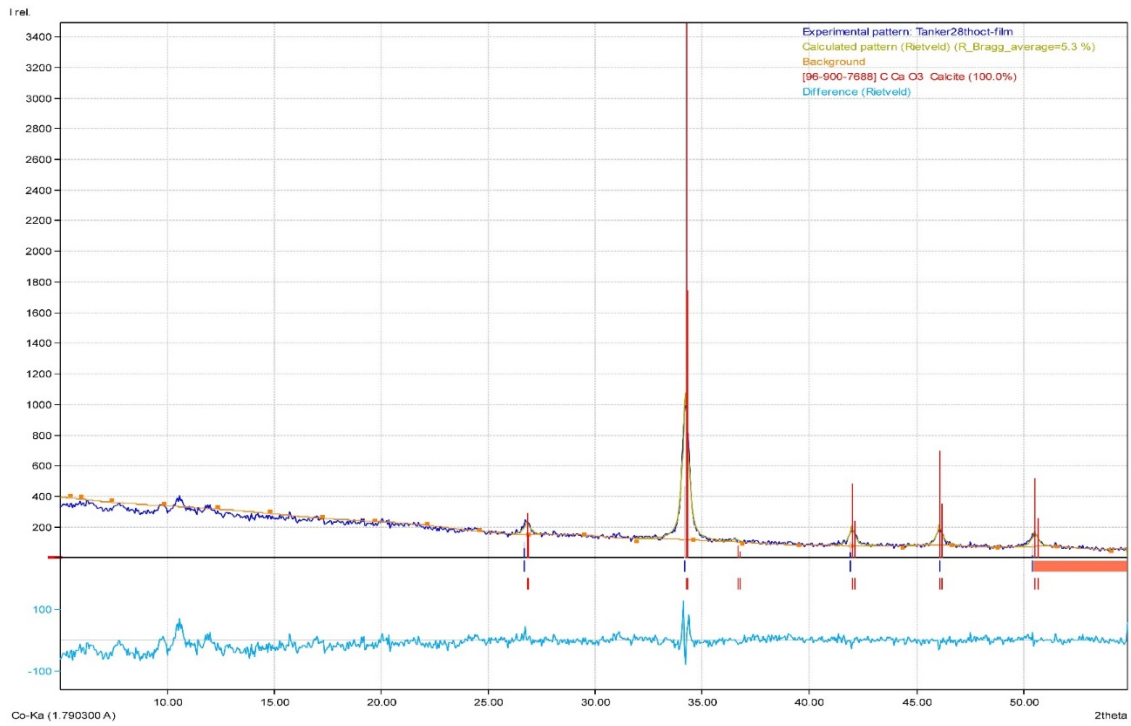


Figure E. Rietveld refinement of preexisting clog sample collected in October 28, 2015 (in front of trailer)

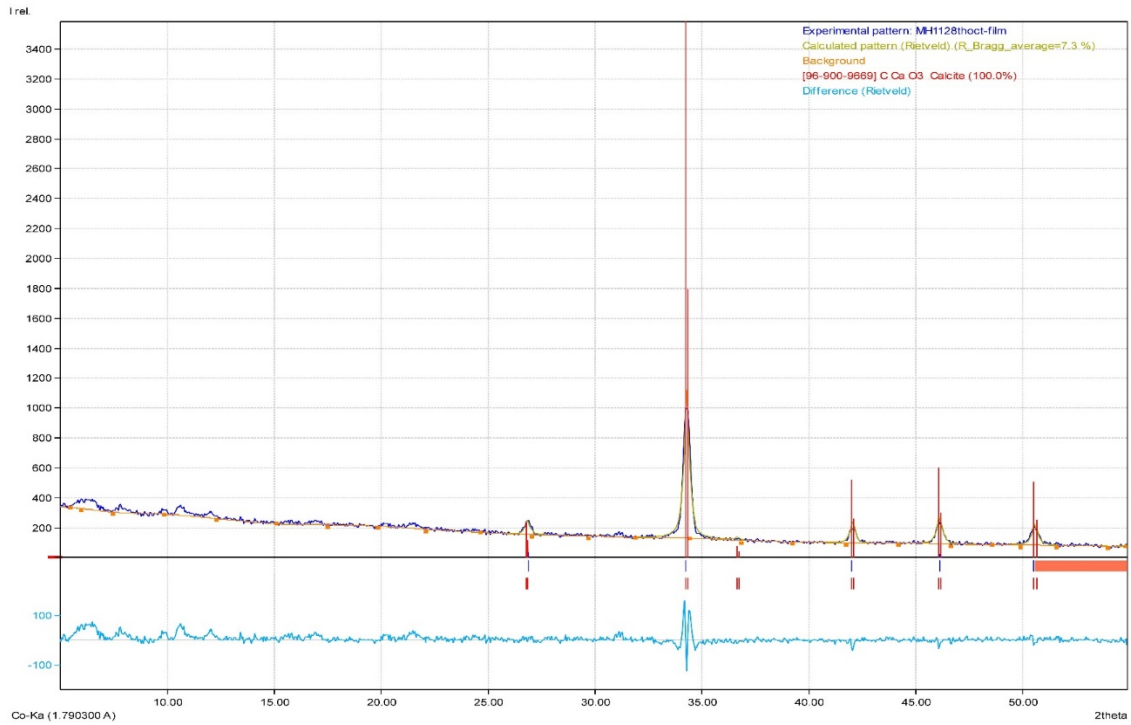


Figure F. Rietveld refinement of preexisting clog sample collected in October 28, 2015 (MH 11)

# Appendix C: Summary of Phase Identification and Rietveld Refinement

## Match! Phase Analysis Report

Bishow Nath Shaha

Sample: Calcite-film

### Sample Data

File name	Calcite-film.bt
File path	D:\Dropbox\Dr. Meeroff\Calcite\processed
Data collected	Oct 19, 2015 12:04:02
Data range	4.904° - 54.820°
Number of points	999
Step size	0.050
Rietveld refinement converged	Yes
Alpha2 subtracted	No
Background subtr.	No
Data smoothed	No
2theta correction	0.01972°
Specimen displacement correction (Bragg-Brentano geometry)	T = (-s/R) = 0.0010126
Radiation	X-rays
Wavelength	1.790300 Å

### Matched Phases

Index	Amount (%)	Name	Formula sum
A	100.0	Calcite	C Ca O3
	3.5	Unidentified peak area	

### A: Calcite (100.0 %)

Formula sum	C Ca O3
Entry number	96-900-7690
Figure-of-Merit (FoM)	0.889275
Total number of peaks	86
Peaks in range	12
Peaks matched	9
Intensity scale factor	0.23
Space group	R-3 c
Crystal system	trigonal (hexagonal axes)
Unit cell	a= 4.9880 Å c= 17.0680 Å
I/c	3.50
Calc. density	2.712 g/cm <sup>3</sup>
Reference	Maslen E. N., Streltsov V. A., Streltsova N. R., Ishizawa N., "Electron density and optical anisotropy in rhombohedral carbonates. III. Synchrotron X-ray studies of CaCO <sub>3</sub> , MgCO <sub>3</sub> and MnCO <sub>3</sub> ", Acta Crystallographica, Section B <b>51</b> , 929-939 (1995)

### Search-Match

#### Settings

Reference database used	COD REV173445 2016.01.04
Automatic zeropoint adaptation	Yes
Minimum figure-of-merit (FoM)	0.60
2theta window for peak corr.	0.29 deg.
Minimum rel. int. for peak corr.	1
Parameter/influence 2theta	0.50
Parameter/influence intensities	0.50
Parameter multiple/single phase(s)	0.50

### Peak List

No.	2theta [°]	d [Å]	I/I0	FWHM	Matched
1	26.76	3.8685	44.62	0.3396	A
2	34.16	3.0477	349.88	0.3258	A
3	41.91	2.5028	52.68	0.3727	A
4	46.07	2.2879	62.26	0.2960	A
5	50.52	2.0978	49.58	0.3450	A

### Rietveld Refinement using FullProf

Automatic refinement	No
Final weighted average Bragg R-factor	1.9
Final reduced chi <sup>2</sup>	3.0
FullProf comment	Your refinement seems to be very good!

### Rietveld Parameter List

Parameter	Final value	Refined
Zero_pat1	0.0197157	+
SyCos_pat1	0.116032	
SySin_pat1	0	
Lambda_pat1	1.7903	
P0_mabs_pat1	0	
Cp_mabs_pat1	1	
Tau_mabs_pat1	0.1	
Bck_0_pat1	1.001	
Bck_1_pat1	0	
Bck_2_pat1	0	
Bck_3_pat1	0	
Scale_ph1_pat1	0.00114784	

Scale_ph1_pat1	0.104181
Bover_ph1_pat1	4.95096
Strain1_ph1_pat1	0
Strain2_ph1_pat1	0
Strain3_ph1_pat1	0
U-Cagl_ph1_pat1	2.14027
V-Cagl_ph1_pat1	-1.52372
W-Cagl_ph1_pat1	0.361122
G-Size_ph1_pat1	0
L-Size_ph1_pat1	0
Cell_A_ph1_pat1	4.99614
Cell_B_ph1_pat1	4.99614
Cell_C_ph1_pat1	17.0773
Cell_D_ph1_pat1	90
Cell_E_ph1_pat1	90
Cell_F_ph1_pat1	120
Or1_ph1_pat1	0
Or2_ph1_pat1	0
Asym1_ph1_pat1	-0.399205
Asym2_ph1_pat1	-0.290801
Asym3_ph1_pat1	1.11607
Asym4_ph1_pat1	0.658631
X_Ca1_ph1	0
Y_Ca1_ph1	0
Z_Ca1_ph1	0
Biso_Ca1_ph1	1
Occ_Ca1_ph1	1
X_C2_ph1	0
Y_C2_ph1	0
Z_C2_ph1	0.25
Biso_C2_ph1	1
Occ_C2_ph1	1
X_O3_ph1	0.256776
Y_O3_ph1	0
Z_O3_ph1	0.25
Biso_O3_ph1	1
Occ_O3_ph1	1

### Integrated Profile Areas

#### Based on Rietveld refinement

<i>Profile area</i>	<i>Counts</i>	<i>Amount</i>
Overall diffraction profile	450320	100.00%
Background radiation	407795	90.56%
Diffraction peaks	42525	9.44%
Peak area belonging to selected phases	39120	8.69%
Peak area of phase A ( <i>Calcite</i> )	39947	8.87%
Unidentified peak area	15921	3.54%

### Peak Residuals

<i>Peak data</i>	<i>Counts</i>	<i>Amount</i>
Overall peak intensity	2308	100.00%
Peak intensity belonging to selected phases	2166	93.82%
Unidentified peak intensity	143	6.18%

### Diffraction Pattern Graphics

